A MATHEMATICAL MODEL FOR SOLID POPULATION BALANCE IN A 7.5 MW FBC POWER PLANT USING COTTON STALK

A Thesis

submitted in partial fulfillment of the requirements for the award of degree of

MASTER OF ENGINEERING

IN

(CAD, CAM & Robotics)

Submitted by

KARAMDEEP SINGH

ROLL NO. 80681010

Under the guidance of

Dr. S. K. MOHAPATRA

Professor and Head,

Mechanical Engineering Department

MECHANICAL ENGINEERING DEPARTMENT

THAPAR UNIVERSITY

PATIALA-147004, INDIA

June, 2008

CERTIFICATE

This is to certify that the Thesis title, *"A MATHEMATICAL MODEL FOR SOLID POPULATION BALANCE IN A 7.5 MW FBC POWER PLANT USING COTTON STALK"*, being submitted by *Karamdeep Singh,* in partial fulfillment of the requirements for the award of degree of **MASTER OF ENGINEERING (CAD/CAM & ROBOTICS) at THAPAR UNIVERSITY, PATIALA** is a bonafide work carried out by him under my guidance and supervision and no part of this thesis has been submitted for the award of any other degree.

Dr. S.K. Mohapatra
Prof. & Head, MED 26/6/08
Thapar University, PATIALA

Dr. S.K. Mohapatra 26/6/08
Prof. & Head, MED
Thapar University, PATIALA

Dr. R.K. Sharma
Dean Academic Affairs
Thapar University, PATIALA

ACKNOWLEDGMENT

The author is deeply indebted to **Dr. S. K. MOHAPATRA**, Professor and Head Mechanical Engineering Department, Thapar University, for acting as supervisor and giving valuable guidance during the course of this investigation.

A note of thanks here is also due to Mr. Jaswant Singh, Chief Engineer at Malwa Power Ltd., Muktsar, for his cooperation and assistance in the completion of this work.

Karamdeep Singh
ROLL NO. 80681010

ABSTRACT

"The arrival time of a space probe traveling to Saturn can be predicted more accurately than the behavior of a fluidized bed chemical reactor!"

Even though the above quotation (Geldart, 1986) is almost 20 years old, it remains true in the new millennium of fluidization engineering. The difficulties in prediction stem in part from the complexity and ambiguity in defining the fundamental parameters such as size, shape and density of the particles. These parameters play an important role in the calculation and prediction of dynamic behavior in fluidized beds. Most physical properties of the particles are estimated indirectly, such as estimating particle shape by the bed voidage. All factors are explicitly and implicitly significant in the estimation of the behavior of fluidization operations. Although new technology is helping us to understand and give more precise prediction in fluidization, more research is still needed.

Either a gas or a liquid can fluidize a bed of particles. In this thesis, the focus is purely on gas-solid fluidization. Taking data from a 7.5 MW FBC power plant, a mathematical model has been developed for solid population balance. The initial part of the development included calculation of physico-chemical parameters, developing a model that fits in the size distribution data and then further extending this model to calculate the carryover probability density and bed charcoal weight.

CONTENTS

LIST OF FIGURES AND TABLES

List of Tables

LIST OF SYMBOLS USED

A	Cross-sectional area of the bed (m^2)
A_b	Cross-sectional area of bed occupied by bubble phase (m^2)
A_{cw}	Cross-sectional area of bed occupied by cloud-wake phase (m^2)
A_{cw_g}	Cross-sectional area of bed available for gas flow in the cloud-wake phase (m^2)
A_{kt}	Attrition rate constant
Ar	Archimedes number
C_o	Initial oxygen concentration (kg-mol/m^3)
C_{avg_n}	Average oxygen concentration leaving stage n (kg-mol/m^3)
C_{avg}	Average oxygen concentration leaving top of bed (kg-mol/m^3)
C_{b_n}	Oxygen concentration leaving stage n in bubble phase (kg-mol/m^3)
C_{cw_n}	Oxygen concentration leaving stage n in cloud-wake phase (kg-mol/m^3)
C_{e_n}	Oxygen concentration leaving stage n in emulsion phase (kg-mol/m^3)
C_p	Oxygen concentration in the particulate phase (kg-mol/m^3)
C_s	Carbon concentration per unit dense phase (kg-mol/m^3)
C_s'	Oxygen concentration at the carbon surface (kg-mol/m^3)
d_p	Feed particle diameter (m)
D_b	Average equivalent bubble diameter (m)
D_{bm}	Fictitious maximum bubble diameter (m)

D_{bo}	Initial bubble diameter (m)
D_R	Bed diameter (m)
D_e	Molecular diffusion coefficient of gas (m^2/s)
dd_p/dt	Particle shrinkage rate (m/s)
f_c	Ratio of cloud volume to the volume of bubble
f_{cw}	Ratio of volume of cloud-wake phase to the volume of bubble
f_w	Ratio of wake volume to the volume of bubble
F_{ME}	Actual molar feed rate of fluidizing air (kg-mole/s)
F_{MTH}	Stoichiometric air feed rate (kg-mole/s)
g	Acceleration due to gravity (m/s)
H	Expanded bed height (m)
H_{mf}	Bed height at minimum fluidization (m)
$(K_{bc})_b$	Gas interchange coefficient between bubble and cloud-wake phases (s^{-1})
$(K_{be})_b$	Gas interchange coefficient between bubble and emulsion phases (s^{-1})
$(K_{ce})_b$	Gas interchange coefficient between cloud-wake and emulsion phases (s^{-1})
K	Overall reaction rate constant (s^{-1})
K_{cw}	Reaction rate in the cloud-wake phase (s^{-1})
K_s	Surface reaction rate constant (m/s)
K_g	Mass transfer coefficient (m/s)
M_c	Molecular weight of carbon (kg/mol)
N	Number of equivalent stages
N_D	Number of orifice openings in distributor plate
P_{av}	Average pressure in the combustor (atm)
R_g	Gas constant (atm-m^3/ kg-mole)

Sh	Sherwood number
T_b	Absolute bed temperature (K)
T_p	Char surface temperature (K)
u_b	Rise velocity of a crowd of bubbles (m/s)
u_{br}	Rise velocity of an isolated single rising bubble (m/s)
U	Superficial velocity (m/s)
U_b	Superficial gas velocity of the bubble phase (m/s)
U_{cw}	Superficial gas velocity of cloud-wake phase (m/s)
U_{mf}	Superficial velocity of fluidizing gas under minimum fluidization (m/s)
W	Fuel feed rate into the combustor (kg/s)
X	Oxygen conversion
XC	Carbon content of the fuel
XH	Hydrogen content of the fuel
XO	Oxygen content of the fuel
XS	Sulphur content of the fuel
XW	Moisture content of the fuel
Z	Bed height above distributor plate (m)

Greek symbols

ρ_g	Density of fluidizing gas (kg/m^3)
ρ_s	Density of feed particle (kg/m^3)
μ_g	Viscosity of fluidizing gas (kg/m.s)
ε_b	Volume fraction of bubbles in the bed
ε_{mf}	Voidage at minimum fluidization
κ^*	Elutriation constant
$\Re$	Shrinkage constant

CHAPTER 1

1.0 Introduction

In India 65 percent energy consumption due to coal fired power generation is dependent on non-coking coal as high ash coal in pulverized form. The total coal consumed for power generation accounts 50% of the coal produced in India including middlings and sinks available from more than 17 Washeries. The quality of Indian coals available for power generation is progressively detoriating with growing emphasis on open cast mining. The high ash content along with highly abrasive nature of the ash causes forced outage of thermal power plants. The average national availability of thermal power plant is between 52 – 53 percent. The existing coal based power plants have reached 36% efficiency. In future programme degradation in quality of coal will cause further reduction of the efficiency of power generation as well as inherent creation of pollution problems. Besides pollution caused by the thermal power station is expected to increase its planned addition of power generation capacity. Therefore, alternate energy conversion system needs to be established to overcome the detoriating trend of generation efficiency.

The possible advanced coal fired generation systems are being developed worldwide to meet the development needs such as:

(i) to meet power generation at economical cost

(ii) to improve thermal efficiency

(iii) to comply with current and expected environmental standards

The above achievements may be gained by introduction of Fluidized Bed Combustion (FBC), in which a fluidized bed of sand like particles is initially heated and then the fuel is thrown on the bed for combustion. FBC technologies based plants incorporating supercritical steam cycles together with some form of flue gas,

desulphurization and low NOx measures. Fluidized bed power generation systems represent significant advantage over conventional coal combustion technologies in a cost effective manner using various fuels effectively with efficient in-situ retention of sulphur oxides and inherent low NOx emissions under improved efficiency of power generation.

1.1 History & State of the Art

The operation of the world's first large-scale, commercial, fluidized bed reactor was started by Fritz Winkler for the gasification of powdered coal in 1926. Since then fluidized beds have been developed vigorously for different physical and chemical operations, such as transportation systems and chemical reaction processes. As the demand for petrol rose in the Second World War, research in catalytic cracking of heavy oils was desperately needed. At this time, a group of researchers at the Massachusetts Institute of Technology had proposed and confirmed experimentally that a completely pneumatic circuit consisting of fluidized beds and transport lines could be operated stably for a satisfactory catalytic cracking process (Kunii and Levenspiel, 1991). Esso engineers concentrated on this idea and built a large-scale pilot plant of an up-flow cracking unit (Geldart, 1986). The Fluid Catalytic Cracking (FCC) process was then on track. The world's first Fluid Catalyst Cracking unit was constructed at the Baton Rouge refinery in Louisiana in 1942, and this type of reactor remains a fundamental and essential reactor in the field of process engineering.

In UK, FBC technology was developed in 1967 and projected that this technology offered advantages with a more compact boiler and very high rate of heat transfer to the tube surfaces in the bubbling bed, level of NOx and SOx was minimum under good achievement of pollution control. In 1983 the First International Conference on FBC technology was organized by Mc-Graw Hill Publication in China. China has installed more than 2000 boilers operating on FBC technology. The main reason for utilization of FBC boilers is low grade coal and washery rejects. In response to First Arab/Israel war and the subsequent oil supply crisis, the International Energy Agency (IEA) established technology development programmes that would reduce the reliance on the oil. Three countries UK, USA and West Germany came together under a test implementing agreement to undertake a large scale demonstration of FBC in Yorkshire.

Major FBC bioler manufacturers in the world are:

- Babcock and Wilcox
- Foster Wheeler
- Lurgi Lentges Babcock
- Tampella Power USA
- ABB Combustion Engineering
- GEC Alsthom Germany etc.

FBC generation on Pilot Scale studies have been conducted by KRW and U Gas in USA using 35 TPD and 15 TPD test rigs respectively. In India BHEL (Bharat Heavy Electricals Ltd.) has set up a pilot scale Process Equipment Development Unit (PEDU) of 18 TPD capacity and also Pilot scale plants of PFBC (Pressurised Fluidised Bed Combustion) and HGCS (Hot Gas Clean up Systems) followed by FBC technology.

Currently a FCC unit is a standard component in the production of gasoline and other fuels from heavy oil components, and is at the heart of practically every oil refinery in the world. The FCC unit is an example application of fluidized bed reactors that have had a major impact on industrial processes. In fact, fluidized bed reactors are already utilized for a wide range of applications where contact between gas and particulate solids is required together with good solids mixing and heat transfer, for example mixing of powders, coating, heat exchange, drying and classifying materials. The complexity of solid movement within the beds depends on a number of parameters such as the geometry of the bed and physical properties of particles. A small difference in those parameters can cause a severe change in terms of the efficiency of fluidized bed reactors. To make sure that a fluidized bed reactor is at optimum efficiency, normally either a small or large pilot model is made and investigated to test the proposed fluidized bed. Even though the experiments and pilot model were tested before building a real unit, problems have often occurred when attempting to construct and operate the large-scale unit.

Since the availability of computers has significantly increased, the use of mathematical models to predict the performance and efficiency of an existing or newly designed fluidized bed also has increased. A number of mathematical models have been proposed for fluidized beds. Most of the models used in chemical engineering and also in

fluidization have been deterministic differential equation models based on conservation equations.

1.2 Review of Fluidization Basics

Fluidization is a process in which solids are caused to behave like a fluid by blowing gas or liquid upwards through the solid-filled reactor. Fluidization is widely used in commercial operations; the applications can be roughly divided into two categories, i.e.

- Physical operations, such as transportation, heating, absorption, mixing of fine powder, etc. and
- Chemical operations, such as reactions of gases on solid catalysts and reactions of solids with gases etc.

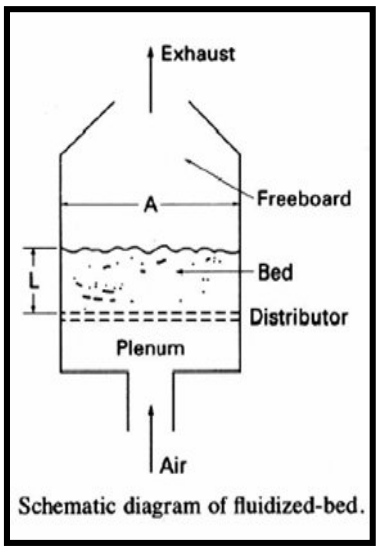

Figure 1.1: FBC

The fluidized bed is one of the best known contacting methods used in the processing industry, for instance in oil refinery plants. Among its chief advantages are that the particles are well mixed leading to low temperature gradients, they are suitable for both small and large scale operations and they allow continuous processing. There are many well established operations that utilize this technology, including cracking and reforming of hydrocarbons, coal carbonization and gasification, ore roasting, Fisher-Tropsch synthesis, coking, aluminum production, melamine production, and coating preparations. The application of fluidization is also well recognized in nuclear engineering as a unit operation for example, in uranium extraction, nuclear fuel fabrication, reprocessing of fuel and waste disposal.

1.2.1 Fluidization Regimes

When the solid particles are fluidized, the fluidized bed behaves differently as velocity, gas and solid properties are varied. It has become evident that there are number of regimes of fluidization, as shown in Figure 1.2. When the flow of a gas passed through a bed of particles is increased continually, a few vibrate, but still within the same height as the bed at rest. This is called a fixed bed (Figure 1.2 A). With increasing gas velocity, a point is reached where the drag force imparted by the upward moving gas equals the weight of the particles, and the voidage of the bed increases slightly: this is the onset of fluidization and is called minimum fluidization (Figure 1.2 B) with a corresponding minimum fluidization velocity, U_{mf}. Increasing the gas flow further, the formation of fluidization bubbles sets in, at this point, a bubbling fluidized bed occurs as shown in Figure 1.2 C. As the velocity is increased further still, the bubbles in a bubbling fluidized bed will coalesce and grow as they rise. If the ratio of the height to the diameter of the bed is high enough, the size of bubbles may become almost the same as diameter of the bed. This is called slugging (Figure 1.2 D). If the particles are fluidized at a high enough gas flow rate, the velocity exceeds the terminal velocity of the particles. The upper surface of the bed disappears and, instead of bubbles, one observes a turbulent motion of solid clusters and voids of gas of various sizes and shapes. Beds under these conditions are called turbulent beds as shown in Figure 1.2 E. With further increases of gas velocity, eventually the fluidized bed becomes an entrained bed in which we have disperse, dilute or lean phase fluidized bed, which amounts to pneumatic transport of solids.

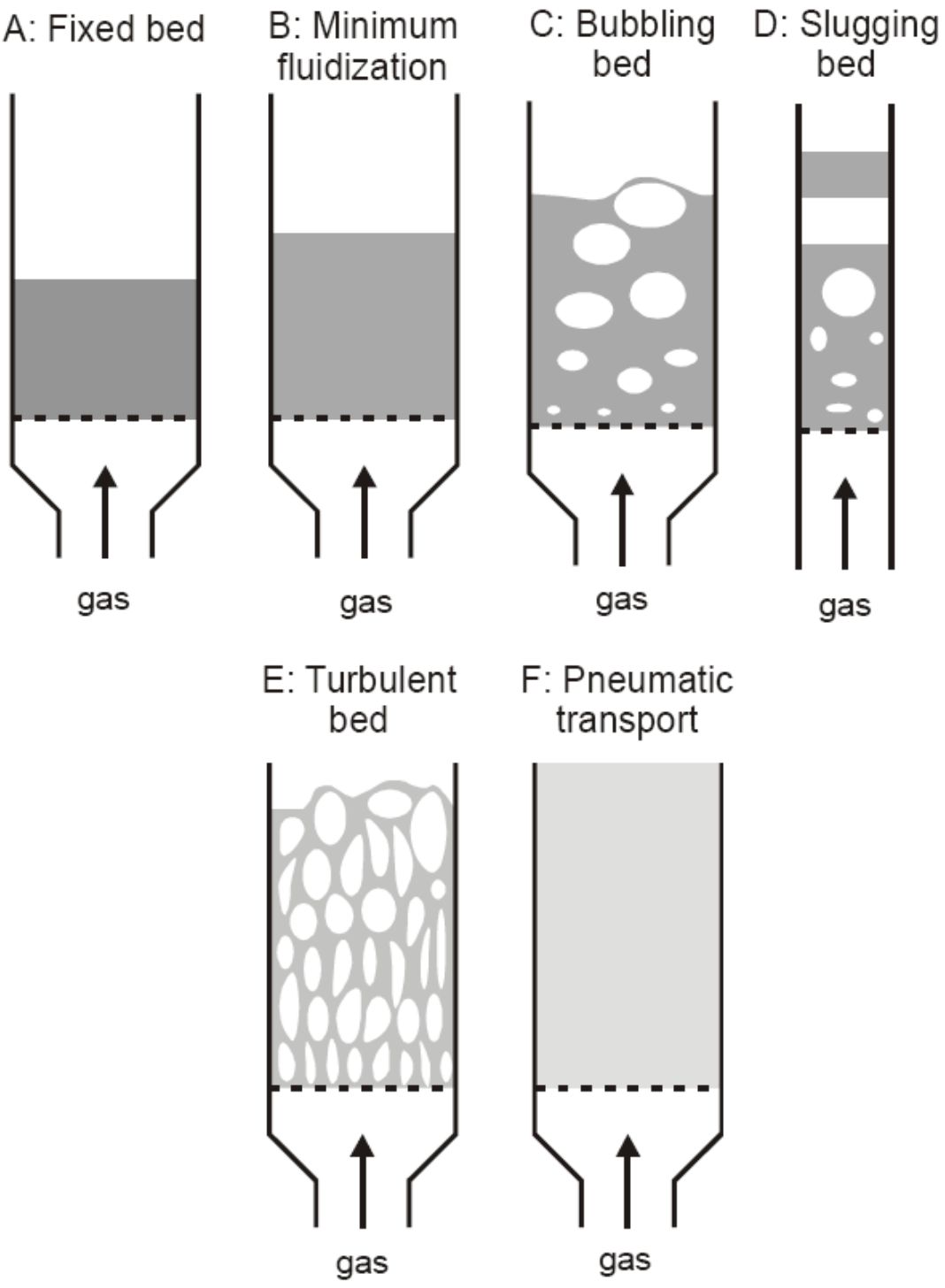

Figure 1.2: Regimes of Fluidization

1.2.2 Geldart's Classification of Powders

Not every particle can be fluidized. The behavior of solid particles in fluidized beds depends mostly on their size and density. A careful observation by Geldart (1973, 1978) is shown in Figure 1.3, in which the characteristics of the four different powder types were categorized as follows:

• Group A is designated as 'aeratable' particles. These materials have small mean particle size (d_p < 30 μm) and/or low particle density (<~1.4 g/cm^3). Fluid cracking catalysts typically are in this category. These solids fluidize easily, with smooth fluidization at low gas velocities without the formation of bubbles. At higher gas velocity, a point is eventually reached when bubbles start to form and the minimum bubbling velocity, U_{mb} is always greater than U_{mf}.

• Group B is called 'sandlike' particles and some call it bubbly particles. Most particles of this group have size 150 μm to 500 μm and density from 1.4 to 4 g/cm^3. For these particles, once the minimum fluidization velocity is exceeded, the excess gas appears in the form of bubbles. Bubbles in a bed of group B particles can grow to a large size. Typically used group B materials are glass beads (ballotini) and coarse sand.

• Group C materials are 'cohesive', or very fine powders. Their sizes are usually less than 30 μm, and they are extremely difficult to fluidize because interparticle forces are relatively large, compared to those resulting from the action of gas. In small diameter beds, group C particles easily give rise to channeling. Examples of group C materials are talc, flour and starch.

• Group D is called 'spoutable' and the materials are either very large or very dense. They are difficult to fluidize in deep beds. Unlike group B particles, as velocity increases, a jet can be formed in the bed and material may then be blown out with the jet in a spouting motion. If the gas distribution is uneven, spouting behavior and severe channeling can be

expected. Roasting coffee beans, lead shot and some roasting metal ores are examples of group D materials.

Geldart's classification is clear and easy to use as displayed in Figure 2.2 for fluidization at ambient conditions and for U less than about $10 \cdot U_{mf}$. For any solid of a known density ρ_s and mean particle size d_p this graph shows the type of fluidization to be expected. It also helps predicting other properties such as bubble size, bubble velocity, the existence of slugs etc.

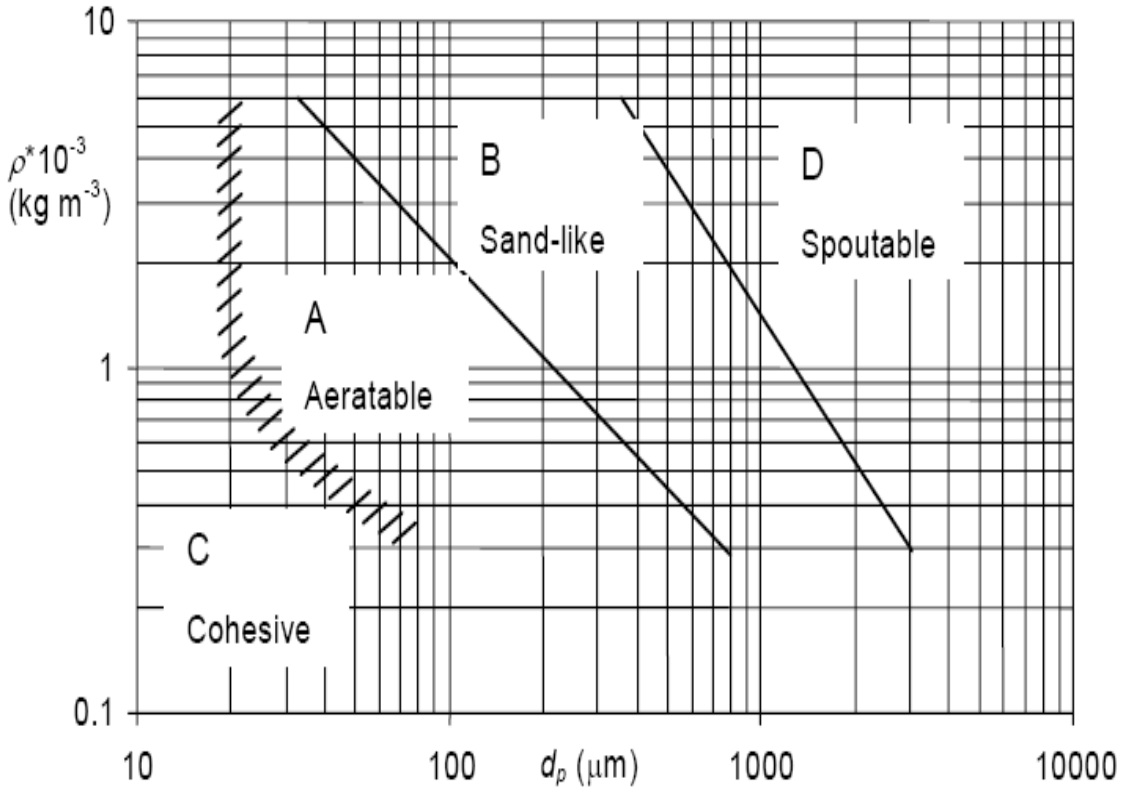

Figure 1.3: Diagram of the Geldart classification of particles (Geldart, 1973)

1.2.3 Fluidization Hydrodynamics

When a fluid is passed upwards through a bed of solid particles at a very low flow rate the fluid percolates through the void space without disturbing the bed. This condition represents a fixed bed. If the upward flow rate is very high the bed mobilizes pneumatically and may be swept out of the vessel. At an intermediate flow rate, the bed expands; the particles are separated by a mean free distance and are supported by the drag force of the fluid. The expanded bed, having some of a fluid's properties, is called a fluidized bed. Typical results of a gas-fluidized bed of particles are shown in Figure 1.4 where the pressure drop across the bed and its height are plotted as a function of the superficial gas velocity: starting from line A, for slowly increasing flow, the overall pressure drop is slightly more than enough to support the weight of the particles. Above point B, a slight increase in flow velocity frees the particles: the pressure drop becomes just enough to support their weight and, consequently, point C is commonly defined as a point of incipient fluidization, characterized by the minimum fluidization velocity Umf and the voidage fraction emf. If the flow rate is decreased from point C, the particles are more loosely packed so the bed height is greater and the pressure drop smaller (point D).

For a gas fluidized bed in which the gas velocity is greater than U_{mf}, some of the gas may pass through the bed as bubbles: these agitate the bed and consequently its height fluctuates as indicated in region E. The formation of bubbles characterizes the bubbling fluidized bed; with still greater flows the bubbles grow and appear more frequently, until the bed becomes slugging. A further increase in flow carries particles out of the combustor according to the phenomena of pneumatic transport. After the gas reaches the minimum fluidization velocity, bubbles form and during their rise to the surface of the bed, not only do they increase in size and coalesce, they are also divided. In general, fluidized bed models consider the division between the bubble phase and the particulate phase, also called emulsion or dense phase, the degree of mixing in the particulate phase and the transfer of gas between the two phases. The reason for developing a conceptual model for the bubbling bed is to estimate its main features, such as velocities of gas and solid, volume fractions and contacting regimes, from very little information about the solid particles in the bed.

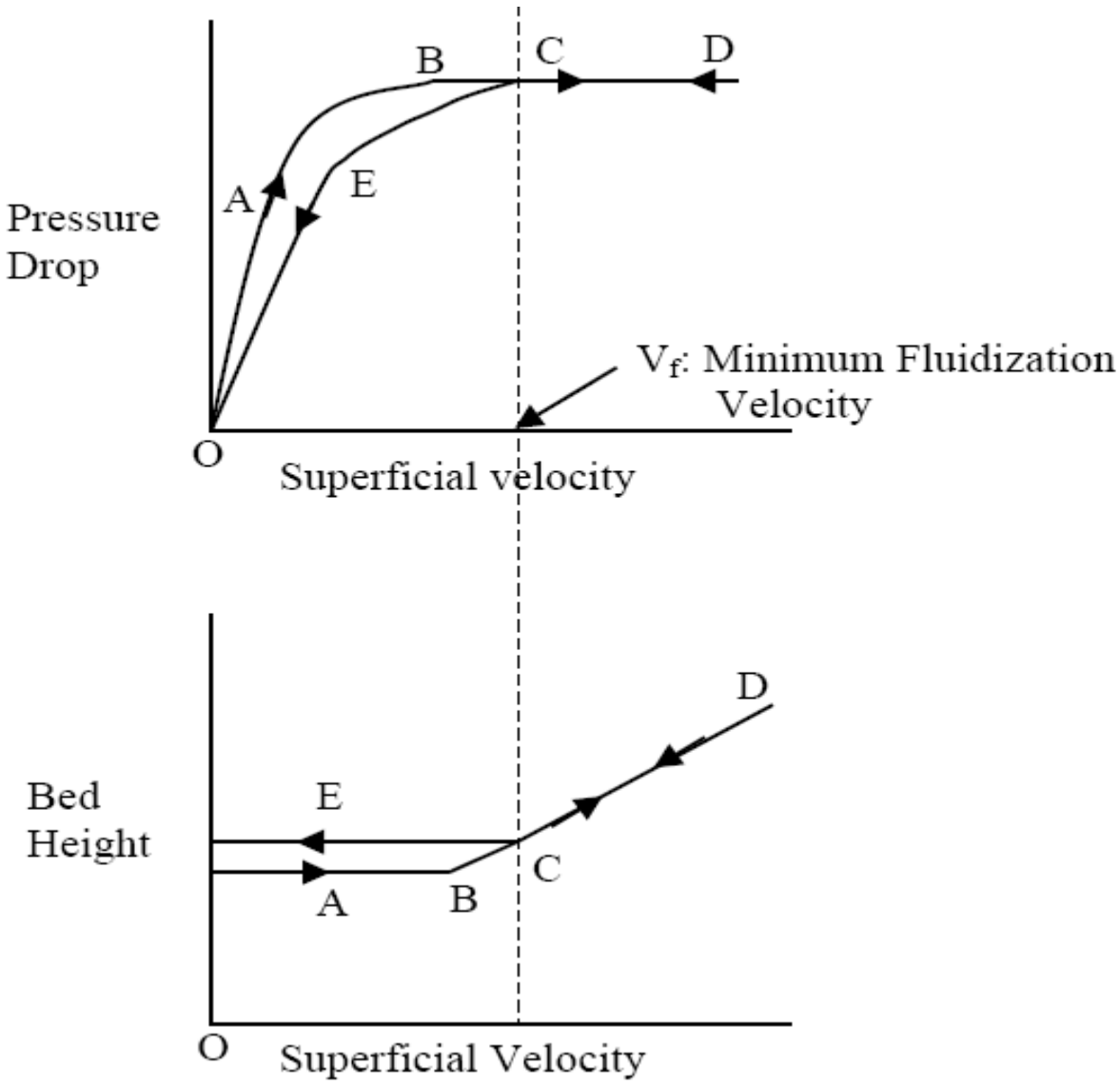

Figure 1.4: Pressure drop across the bed

The first significant breakthrough was made by Davidson who proposed a straightforward, simple model for single rising bubbles, based on the following postulates: a gas bubble is solid-free and circular in shape; as a bubble rises, particles move aside. The emulsion behaves like an incompressible fluid through which the gas flows as an incompressible viscous fluid. Pressure in the bubble is assumed to be constant. One of the most appreciable results of this model is the pressure distribution near a 3-D bubble: the pressure in the lower part of the bubble is lower than that of the

surrounding bed, whereas in the upper part it is higher. Hence, gas flows into the bubble from below and leaves at the top. Although the circular shape of the bubble is not a realistic hypothesis, the Davidson model fits the data quite well. A significant attempt to understand the behaviour of a bubbling bed as a whole was made by Toomey and Johnstone [36], the fathers of the two-phase theory of fluidization. Since experiments in bubbling beds indicate roughly that all gas in excess of that needed to fluidize the bed passes through the bed as bubbles and the emulsion phase remains close to minimum fluidizing conditions, they considered the bubbling bed to be composed of two phases: the bubbling phase and the emulsion phase. The emulsion flow rate is equal to the flow rate for incipient fluidization (U_{mf}) while the bubble phase carries the additional flow of fluidizing fluid ($U - U_{mf}$). Comparison between predicted and experimental data makes it clear that the two-phase theory overestimates the volume of gas passing through the bed as bubbles. Besides, evaluation of solids movement in the bed is not considered.

A more detailed description of the bubbling bed was proposed by Kunii and Levenspiel [15]. They introduced a new phase called ‘‘cloud’’ thus their contribution is also known as the three-phase theory (Figure 1.5). Consider the following flow patterns: if the emulsion gas rises faster than the bubble, it enters the bottom of the bubble and leaves at the top; this generates an annular ring of gas that circulates within the bubble. On the contrary, if the bubble rises faster than the emulsion, the gas leaving the top of the bubble is swept around and returns to the base of the bubble. The region around the bubble covered by this circulating gas is the cloud: slow bubbles are cloudless whereas, in the case of fast bubbles, cloud cannot be neglected. In addition, this model is the first to show that solids are dragged up the bed behind bubbles and drift downwards in the emulsion. Although, the volume fraction of particles dispersed in rising bubbles might be less than 0.1%, these could enormously affect processes in which rapid kinetics occurs. Unlike the previous theory, bubbles are not spherical but have a flattish or even concave base (Figure 1.6). The region just below the bubble is the wake: this leaks the solid matter that a rising bubble drags up, assuring an interchange with the emulsion. This model hypothesizes that all the fluid passes through the bubble phase (the gas flow through the emulsion is negligible) and solid matter mixes perfectly with the gas in the emulsion phase.

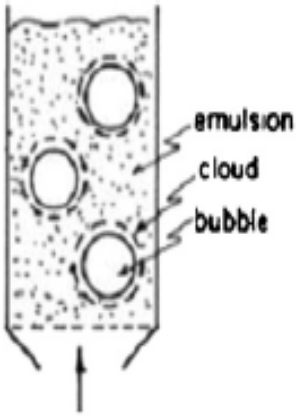

Figure1.5: Representation of 3-phases in Fluidized bed

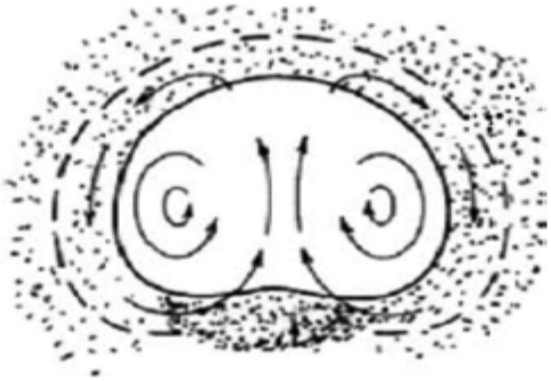

Figure1.6: Gas flow pattern in and around the bubble acc. to Kunni & Levenspiel

The three-phase theory has been the object of controversies for some time since its complexity cannot often assure better results than the simpler two-phase theory. However, investigations by many researchers demonstrated that, among others models, it adapts better to different operating conditions. In order of rising complexity, the last fluidization model was developed by Werther [8] who was inspired by studies of bed expansion and bubble size distribution. By analogy with gas–liquid reactors, he adopts known mass-transfer phenomena with concentration profiles around the bubbles. The key assumption is concerned with defining a height below which bubble size does not change. Additional hypotheses include the following: the gas flow through the emulsion phase is negligible whereas the one in the bubble phase is a plug flow; the coefficient of mass transfer and the interfacial film between bubble and emulsion are considered independent of the height in the bed.

1.3 Types of Fluidized Bed Combustion

There are three basic types of fluidized bed combustion boilers:

1. Atmospheric (classic) Fluidized Bed Combustion System (AFBC)
2. Atmospheric circulating Fluidized Bed Combustion System (CFBC)
3. Pressurized Fluidized Bed Combustion System (PFBC).

1.3.1 Atmospheric Fluidized Bed Combustion (AFBC)

In AFBC, the fuel is chipped and broken to a size of 1 – 30 mm depending on the rank of coal, type of fuel feed and fed into the combustion chamber. The atmospheric air, which acts as both the fluidization air and combustion air, is delivered at a pressure and flows through the bed after being preheated by the exhaust flue gases. The velocity of fluidizing air is in the range of 1.2 to 3.7 m /sec. The rate at which air is blown through the bed determines the amount of fuel that can be reacted. Almost all AFBC/ bubbling bed boilers use in-bed evaporator tubes in the bed of limestone, sand and fuel for extracting the heat from the bed to maintain the bed temperature. The bed depth is usually 0.9 m to 1.5 m deep and the pressure drop averages about 1 inch of water per inch of bed depth. Very little material leaves the bubbling bed – only about 2 to 4 kg of solids is recycled per ton of fuel burned. Typical fluidized bed combustor of this type is shown in Figures 1.7.

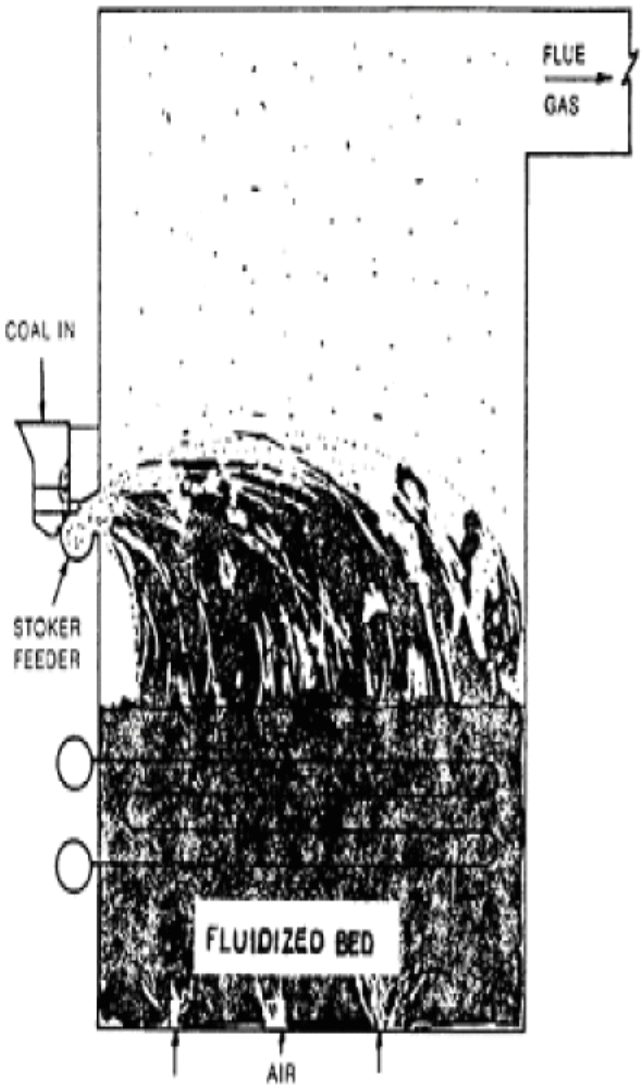

Figure 1.7: AFBC

The combustion gases pass over the super heater sections of the boiler, flow past the economizer, the dust collectors and the air pre-heaters before being exhausted to atmosphere. The main special feature of atmospheric fluidized bed combustion is the constraint imposed by the relatively narrow temperature range within which the bed must be operated. With coal, there is risk of clinker formation in the bed if the temperature exceeds 950°C and loss of combustion efficiency if the temperature falls below 800°C. For efficient sulphur retention, the temperature should be in the range of 800°C to 850°C.

1.3.1.1 General Arrangements of AFBC Boiler

AFBC boilers comprise of following systems:

i) Fuel feeding system

ii) Air Distributor

iii) Bed & In-bed heat transfer surface

iv) Ash handling system

Many of these are common to all types of FBC boilers

Fuel feeding system

For feeding fuel, sorbents like limestone or dolomite, usually two methods are followed: under bed pneumatic feeding and over-bed feeding.

Under Bed Pneumatic Feeding

If the fuel is coal, it is crushed to 1-6 mm size and pneumatically transported from feed hopper to the combustor through a feed pipe piercing the distributor. Based on the capacity of the boiler, the number of feed points is increased, as it is necessary to distribute the fuel into the bed uniformly.

Over-Bed Feeding

The crushed coal, 6-10 mm size is conveyed from coal bunker to a spreader by a screw conveyor. The spreader distributes the coal over the surface of the bed uniformly. This

type of fuel feeding system accepts over size fuel also and eliminates transport lines, when compared to under-bed feeding system.

Air Distributor

The purpose of the distributor is to introduce the fluidizing air evenly through the bed cross section thereby keeping the solid particles in constant motion, and preventing the formation of de-fluidization zones within the bed. The distributor, which forms the furnace floor, is normally constructed from metal plate with a number of perforations in a definite geometric pattern. The perforations may be located in simple nozzles or nozzles with bubble caps, which serve to prevent solid particles from flowing back into the space below the distributor.

The distributor plate is protected from high temperature of the furnace by:

i) Refractory lining

ii) A static layer of the bed material

iii) Water cooled tubes

Bed & In-Bed Heat Transfer Surface:

Bed

The bed material can be sand, ash, crushed refractory or limestone, with an average size of about 1 mm. Depending on the bed height these are of two types: shallow bed and deep bed. At the same fluidizing velocity, the two ends fluidize differently, thus affecting the heat transfer to an immersed heat transfer surfaces. A shallow bed offers a lower bed resistance and hence a lower pressure drop and lower fan power consumption. In the case of deep bed, the pressure drop is more and this increases the effective gas velocity and also the fan power.

In-Bed Heat Transfer Surface

In a fluidized in-bed heat transfer process, it is necessary to transfer heat between the bed material and an immersed surface, which could be that of a tube bundle, or a coil. The heat exchanger orientation can be horizontal, vertical or inclined. From a pressure drop point of view, a horizontal bundle in a shallow bed is more attractive than a vertical bundle in a deep bed. Also, the heat transfer in the bed depends on number of parameters

like (i) bed pressure (ii) bed temperature (iii) superficial gas velocity (iv) particle size (v) Heat exchanger design and (vi) gas distributor plate design.

Ash Handling System

Bottom ash removal

In the FBC boilers, the bottom ash constitutes roughly 30 - 40 % of the total ash, the rest being the fly ash. The bed ash is removed by continuous over flow to maintain bed height and also by intermittent flow from the bottom to remove over size particles, avoid accumulation and consequent de-fluidization. While firing high ash coal such as washery rejects, the bed ash overflow drain quantity is considerable so special care has to be taken.

Fly ash removal

The amount of fly ash to be handled in FBC boiler is relatively very high, when compared to conventional boilers. This is due to elutriation of particles at high velocities. Fly ash carried away by the flue gas is removed in number of stages; firstly in convection section, then from the bottom of air pre-heater/economizer and finally a major portion is removed in dust collectors.

The types of dust collectors used are cyclone, bag-filters, electrostatic precipitators (ESP's) or some combination of all of these. To increase the combustion efficiency, recycling of fly ash is practiced in some of the units.

1.3.2 Circulating Fluidized Bed Combustion (CFBC)

Circulating Fluidized Bed Combustion (CFBC) technology has evolved from conventional bubbling bed combustion as a means to overcome some of the drawbacks associated with conventional bubbling bed combustion (see Figure 6.5). This CFBC technology utilizes the fluidized bed principle in which crushed (6 –12 mm size) fuel and limestone are injected into the furnace or combustor. The particles are suspended in a stream of upwardly flowing air (60-70% of the total air), which enters the bottom of the furnace through air distribution nozzles. The fluidizing velocity in circulating beds ranges from 3.7 to 9 m/sec. The balance of combustion air is admitted above the bottom of the furnace as secondary air. The combustion takes place at 840-900 ^{o}C, and the fine particles

(<450 microns) are elutriated out of the furnace with flue gas velocity of 4-6 m/s. The particles are then collected by the solids separators and circulated back into the furnace. Solid recycle is about 50 to 100 kg per kg of fuel burnt.

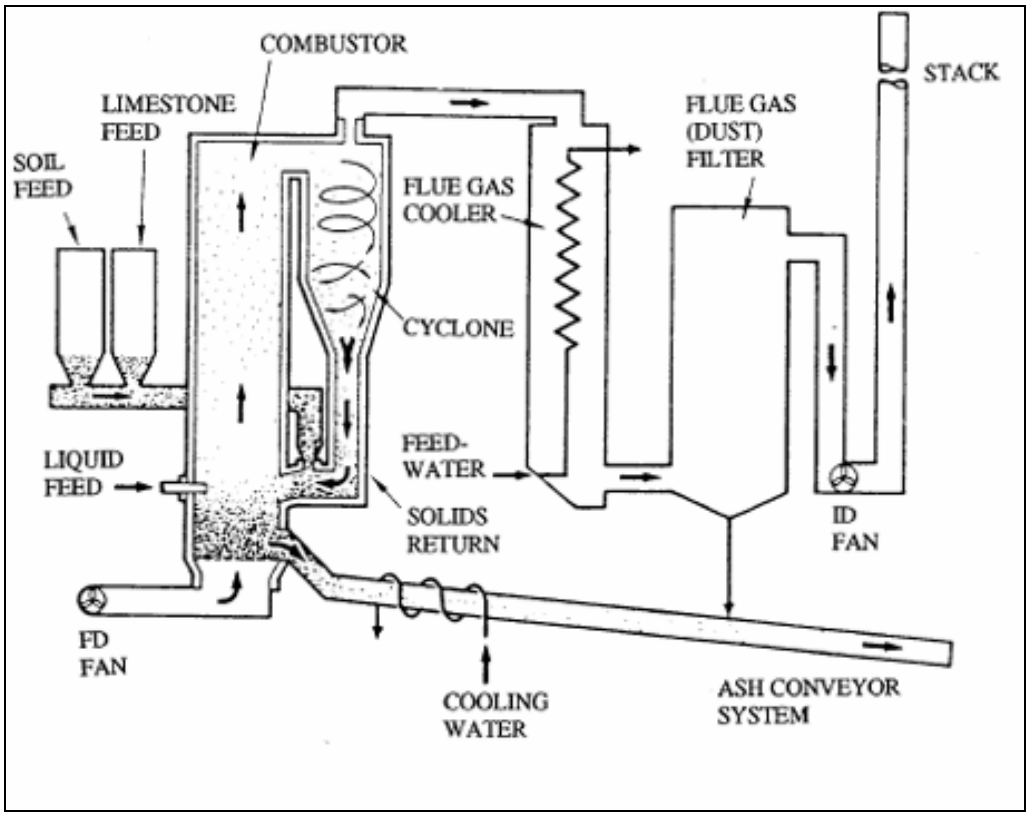

Figure 1.8: Schematic diagram of CFBC

There are no steam generation tubes immersed in the bed. The circulating bed is designed to move a lot more solids out of the furnace area and to achieve most of the heat transfer outside the combustion zone - convection section, water walls, and at the exit of the riser. Some circulating bed units even have external heat exchanges.

The particles circulation provides efficient heat transfer to the furnace walls and longer residence time for carbon and limestone utilization. Similar to Pulverized Coal (PC) firing, the controlling parameters in the CFB combustion process are temperature, residence time and turbulence. For large units, the taller furnace characteristics of CFBC boiler offers better space utilization, greater fuel particle and sorbent residence time for

efficient combustion and SO_2 capture, and easier application of staged combustion techniques for NOx control than AFBC generators. CFBC boilers are said to achieve better calcium to sulphur utilization – 1.5 to 1 vs. 3.2 to 1 for the AFBC boilers, although the furnace temperatures are almost the same. CFBC boilers are generally claimed to be more economical than AFBC boilers for industrial application requiring more than 75 – 100 t/hr of steam. However, CFBC requires huge mechanical cyclones to capture and recycle the large amount of bed material, which requires a tall boiler.

A CFBC could be good choice if the following conditions are met.

- Capacity of boiler is large to medium
- Sulphur emission and NOx control is important
- The boiler is required to fire low-grade fuel or fuel with highly fluctuating fuel quality.

Major performance features of the circulating bed system are as follows:

a) It has a high processing capacity because of the high gas velocity through the system.

b) The temperature of about 870°C is reasonably constant throughout the process because of the high turbulence and circulation of solids. The low combustion temperature also results in minimal NOx formation.

c) Sulfur present in the fuel is retained in the circulating solids in the form of calcium sulphate and removed in solid form. The use of limestone or dolomite sorbents allows a higher sulfur retention rate, and limestone requirements have been demonstrated to be substantially less than with bubbling bed combustor.

d) The combustion air is supplied at 1.5 to 2 psig rather than 3-5 psig as required by bubbling bed combustors.

e) It has high combustion efficiency.

f) It has a better turndown ratio than bubbling bed systems.

g) Erosion of the heat transfer surface in the combustion chamber is reduced, since the surface is parallel to the flow. In a bubbling bed system, the surface generally is perpendicular to the flow.

1.3.3 Pressurized Fluidized Bed Combustion (PFBC)

Pressurized Fluidized Bed Combustion (PFBC) is a variation of fluid bed technology that is meant for large-scale coal burning applications. In PFBC, the bed vessel is operated at pressure up to 16 kg/cm^2. The off-gas from the fluidized bed combustor drives the gas turbine. The steam turbine is driven by steam raised in tubes immersed in the fluidized bed. The condensate from the steam turbine is pre-heated using waste heat from gas turbine exhaust and is then taken as feed water for steam generation.

The PFBC system can be used for cogeneration or combined cycle power generation. By combining the gas and steam turbines in this way, electricity is generated more efficiently than in conventional system. The overall conversion efficiency is higher by 5% to 8%. (Refer Figure 6.6).

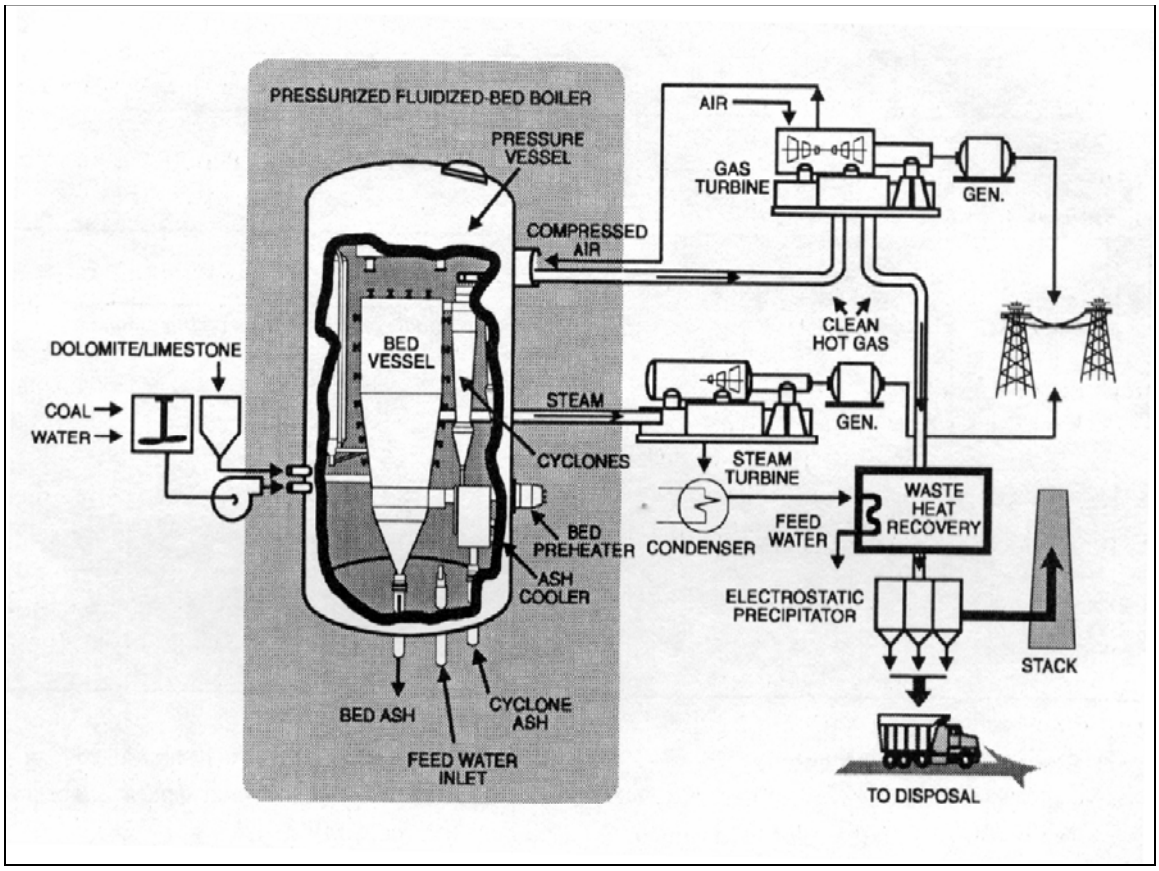

Figure 1.9: Schematic representation of PFBC

1.4 Advantages of Fluidized Bed Combustion Boilers

1. High Efficiency

FBC boilers can burn fuel with a combustion efficiency of over 95% irrespective of ash content. FBC boilers can operate with overall efficiency of 84% (plus or minus 2%).

2. Reduction in Boiler Size

The high heat transfer rate over a small heat transfer area immersed in the bed result in overall size reduction of the boiler.

3. Fuel Flexibility

FBC boilers can be operated efficiently with a variety of fuels. Even fuels like flotation slimes, washery rejects, agri waste can be burnt efficiently. These can be fed either independently or in combination with coal into the same furnace.

4. Ability to Burn Low Grade Fuel

FBC boilers would give the rated output even with inferior quality fuel. The boilers can fire coals with ash content as high as 62% and having calorific value as low as 2,500 kcal/kg. Even carbon content of only 1% by weight can sustain the fluidised bed combustion.

5. Ability to Burn Fines

Coal containing fines below 6 mm can be burnt efficiently in FBC boiler, which is very difficult to achieve in conventional firing system.

6. Pollution Control

SO_2 formation can be greatly minimized by addition of limestone or dolomite for high sulphur coals. 3% limestone is required for every 1% sulphur in the coal feed. Low combustion temperature eliminates NO_x formation.

7. Low Corrosion and Erosion

The corrosion and erosion effects are less due to lower combustion temperature, softness of ash and low particle velocity (of the order of 1 m/sec).

8. Easier Ash Removal – No Clinker Formation

Since the temperature of the furnace is in the range of 750 – 900 ^{o}C in FBC boilers, even coal of low ash fusion temperature can be burnt without clinker formation. Ash removal is easier as the ash flows like liquid from the combustion chamber. Hence less manpower is required for ash handling.

9. Less Excess Air – Higher CO_2 in Flue Gas

The CO_2 in the flue gases will be of the order of 14 – 15% at full load. Hence, the FBC boiler can operate at low excess air - only 20 – 25%.

10. Simple Operation, Quick Start-Up

High turbulence of the bed facilitates quick start up and shut down. Full automation of start up and operation using reliable equipment is possible.

11. Fast Response to Load Fluctuations

Inherent high thermal storage characteristics can easily absorb fluctuation in fuel feed

rates. Response to changing load is comparable to that of oil fired boilers.

12. No Slagging in the Furnace-No Soot Blowing

In FBC boilers, volatilisation of alkali components in ash does not take place and the ash is non sticky. This means that there is no slagging or soot blowing.

13 Provisions of Automatic Coal and Ash Handling System

Automatic systems for coal and ash handling can be incorporated, making the plant easy to operate comparable to oil or gas fired installation.

14 Provision of Automatic Ignition System

Control systems using micro-processors and automatic ignition equipment give excellent control with minimum manual supervision.

15 High Reliability

The absence of moving parts in the combustion zone results in a high degree of reliability and low maintenance costs.

16 Reduced Maintenance

Routine overhauls are infrequent and high efficiency is maintained for long periods.

17 Quick Responses to Changing Demand

A fluidized bed combustor can respond to changing heat demands more easily than stoker fired systems. This makes it very suitable for applications such as thermal fluid heaters, which require rapid responses.

18 High Efficiency of Power Generation

By operating the fluidized bed at elevated pressure, it can be used to generate hot pressurized gases to power a gas turbine**.** This can be combined with a conventional steam turbine to improve the efficiency of electricity generation and give a potential fuel savings of at least 4%.

CHAPTER 2

Literature Review

2.1 Significance of mathematical modeling

Making use of commercial fluidized bed processes to recover energy from waste or biomass is becoming more and more frequent; as a result, need for models simulating commercial equipment is becoming urgent. Models differ from one another in the context of hypothesis about devolatilization, elutriation of fine particles etc.

While it may be rewarding to arrive at viable conclusion for a specific problem, it is more rewarding to develop a scheme that provides insight into otherwise a complex process. The importance of mathematical modeling in our modern world is well appreciated and it has helped to alter the landscape of curricula at both the graduate and under graduate levels. An important feature of modeling is that it has brought the rigor and analysis of mathematics to the doorstep of our fellow scientists in the natural and physical sciences. The importance of mathematical modeling in this context is that it helps in deciding the optimum values for the operating parameters, which result in an efficient operation of the fluidized bed system.

2.2 Description of some popular models

In the past a lot of work has been done on mathematical modeling of fluidized bed combustion, using different fuels, but when we talk about fluidized bed combustion using rice husk, not many people have done research in this area. Given below are some popular models related to the mathematical modeling of fluidized bed combustors, which can be used for the development of mathematical model for fluidized bed combustor using rice husk.

Mihalyko et al. [23] presented a mathematical model for particle-to-particle heat transfer in gas-solid systems. In developing the model, simple kinetic equations were assumed to describe the inter-particle heat transfer process, and the particle-particle interactions were considered stochastic. A stochastic approach was used to derive the population balance

equation describing the variation of density function of temperature distribution of the particulate phase. The moment equations and numerical solution of the partial integro-differential equation of the population balance model were derived and used to analyze the behavior of a batch gas-solid system. The results, as shown in Figures 2.1, 2.2, indicated that the population balance approach, used for developing the model describing the inter-particle contact heat conduction during collision was capable to take into account a number of parameters affecting the process & can be applied also for predicting heat transfer in gas-solid processing systems.

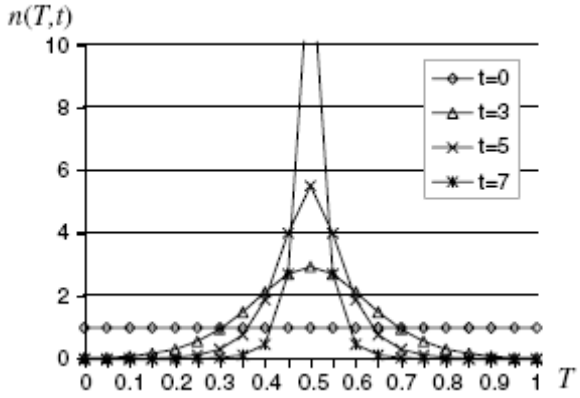

Figure 2.1: Population density function at different moments of time

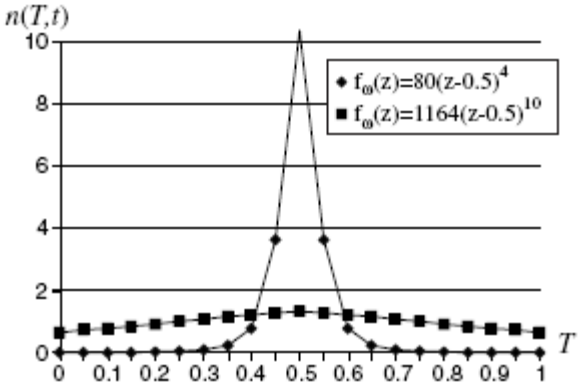

Figure 2.2: Comparision of two population density function

Grosso et al. [10] analyzed particle size distributions in the output stream of commercial, fluidized-bed reactors for ethylene polymerization using a mathematical model. They also studied the impact on the overall reactor performance of the universe of sizes for the

particles in the bed. For the output stream, product size distribution was modeled using triangular and generalized gamma functions. They employed extraction system parameters to model the particle quantity and sizes. From the results they concluded that it would be appropriate to include both product and bed particle diameter distribution when studying the rector performance.

Mancuhan Ebru [19] developed a computerized model for any low rank coal with a known particle size distribution and mass fraction. When the coal is fed into the bed, the volatile matter was assumed to be released instantaneously and a new particle size distribution was achieved within the bed. The effect of elutriation and chemical reactions were also taken into account. It considered the particle size distribution of the semi-coke and the mass fraction values within the bed at steady-state conditions (BSSC), effect of the excess air on elutriation and the particle size distribution both in the bed and the freeboard. Model developed investigated the effect of volatile matter on bed temperature, effect of coal properties on bed temperature (as sown in Fig. 2.3, 2.4 & 2.5), excess air on elutriation, particle size distribution of the semi-coke and the mass fraction values within the bed at steady state conditions. The excess air ranged from 1 to 1.48. It also took into account, the effect of coal type on the bed temperature. The results of the model simulation studies were compared with a limited amount of experimental work available for Turkish lignites and the agreement between the model prediction and the experimental data was reasonably good. Closer to distributor plate the bed temperature prediction of the model was low, but agreement improved as the active bed surface was reached.

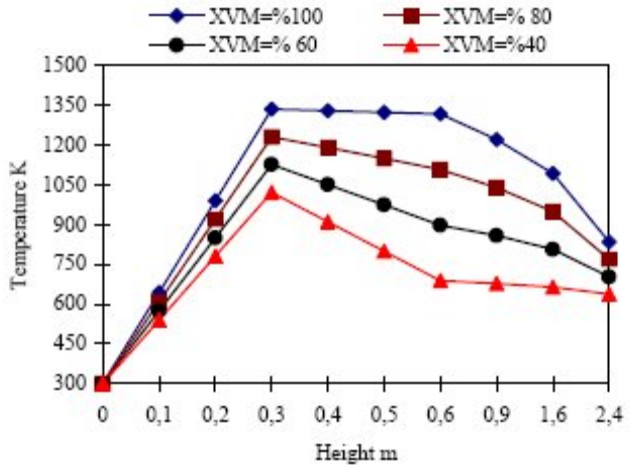

Figure 2.3: Effect of volatile matter on bed temperature

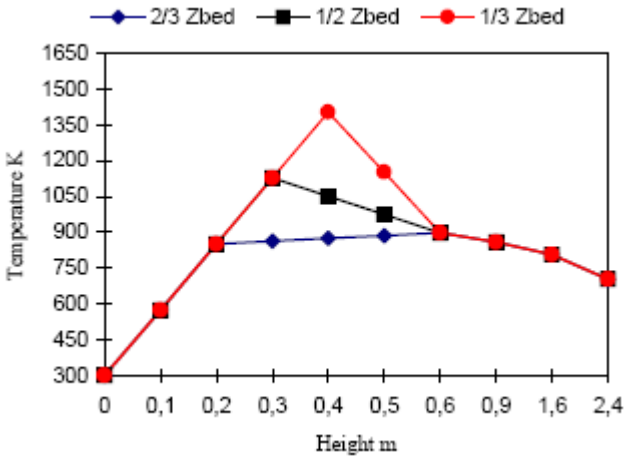

Figure 2.4: Effect of the position of heat transfer on bed temperature

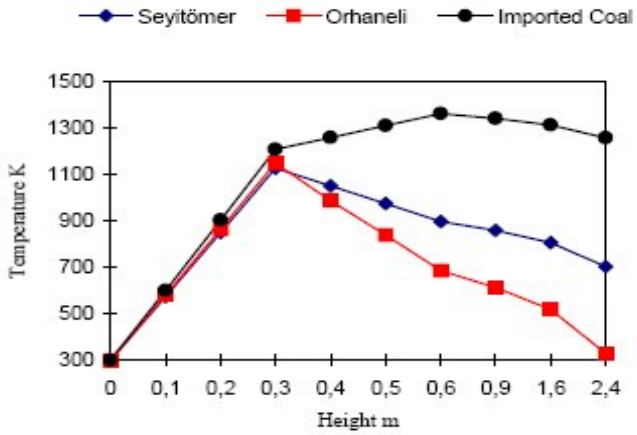

Figure 2.5: Effect of coal properties on bed temperature

Choi et al. [4] determined the particle entrainment rate and the size distribution of entrained particles in two large-scale fluidized bed combustors and a cold model fluidized bed. For which they developed a model to predict the particle entrainment rate in which the vertical velocity distribution of entrained solids at the bed surface was considered. They concluded that the entrainment rate increases with increase in gas velocity and coal feed rate and the effect of gas velocity on the entrainment rate is less pronounced in the combustor than in the cold model fluidized bed. However the vertical velocity of entrained particles at the bed surface of the combustors is higher than that in the cold model fluidized bed.

Janvijitsakul et al. [11] in their work, co-fired rice husk and bagasse in a cone-shaped fluidized bed combustor with the aim of effective and environmentally friendly utilization of the biomass fuels. Temperature and volume gas concentrations (O_2, CO and NO) were measured at different location points along the combustor height. The axial temperature profiles were found to be almost independent of excess air and strongly affected by the rice husk energy fraction i.e. contribution by rice husk to the heat input when rice husk and bagasse co-firing. The CO emissions in the flue gas leaving the combustor were found to reduce for higher values of Excess air and Energy fraction of rice husk. They concluded that co-firing of rice husk and begasse lead to higher combustion efficiency at reduced environmental impacts compared with those in the case of firing rice husk only as shown in Figure 2.5 & 2.6. The table 2.1 gives the detail of proximate and ultimate analysis of rice husk and bagasse.

Analysis	Rice husk	Bagasse
Ultimate analysis (wt.%, "dry and ash-free" basis):		
Carbon	44.99	42.64
Hydrogen	6.39	6.62
Oxygen	48.15	50.48
Nitrogen	0.42	0.19
Sulfur	0.05	0.07
Proximate analysis (wt.%):		
Moisture ("as-received" basis)	11.0	48.8
Ash ("dry" basis)	14.16	2.15
LHV (MJ/kg)	12.34	6.68

Table 2.1: Proximate & Ultimate analysis of rice husk & bagasse

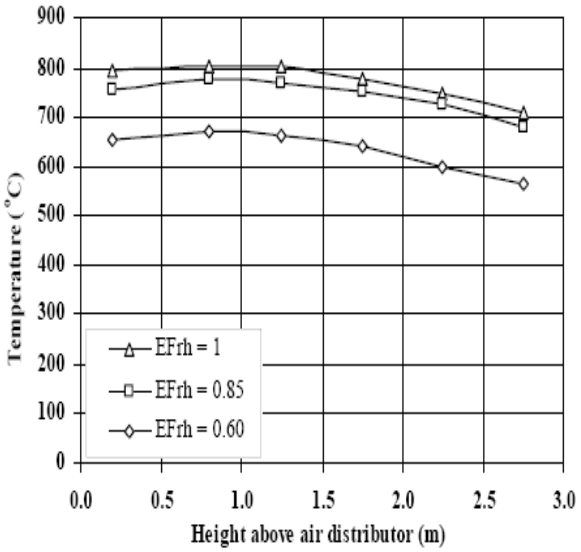

Figure 2.6: Effect of rice husk energy Fraction on temperature

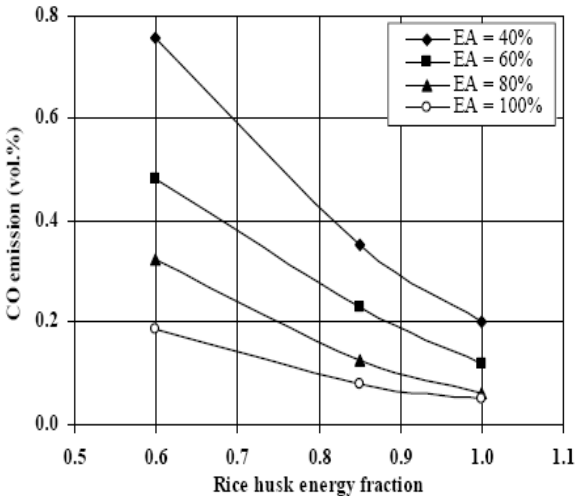

Figure 2.7: CO emissions for various excess air fractions

Kim et al. [14] examined the heat and mass transfer characteristics in three-phase fluidized beds to provide prerequisite knowledge for reactor design. The effects of gas and liquid velocities, solid and liquid properties on the heat and mass transfer coefficients

in three-phase fluidized beds were determined. The various correlation and models to predict the heat and transfer coefficients in the literature had been examined and the unified correlations based on the concepts of surface renewal theory and energy dissipation rate in the beds had been proposed. The analogy between the heat and the mass transfer in three-phase fluidized beds were discussed. They also recommended the areas wherein future research should undertake to improve the state of the present knowledge.

Garbett et al. [9] studied the influence of particle size distribution on the combustion rates in a batch fed fluidized bed. The model which they employed was the two-phase bubbling bed model of Avedesian and Davidson where a bed of inert particles at temperature Tb is fluidized by air at a superficial velocity Uo and a minimum fluidized velocity Umf. The model predicted the change in size distribution during burnaway, burn-out times and particulate phase oxygen concentrations as a function of original particle size distribution in a batch fed fluidized bed. They also concluded that if the original size distribution is accurately known, a batch fed experiment could be devised to determine the role of the chemical kinetics for a given type of coal and would thus be an aid to modeling of fluidized bed combustion.

Chang et al. [3] studied mass transfer in two and three phase fluidized beds. They used a 6.64 cm I.D and 1.8 m high Plexigas column to determine mass transfer characteristics of gas-solid and gas-liquid-solid fluidized beds in terms of gas-liquid mass transfer coefficient and interfacial area. The effects of liquid velocity, gas velocity, liquid-phase ionic strength and particle size on mass transfer and the interfacial area were determined. The volumetric mass transfer coefficient, k_L, and the gas/liquid interfacial area, A, increased with increasing gas velocity, particle size and liquid phase ionic strength in three-phase fluidized beds. They concluded that the liquid side mass transfer coefficient can be correlated in terns of Sherwood number with Schmidt and modified Reynolds number based on isotropic turbulence theory.

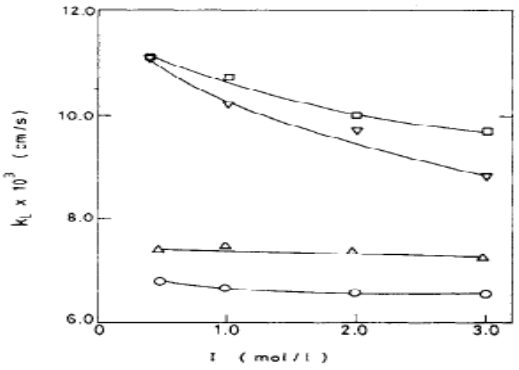

Figure 2.8: Effect of I on k_L in three phase fluidized beds

Niu et al. [27] studied fluidization of particles with supercritical carbon dioxide. They investigated and concluded that nearly spherical glass and amberlite particles ranging in size from 0.18 to 1.0 mm can be successfully fluidized by supercritical carbon dioxide and the bed expansion has weak temperature and pressure dependences due to counteracting effects of the density and viscosity variations of supercritical carbon dioxide. For a given packing material the length of the expanded bed varies exponentially with CO_2 mass flow rate. This is attributed to opposing effects of density and viscosity changes of the fluidizing medium on the bed expansion. The minimum fluidization velocity values measured experimentally were consistent with the correlations, from which they proved that conventional correlations may be used for designing CO_2 based fluidization processes.

Rawlings et al. [31] in their paper provide an overview of modeling measurement and control issues arising in systems modeled by population balances. The population balance, according to them, is a partial differential equation describing the dynamics of some particle size distribution. They conclude that the general population balance modeling framework very successfully describes the dynamic and overall reactor properties for a variety of chemical systems.

Khan et al. [13] presented a model of 10 MW atmospheric bubbling fluidized combustor burning waste wood fuel. The model incorporates both the solid and gas phases. The bed

is assumed to consist of two phases, of which the emulsion phase takes both gas and solids in to account, while the bubble phase consists only of gas. A wide size distribution of biomass feed has been assumed. The model calculates the gas composition, velocities and other hydrodynamic parameters in both the emulsion and bubble phase as shown in figure 2.9, 2.10 and 2.11. They included a particle size distribution model to calculate elutriation losses of fine char particles. Their approach took into consideration devolatilization, fragmentation, and attrition of the solid phase along with gaseous profiles.

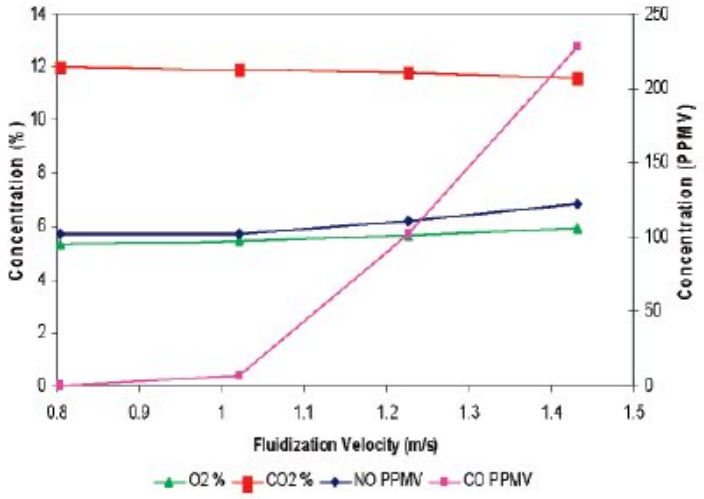

Figure 2.9: Effect of fluidization velocity on gaseous emissions

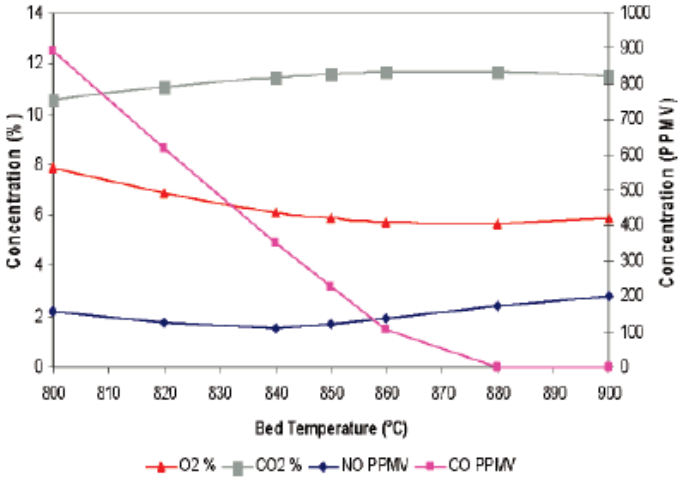

Figure 2.10: Effect of temperature on gaseous emissions

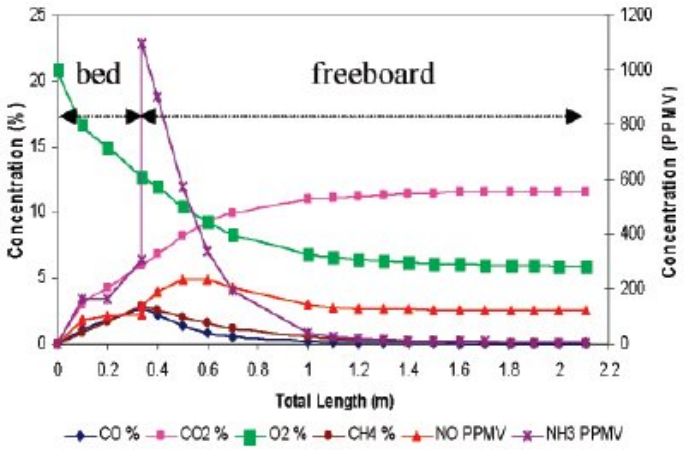

Figure 2.11: Predicted species concentration along the boiler length

Muthukrishnan et al. [25] in their paper gave valuable insight into the world's first rice straw fired fluidized bed boiler in a 10 MW power plant. Bases on the analysis of the observations of the plant, they proposed some modifications such as increasing the quantity of secondary air to about 30% of the total air which further assisted in release and completion of combustion of volatile and char in the immediate vicinity of the bed; in order to ensure proper fluidization, the bed particle diameter was reduced to 1.5mm from 3mm; a pneumatic feeding system was designed so that limestone could be continuously added into the fluidized bed. The major conclusion given by the authors is that though rice straw is a low density fuel and warrants handling in huge volume but by unique handling, transportation it can be used as a fuel for a power plant and by proper adoption the system can be easily scaled up for larger capacities.

Skrifvars et al. [34] have done research in the thermal behavior of the fuel ash components in the furnace and the flue gases. For this they employed a method that was a combination of advanced fuel analysis technique "chemical fractionation analysis" and thermodynamic phase equilibrium calculations. The main aim of the research being, the ease for estimating the behavior of any new fuels or fuel mixtures in advance before trying them in full-scale unit, as burning a great variety of fuels is one of the key advantage of the fluidized bed combustion technology. To evaluate the predictions arrived at by above technique, they compared some selected results with two multi-fuel

fired fluidized boilers and concluded that advanced fuel analysis in combination with a thermodynamic model for description of the main chemical conversions in the FBC furnace opens promising pathways for improved predictions of the fuel ash behavior.

Yagi and Kunni [38] made the first attempt to model a fluid bed combustor in **1955**. They derived equations for the combustion of a single carbon particle of a fixed size, as well as for a particle which is shrinking due to reaction, taking into account the intermediate diffusion and chemical reaction. Assuming single phase theory, they formulated an expression for solids population balance and carbon load in the bed. The proposed theory was tested and compared with the combustion of coke particles in laboratory scale combustor with reasonable accuracy. Though the model received widespread consideration in fluidized bed combustor models, it has following limitations:

(i) Only an isothermal bed is considered.

(ii) No consideration was given to the existence of a dilute phase.

(iii) Single carbon particle of fixed size was considered.

(iv) Only the simplest kinetic behavior, namely, the direct formation of carbon dioxide from carbon and oxygen was considered.

(v) No validation with data from industrial fluidized bed combustor was made.

Ohamn et al. [28] studied the bed agglomeration characteristics during burning of biomass fuels. The in-bed behavior of ash-forming elements in fluidized bed combustion of different biomass fuels was examined by analysis of the samples collected during controlled agglomeration test runs. Eight fuels were chose for the test. The bench scale reactor bed samples were finally compared with bed samples collected from biomass-fired full-scale fluidized bed boilers. In all the analyzed samples, the bed particles were coated with a relatively homogenous ash layer. The results indicated that the partial melting of the coating of the bed particles was directly responsible for the agglomeration.

Degirmenci et al. [5] presented a comprehensive model for continuous combustion of lignite with wide size distribution burning in its own ash in an atmospheric bubbling

fluidized bed combustor (AFBC) and used it to correlate the data from a 0.3 MW AFBC test rig. The model consists of submodels for hydrodynamics, volatile release and combustion, char combustion, particle size distribution, entrainment and elutriation and is based on conservation equations for energy and chemical species. The volatile release model is based on a particle movement model for estimation of portion of volatiles released in bed and a devolatilization kinetics model described by the distributed activation energy model for determination of time-resolved devolatilization profile of lignite particles. Predictions of the model were compared with measured concentration and temperature profiles and good agreement was obtained.

Ngampradit et al. [26] developed a rigorous mathematical model to predict the proper amount of mixed fuel and to reduce the emission from coal burning. The model was divided into three parts: reaction, hydrodynamic, and gas emission. In the first part, the reactions in the combustor were represented by a continuous stirred tank reactor module. The module was modified by adding the shrinking core model for calculating the size and weight fraction of particles in each region. In the second part, the hydrodynamic in CFBC were divided into two regions: a lower region with one interval and an upper region with three intervals. In each region the characteristics, such as the height of the bed, void, and the volume were calculated. In third part, gas emission models were used to calculate the kinetic rates of NO, N_2O and the conversion of SO_2 to predict the emission to the environment.

Mansaray et al. [20] validated the two compartment model developed for fluidized bed gasification of biomass. The fluidized bed was operated on rice husk at various bed heights (19.5, 25.5, 31.5 cm), fluidization velocities (0.22, 0.28, 0.33 m/s) and equivalence ratios (0.25, 0.30, 0.35). The model gave reasonable predictions of the core, annulus and the exit temperatures. The corresponding data given in Table 3.1 was analyzed to verify the model predictions.

Bed height (cm)	Fluidization Velocity(m/s)	Equivalence Ratio	Core Temperature (°C)	Annulus Temperature (°C)	Exit Temperature (°C)
19.5	0.22	0.25	703	703	623
		0.30	796	800	710
		0.35	845	852	793
	0.28	0.25	723	726	683
		0.30	816	822	779
		0.35	871	877	846
	0.33	0.25	742	745	713
		0.30	830	834	795
		0.35	876	882	856
25.5	0.22	0.35	691	693	616
		0.30	774	777	709
		0.35	837	842	775
	0.28	0.25	716	718	681
		0.30	800	803	765
		0.35	850	852	810
	0.33	0.25	722	721	696
		0.30	819	820	786
		0.35	851	853	815
31.5	0.22	0.25	662	666	607
		0.30	742	744	692
		0.35	809	812	748
	0.28	0.25	670	670	641
		0.30	747	753	714
		0.35	819	822	782
	0.33	0.25	698	700	675
		0.30	764	767	734

Table 2.2: Temperature readings in the gasifier

Loffler et al. [18] had developed chemical kinetic modeling of a single fuel particle in a laboratory-scale fluidized bed. NOx and N_2O are known as harmful pollutants. In FBC these are formed from the nitrogen in the fuel. To develop effective primary measures reducing the emissions, more knowledge on the mechanism of formation and destruction ongoing in fluidized beds has to be obtained. In this work, a detailed chemistry model is combined with a two phase model for a stationary fluidized bed to calculate the emissions of the single fuel particle in a laboratory-scale stationary fluidized bed. The single particle model consists of a simple model for the H_2O release during drying, a model for the volatiles composition, and a model for the nitrogen chemistry during char combustion. The related reaction mechanism consists of the homogeneous part, heterogeneously catalyzed reactions on the bed material, and the radical recombination reactions on the solids surface. The results confirm that devolatilization, and char combustion are of nearly equal importance for NO and N_2O formation. During devolatilization, NO is formed from HCN and NH_3, while N_2O is formed almost exclusively from HCN. During char combustion, NO is mostly formed by heterogeneous oxidation of HCN. On the other hand, there is also a back coupling of NO on the homogeneous burnout of the carbon containing species, by sensitizing the oxidation of CH_4.

Faravelli et al. [7] modeled homogeneous combustion in bubbling beds burning liquid fuels. They introduces a model for the description of the homogeneous combustion of various fuels in fluidized bed combustors (FBC) at temperatures lower than the classical value for solid fuels, i.e., 850°C. The model construction is based on a key bubbling fluidized bed feature: A fuel-rich (endogenous) bubble is generated at the fuel injection point, travels inside the bed at constant pressure, and undergoes chemical conversion in the presence of mass transfer with the emulsion phase and of coalescence with air (exogenous) bubbles formed at the distributor and, possibly, with other endogenous bubbles. The model couples a fluid-dynamic submodel based on two-phase fluidization theory with a submodel of gas phase oxidation. To this end, the model development takes full advantage of a detailed chemical kinetic scheme, which includes both the low and high temperature mechanisms of hydrocarbon oxidation, and accounts for about 200

molecular and radical species involved in more than 5000 reactions. Simple hypotheses are made to set up and close mass balances for the various species as well as enthalpy balances in the bed. First, the conversion and oxidation of gaseous fuels (e.g., methane) were calculated as a test case for the model; then, n-dodecane was taken into consideration to give a simple representation of diesel fuel using a pure hydrocarbon. The model predictions qualitatively agree with some of the evidence from the experimental data reported in the literature. The fate of hydrocarbon species is extremely sensitive to temperature change and oxygen availability in the rising bubble. A preliminary model validation was attempted with results of experiments carried out on a pre-pilot, bubbling combustor fired by under-bed injection of a diesel fuel. Specifically, the model results confirm that heat release both in the bed and in the freeboard is a function of bed temperature. At lower emulsion phase temperatures many combustible species leave the bed unburned, while post-combustion occurs after the bed and freeboard temperature considerably increases. This is a well-recognized undesirable feature from the viewpoint of practical application and emission control.

Delebarre et al. [6] worked on the phenomenon that the minimum fluidization does exist or not. This work proposes an equation giving the pressure drop of a gas flowing through a porous medium or a granular bed. The consequences for the onset of the fluidization are then discussed. It appears that the notion of minimum gas mass-flow rate would improve the description of the transition between fixed and fluidized bed regimes. An equation is then proposed to calculate the minimum fluidization gas mass-flow rate. It is then proved that the minimum fluidization is not only a function of the medium and fluid characteristics but also that it increases with bed inventory. It is then shown that a batch of particles has a minimum fluidization depending on its arrangement in a column and that in some cases, this minimum does not exist at all. As a consequence, the minimum of fluidization, whether it is a velocity or a mass flow rate, cannot be considered as a criterion to characterize a powder.

Jiang et al. [12] designed a novel fluidized bed gasifier in which rice husk was fluidized and gasified without inert additives. The gas compositions were determined by an online

analyzer and gas chromatography. The results showed that low fluidized velocity and low gasification temperature (550-650°C) were beneficial to the production of syngas with a high composition of CO. The composition of H_2 was influenced slightly by the equivalent ratio. The average composition of H_2 was almost unchangeable to different fluidized velocities. The minimum fluidization velocity U_{mf} of rice husk without inert additives experimentally determined was 0.495 m/s, which was higher than that of two-component system containing rice husk and sand. The throughput of rice husk in the reactor was higher than that in a fixed bed with same volume.

Subramani et al. [35] in their paper addressed the determination of minimum fluidization velocities at elevated temperatures for Geldart's group B-powders. New experiments were carried out to obtain bed porosity and air velocity at incipient fluidization over a wide range of temperatures between 298 K and 973 K using ilmenite, sand, limestone and quartz magnetite of varying sizes. A relatively simple linear empirical correlation between Reynolds number and Archimedes number were developed to predict minimum fluidization velocity at high temperatures. The predicted values were in good agreement with the new experimental results and already existing data in open literature within an error of ±15%.

Liu Huie et al. [17] devised a method for fluidization quality improvement for cohesive particles by a dry coating method. In this method a fine powder was used to improve the fluidization quality for cornstarch particles, belonging to Geldart's C group, which can not fluidize normally. Two kinds of SiO_2 fine powders are used to coat cornstarch particles. Both a conventional fluidized bed and a magnetic fluidized bed were employed for coating the cornstarch particles. The coated particles were observed via the scanning electron microscope (SEM) images. Furthermore, the fluidization behaviors pf the coated particles were investigated. The results showed that the coating with fine SiO_2 powder is an effective method to improve the fluidization quality of cohesive particles. However, no significant difference in fluidization quality was observed between particles coated in a conventional fluidized bed and those coated in a MFB.

Ahmadzadeh et al. [1] expressed in their paper that to enhance the efficiency of fluidized-bed reactors, there must be more flexibility in controlling the residence time of particles of different sizes, particularly very fine particles. To achieve this goal, they studied gas and particle flow patterns in a vertical rotating fluidized bed. They limited the study to the quasi-three dimensional simulation of an isothermal RFB with constant particle size and no chemical reaction to examine the predictability of a computational fluid dynamics approach to the analysis of RFB systems. Simulation results showed that the particle residence time distribution could be controlled by the manipulation of rotational speed and inlet gas velocity.

Ramirez et al. [29] designed a fluidized bed gasifier for rice husk and developed it on a pilot scale. The gasifier equipment, made up of a reaction chamber of 0.3 m of internal diameter and 3 m of overall height, was designed by them, from theoretical and experimental information available in the literature and their past research experience. A design procedure was elaborated for each one of the seven parts or sub-systems in which the gasifier equipment was divided. Experimental tests performed with the gasifier fabricated according to the designs showed that the developed procedure was adequate.

CHAPTER 3

Plant details

Malwa power limited, Muktsar, a 7.5 MW FBC based power plant is the plant from which the data for the present work was collected. It is located in the south-western district of Punjab, named Muktsar. This area of Punjab is popularly called cotton belt of Punjab. As the soil is quite conducive for cotton, so the farmers of south-western Punjab prefer growing cotton. Above all, many farmers grow cotton twice a year.

A large amount of cotton waste is left in the fields after the cotton has been harvested from the plants. This waste is called 'cotton stalk' and has a height varying from 3 feet to 5 feet. Cotton stalk is quite rich in carbon content. Traditionally, this was used for domestic cooking and water heating purposes which caused a lot of pollution.

Malwa power plant was setup in 2005; primarily it is based upon the combustion of cotton stalk. The plant collects the cotton stalk directly from the farmers and stores it in the vast land area acquired by it.

Some important parameters of the plant as given below:

1. Capacity: 7.5MW
2. Auxilliary consumption: 11.5%
3. Type of bed: AFBC
4. Bed temperature: 750-800°C
5. Bed cross-sectional area: 19.43 sq. metres
6. Distribution plate: Nozzle type
7. Bed material: 50% alumina
8. Fuel used: Cotton stalk
9. Fly-ash collector: ESP
10. Fuel feed rate: 10 tonne/hr
11. Steam temperature: 475°C
12. Exit gas temperature: 150°C
13. Feed water temperature: 100°C
14. Steam production rate: 34 tonne/hr

3.1 Process flow:

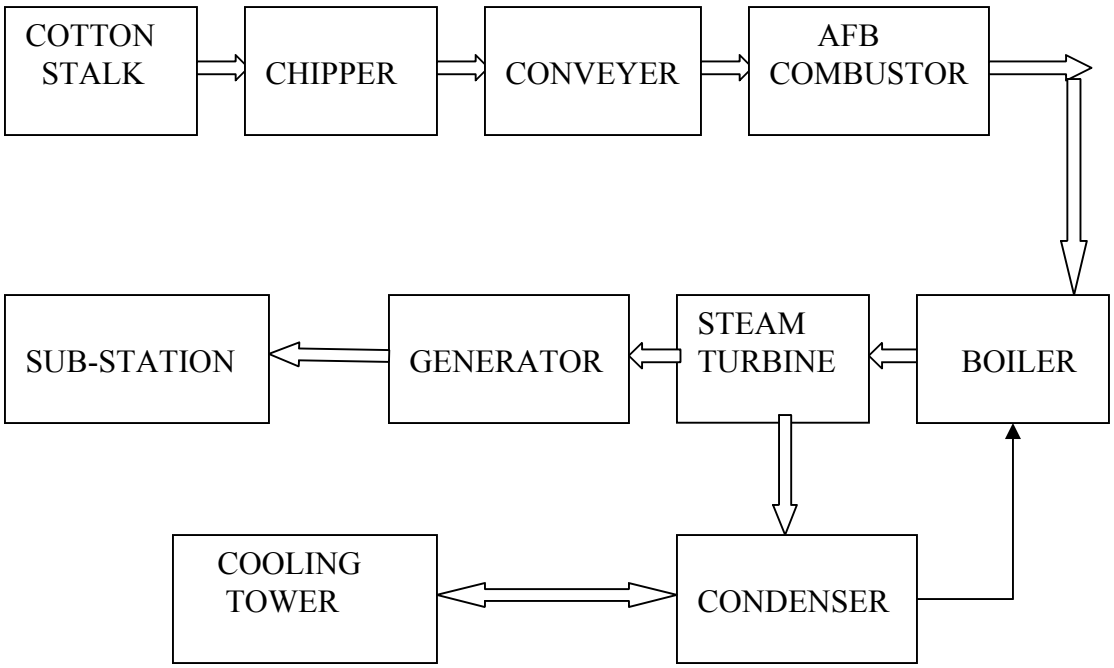

Figure 3.1: Process flow of the power plant

First of all the collected and stored cotton stalk is passed through a wood chipper for breaking the stalk into appropriate size for the combustor. The usual size to which the stalk is cut, is around 2.5 cm to 4 cm. Then the chipped material is moved with the help of semi-automatic trucks and heaps of it are prepared. The chipped fuel is manually loaded onto a belt conveyor. The belt conveyor drops the material into two compartments fitted with screw feeders, which then supply the fuel to the fluidized bed combustor. Before running the combustor on cotton stalk, it is fired with the help oil and coal. When the combustor reaches a temperature of around 700°C, then the cotton stalk is continuously supplied.

The boiler is supplied with the filtered and treated water from water treatment plant. Superheated steam at temperature of 475°C and around 67 bar pressure is produced in the boiler and is stored in the steam drum before passing on to the turbine. The turbine

is coupled with the generator, which produces power. The generated power is stepped up, synchronized and is transmitted to the nearest 32KV sub-station of the electricity board.

3.2 Salient features of the plant

3.2.1 Air and flue gas circuit

The combustion air is provided by a forced draught (FD) fan. This air, before being passed on to the combustion chamber, is first heated up, by passing it through an air pre-heater. Some portion of forced draught fan outlet air is further pressurized by secondary air fan. This air is used to carry the fuel particles into combustion chamber. The flue gas produced due to the combustion of fuel in water cooled combustion chamber is at 650°C. The flue gas gets cooled to 150°C while passing through water wall tubes, super-heater tubes, bank tubes, and economizer. The flue gas is then passed through dust collecting system and then it is sucked by induced draught Fan (ID). The flue gas is then finally passed out to the atmosphere through chimney.

3.2.2 Fuel and ash circuit

An automatic belt conveyer system is used for conveying cotton stalk to the boiler. The belt conveyer conveys chipped fuel to the main bunker. As, the unit is having two compartments, from this main bunker, fuel gets distributed to separate feeders for each of the two compartments. Fuel is then fed to each compartment by screw feeders. The amount of fuel can be varied from the control desk by using the regulators connected to the conveyor. The ash produced due to combustion of fuel is trapped & collected with the help of electro-precipitator unit.

3.2.3 Water and steam circuit

Feed water is filtered of dissolved salts & oxygen in the water treatment plant (Figure 3.1) & pushed into the steam drum by feed pumps, after it has been heated in the economizer. Then, water passes into mud drum through bank tubes. While passing through the bank tubes, water gets heated up by the flue gas passing over the tubes. Then, this hot water enters into bed coils through downcorner tubes and gets heated up again.

Then the steam water mixture rises through the waterwall panel enters into the upper drum through riser tubes. From steam drum, the saturated steam finally enters into

the convection superheater tubes and gets superheated. Then the superheated steam is taken to the process turbine by main steam stop valve.

3.2.4 The distributor plate

The distributor plate is the heart of the FBC system. This is made up of carbon steel base plate with cast iron air nozzles. The air nozzles distribute the fluidizing air from FD fan uniformly over the entire bed.

Figure 3.2: Water treatment plant

Figure 3.3: Cooling tower

Figure 3.4: Chipper in progress

Figure 3.5: Electro-static precipitator

Figure 3.6: Ash under the ESP

Figure 3.7: Belt Conveyor carrying fuel

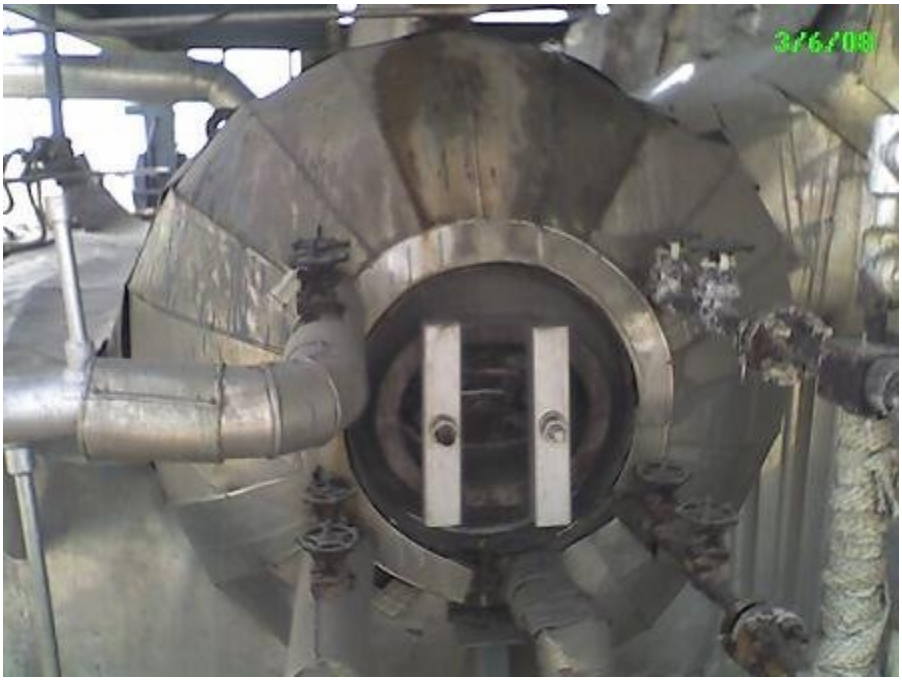

Figure 3.8: Steam drum

Figure 3.9: Turbine ventilators

Figure 3.10: Sample of cotton stalk

CHAPTER 4

Experimental Analysis

Fuel samples collected from the Malwa Power Pvt. Ltd., Muktsar, Punjab, a power plant, using FBC system for generating steam and subsequently power, were subjected to proximate analysis in the laboratory.

4.1 Proximate analysis of fuel

The term proximate analysis is defined as the determination of moisture, ash, volatile matter and fixed carbon.

4.1.1 Determination of moisture

Moisture is defined as the difference in weight of sample when the same is heated at 110°C for one hour under specified conditions.

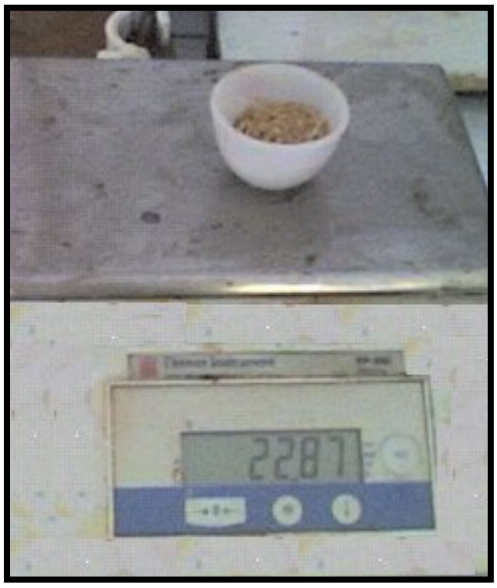

Figure 4.1 Fuel sample being weighed before heating

4.1.1.1 Apparatus required

1. **Air oven**

Ventilated drying oven in which constant and uniform temperature of 110°C can be maintained.

2. **Silica crucible**

One silica crucible is required.

3. **Weighing machine**

Weighing machine is required for weighing sample.

4.1.1.2 Procedure

Silica crucible was taken, cleaned and dried in an oven at 110°C for one hour. It was cooled for 15 minutes and then weighed accurately. Approximately one gram of sample was weighed and put into the silica crucible. Then crucible was kept in an air-dried oven which was maintained at 110°C for one hour. After one hour crucible was removed from

the oven cooled in a desicator and then weighed accurately.

4.1.1.3 Calculations

Weight of dried and empty crucible with lid	=	a gm
Weight of sample and crucible	=	b gm
Weight of sample and crucible after heating	=	c gm
Therefore, weight of sample after heating moisture	=	(b-a) gm
Moisture	=	(b-c) gm
Percentage of moisture	=	{(b-c)/(b-a)} x 100

4.1.2 Determination of volatile matter

Volatile matter is defined as the loss of weight of sample when the same is heated under specified conditions in the absence of air at 900°C for 9 minutes.

4.1.2.1 Apparatus required

1. Muffle furnace

A muffle furnace capable of giving uniform temperature of 900°C with the necessary thermocouples and pyrometers.

2. Silica crucible

A translucent silica crucible with lid having external diameter of 25 mm should be used. The total height of crucible should not exceed 38 mm and internal diameter should not be less than 22 mm.

4.1.2.2 Procedure

For the determination of volatile matter, a crucible with lid was taken and then weighed accurately. Now one gram of sample was weighed accurately into the crucible and spread evenly in the crucible by gentle tapping the crucible with the lid was transferred in the furnace at 900°C for nine minutes.

After nine minutes, the crucible was removed from the furnace and placed on a cooled iron plate to ensure rapid cooling. Then the crucible was placed in a desicator for 15 minutes for further cooling and then weighed accurately.

4.1.2.3 Calculations

Weight of dried and empty crucible with lid = a gm

Weight of sample and crucible = b gm

Weight of sample and crucible after heating = c gm

Therefore, weight of sample after before loss of weight = (b-a) gm

Loss of weight = (b-c) gm

Percentage of volatile matter = {(b-c)/ (b-a)} x100

4.1.3 Determination of ash

Ash is defined as the weight of residue left when a known weight of sample is burnt at 800°C for one hour under specified conditions.

4.1.3.1 Apparatus required

1. Muffle furnace

A muffle furnace capable of giving uniform temperature of 900°C with the necessary thermocouples and pyrometers.

2. Silica crucible

A translucent silica crucible with lid having external diameter of 25 mm should be used. The total height of crucible should not exceed 38 mm and internal diameter should not be less than 22 mm.

Figure 4.2 Figure showing fuel sample being placed in muffle furnace

4.1.2.2 Procedure

For the determination of ash, a silica dish was taken, heated at 800°C for one hour. Then

the dish was cooled for 20 minutes and then weight of empty dish was taken. Now one gram of sample was weighed accurately into the crucible and spread evenly in the crucible by gentle tapping the crucible with the lid.

The silica dish was transferred in the furnace at 450°C for half an hour. Then the temperature of the furnace was raised to 800°C. The dish was kept at this temperature for another one hour. The crucible was removed from the furnace, cooled and then weighed accurately.

4.1.2.3 Calculations

Weight of dried and empty crucible with lid = a gm

Weight of sample and crucible = b gm

Weight of sample and crucible after heating = c gm

Therefore, weight of sample after heating = (b-a) gm

Weight of ash = (c-a) gm

Percentage of ash = {(c-a)/ (b-a)} x100

4.2 Specific gravity

It is defined as the ratio of mass per unit volume of particle to mass per unit volume of water at 4^{o}C.

4.2.1 Procedure

For the determination of specific gravity, first of all the specific gravity bottle was cleaned. Dried, and weighed with tip. Water was filled up to the marked level of the bottle, and weighed. After removing the water, the bottle was dried and about 2 gm of fuel sample was kept and weighed. Then water was filled up to certain level in the specific gravity bottle, and placed in hot water bath at 50^{o}C for 30 minutes to remove air bubble, then water was further filled up to the marked level and weighed with the tip.

4.2.2 Calculation

Weight of specific gravity bottle with tip = a gm

Weight of specific gravity bottle with tip + water = b gm

Weight of specific gravity bottle with tip + fuel = c gm

Weight of specific gravity bottle with tip + fuel +water = d gm

Weight of fuel = (c-a) gm

Weight of water = (b-a) gm

Weight of water of the volume replaced by fuel = (b-a)-(d-c) gm

Specific gravity of fuel $= \frac{(c - a)}{(b - a) - (d - c)}$

Components	Percentage
Moisture	13.88 %
Ash	4.0%
Volatile matter	60.5%
Fixed carbon	21.62%

Table 4.1 Proximate analysis of fuel

4.3 Ultimate Analysis of Fuel:

The ultimate analysis of the fuel was carried out at the Centre with potential for excellence in Biomedical Sciences at Punjab University, Chandigarh. The results obtained are given in Table no.4.2. These values were then directly used in the calculations.

Components	Percentage
C	42.37 %
H	5.67 %
S	0.00 %
0	36.58 %
N	1.50 %

Table 4.2 Ultimate analysis of fuel

4.4 Thermo-gravimetric analysis

The thermo-gravimetric analysis on the fuel sample was conducted in the Thapar University's laboratory. It was conducted to determine the loss in the weight of the fuel sample with temperature and time. A curve was obtained for the same which indicated 50% loss in weight at about 300°C. The particular graph has been shown in figure 4.3.

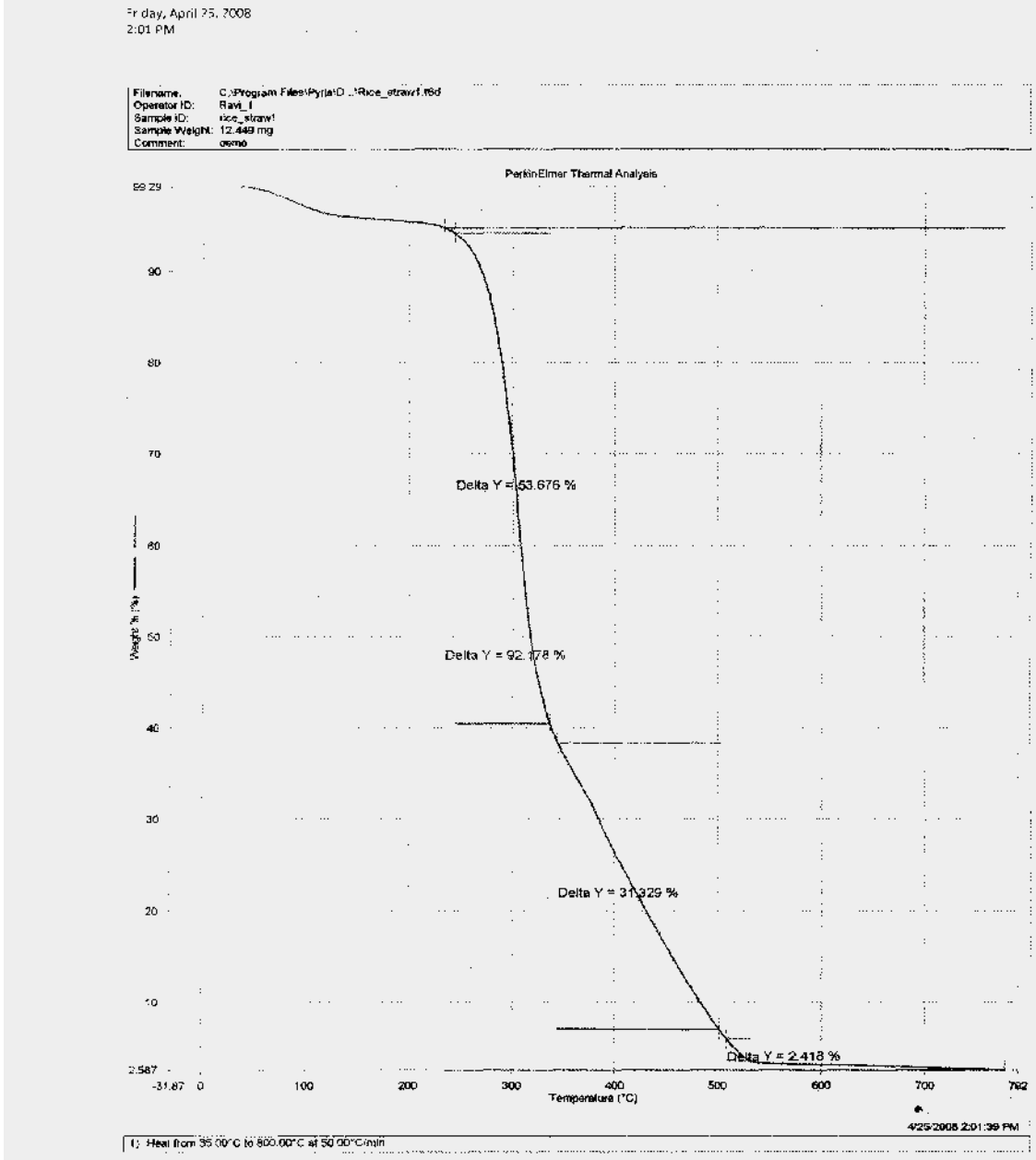

Figure 4.3: Thermo-gravimetric analysis of fuel sample

CHAPTER 5

Mathematical modeling

A mathematical model has been developed in the present work, for an atmospheric bubbling fluidized bed combustor that uses cotton stalk as fuel, it incorporates the following:

- Physico-chemical parameters in the bed i.e., minimum fluidizing velocity, bubble properties, operating velocity etc.
- Solid population balance to find out p_0 (d_p) & p_1 (d_p).

5.1 Model assumptions

The mathematical model developed in the present study is based on the following assumptions;

- The bed is assumed to consist of a number of equivalent stages. The height of each stage is equal to the average equivalent bubble diameter of bed.
- Each stage consists of bubble, cloud-wake and emulsion phase.
- It is assumed that bubbles are solid (carbon) free, uniform in size and equally distributed throughout the bed. The gas flow through the bubble phase is considered to be in plug flow.
- The bubble and its cloud and wake rise at the same absolute velocity. The voidage in the cloud and wake phase is assumed to be the same as in the emulsion phase.
- The gas flowing through the emulsion phase is considered to be completely mixed within each stage. The voidage in the emulsion phase is constant and equal to the voidage at incipient fluidisation and it remains the same as that under minimum fluidisation condition.

- The gas flowing through the cloud-wake phase is considered to be completely mixed within each stage.
- The gas flow rate through the emulsion phase is assumed to remain the same as that under minimum fluidisation condition.

5.2 Physico-chemical parameters in a fluidised bed combustor

In the following text, mathematical relations for some of Physico-chemical parameters in fluidized bed combustors have been given. These relations form the base for developing models for fluidized bed combustors and the values of these parameters directly affect the performance of the combustors.

5.2.1 Superficial velocity

Superficial velocity or the operating velocity is calculated as below;

$$U = \frac{F_{ME} R_g T_b}{P_{av} A} \quad m/s \qquad (5.1)$$

Where, R_g : Gas constant = 0.08206 atm-m^3/ (kg-mole) (K)

P_{av} : Average pressure in the combustor (atm)

T_b : Absolute bed temperature (K)

A : Cross-sectional area of the bed (m^2)

F_{ME} : The actual molar feed rate of fluidising air and is calculated as below;

$$F_{ME} = F_{MTH}(1.0 + Ex_{air}) \text{ (Kg-mole/s)} \qquad (5.2)$$

Where Ex_{air}: Fractional excess air;

F_{MTH} is the stoichiometric air feed rate, which is determined from the fuel composition and fuel feed rate using the simple stochiometrical relationship given below;

$$F_{MTH} = W\,(1.0 - XW)\left\{\frac{\left[\frac{XC}{12} + \frac{XH}{4} + \frac{XS}{32} - \frac{X0}{32}\right]}{0.21}\right\} \qquad (5.3)$$

Where W is the fuel feed rate into the combustor (Kg/sec), and XC, XH, XS, XO, and XW are the ultimate carbon, hydrogen, sulphur, oxygen and moisture content of the fuel.

5.2.2 Minimum fluidization velocity

A number of correlations are available in literature (Table 5.1) to define minimum fluidization velocity, the application of which varies to a great extent depending upon the particle size in the bed. According to Kunni & Levenspiel, the equation (5.4) recommended by Chitester et. al. gives the best results for coarse particles.

$$U_{mf} = \left(\frac{\mu}{d_p \rho_g}\right)\left[\left\{(28.7)^2 + \frac{0.0494 d_p^{\,3} \rho_g (\rho_p - \rho_g)(g)}{\mu^2}\right\}^{1/2} - 28.7\right] \qquad (5.4)$$

Chitester et. al.'s correlation was used to calculate the minimum fluidization velocity in the present model because the particle size is greater than 100µm.

5.2.3 Viscosity of fluidizing gas

Subramani et. al.(2007) gave an equation for estimating the viscosity of fluidizing air, which is a function of bed temperature only and is presented below;

$$\mu_g = \left[1.46\,(10^{-6})\,\left(\frac{T_b^{1.504}}{T_b + 120}\right)\right] \qquad (5.5)$$

5.2.4 Density of fluidizing gas

The density of fluidizing gas can be found from the work of Bird et al. (1960). The final expression for density of fluidizing gas, which is a function of bed temperature only, is presented below;

$$\rho_g = \frac{353.2}{\sqrt{T_b}} \qquad (5.6)$$

Table 5.1 Expressions for minimum fluidization velocity

Sr. No.	Empirical correlation	Authors
1.	$U_{mf} = \left(\frac{\mu}{d_p \rho_g}\right)\left[\left\{(33.7)^2 + \frac{0.0408 d_p^{\,3} \rho_g (\rho_p - \rho_g)(g)}{\mu^2}\right\}^{1/2} - 33.7\right]$	Wen and Yu (1966)
2.	$U_{mf} = \left(\frac{\mu}{d_p \rho_g}\right)\left[\left\{(25.25)^2 + 0.0651 Ar\right\}^{1/2} - 25.25\right]$	Babu et al. (1978)
3	$U_{mf} = \frac{Ar}{(1400 + 5.22 Ar^{0.5})}$	Todes et al. (1981)
4.	$U_{mf} = \left(\frac{\mu}{d_p \rho_g}\right)\left[\left\{(25.46)^2 + 0.0382 Ar\right\}^{1/2} - 25.46\right]$	Bourgeoi & Grenier(1968)
5.	$U_{mf} = \left(\frac{\mu}{d_p \rho_g}\right)\left[\left\{(25.28)^2 + 0.0571 Ar\right\}^{1/2} - 25.28\right]$	Saxena & Vogel(1977)
6.	$U_{mf} = \left(\frac{\mu}{d_p \rho_g}\right)\left[\left\{(18.75)^2 + 0.03125 Ar\right\}^{1/2} - 18.75\right]$	Zheng et.al. (1985)
7.	$U_{mf} = \left(\frac{\mu}{d_p \rho_g}\right)\left[\left\{(30.1)^2 + 0.0417 Ar\right\}^{1/2} - 30.1\right]$	Sathyanaryana &Rao(1989)
8.	$U_{mf} = \left(\frac{\mu}{d_p \rho_g}\right)\left[0.00138\, A_r / \left(A_r + 19\right)^{0.11}\right]$	Ilavsky & Bena(1967)

Where $Ar = \frac{d_p^{\,3} \rho_g (\rho_p - \rho_g)(g)}{\mu^2}$

Table 5.1: Expressions for minimum fluidization velocity

5.2.5 Terminal velocity

To avoid the particles from getting blown out of the bed, the superficial velocity must be limited under the maximum fluidization velocity, that is called terminal velocity of the particles.

The terminal velocity of the particles as given by Geldart et. al. (1984) is:

$$U_t = \sqrt{\frac{4gd_p}{3C_d}\frac{\left(\rho_s - \rho_g\right)}{\rho_g}} \tag{5.7}$$

where C_D is the drag coefficient for a spherical particle.

The relationships between drag coefficient (C_D) and Reynolds number (Re) was given by Kunni & Levenspiel (1969) as:

$$C_D = \frac{24}{\mathrm{Re}} \qquad \text{if } \mathrm{Re} < 0.4 \tag{5.8}$$

$$C_D = \frac{10}{\sqrt{\mathrm{Re}}} \qquad \text{if } 0.4 < \mathrm{Re} < 500 \tag{5.9}$$

$$C_D = 0.43 \qquad \text{if } 500 < \mathrm{Re} < 200000 \tag{5.10}$$

The given equations 5.,5.,5. are substituted into equation 5. to obtain 3 terminal velocities Ut of particles. These values of Ut are used to find out the Reynolds number (Re) and its consistency is verified.

Cheremisinoff et. al. also gave few similar empirical correlation for terminal velocity, given as under:

$$U_t = \left[\left(\frac{4}{225}\right)\frac{\left(\rho_s - \rho_g\right)^2 g^2}{\rho_g \mu}\right]^{1/3} \times d_p \qquad \text{if } 0.4 < \mathrm{Re} < 500 \tag{5.11}$$

$$U_t = \left[\frac{3.1 d_p \left(\rho_s - \rho_g\right) g}{\rho_g}\right]^{1/2} \qquad \text{if } 500 < \mathrm{Re} < 200000 \tag{5.12}$$

5.2.6 Voidage at minimum fluidization

Observing that parameters like the bed porosity at minimum fluidization (ε_{mf}), Re_{mf} and A_r change with temperature, Subramani et. al. attempted to develop an empirical correlation to predict ε_{mf} as a function of Re_{mf} and A_r , using least square method:

$$\varepsilon_{mf} = 0.3507 A_r^{0.0387}\, \mathrm{Re}_{mf}^{-0.0704} \tag{5.13}$$

5.2.7 Transport disengagement height (TDH)

The gases exiting from the combustor carry some suspended particles. This flux of solids is called entrainment or carryover. Freeboard of the vessel is the section between the upper surface of the dense phase and the point of exit of the gas stream, its height is called freeboard height. The density of the solids decreases wit height in the freeboard, increasing the freeboard decreases the entrainment from the bed. Eventually, a freeboard height is reached above which entrainment does not change appreciably. This is called transport disengagement height.

Khan et al. gave an empirical relation for TDH as:

$$TDH = 4.47 d_b^{0.5} \tag{5.14}$$

5.2.8 Average equivalent bubble diameter

Various correlations can be found in literature for the estimation of bubble diameter in a fluidized bed. One of the widely used correlations was proposed by Khan et al. in 2007 taking into account the effect of bed diameter and distributor type on bubble diameter as follows;

$$d_{\mathrm{b}} = d_{\mathrm{bm}} - (\mathrm{d}_{\mathrm{bm}} - d_{\mathrm{bo}}) \exp\left(-\frac{0.3\mathrm{z}}{d_{\mathrm{t}}}\right) \tag{5.15}$$

$$\text{Where, } d_{bm} = 1.633\,[0.785 d_t^2\ (U - U_{mf})]^{0.4} \tag{5.16}$$

$$\text{And } d_{bo} = 0.283\left(U - U_{mf}\right)^2 \tag{5.17}$$

where db_0 is the initial bubble size formed near the bottom of bed.

Rowe (1976) also presented an expression to estimate bubble diameter for fluidized bed combustors, which is given below;

$$d_b=(U - U_{mf})Z^{0.75}g^{-0.25} \quad (5.18)$$

Stubington et al.(1984) modified the above expression for tuyer cap type distributors as follows;

$$d_b=0.43(U - U_{mf})^{0.4}(Z+4\sqrt{A})^{0.8}g^{-0.2} \quad (5.19)$$

Kunni & Levenspiel (1990) presented some expressions for low and high gas flow which took into account the number of orifices, spacing between orifices etc. These are given as under:

$$U - U_{mf} = N_{or} v_{or} \quad (5.20)$$

Where N_{or} = number of orifices per unit area;

v_{or}= volumetric flow rate through an orifice (m^3/s);

$$d_{b0} = 1.30 \frac{v_{or}^{0.4}}{g^{0.2}} \quad (5.21)$$

Hence the bubble diameter just above the distributor becomes;

For low gas flow rate:

$$d_{b0} = \frac{1.30}{g^{0.2}} \left[\frac{U - U_{mf}}{N_{or}} \right]^{0.4} ; \qquad \text{if } d_{b0} \le l_{or} \quad (5.22)$$

Where l_{or} is the spacing between adjacent holes;

For high gas flow rate:

$$d_{b0} = \frac{2.78}{g} \left(U - U_{mf} \right) ; \qquad \text{if } d_{b0} > l_{or} \quad (5.23)$$

In another approach, Werther gave the following expression for bubble size at any height ‘z’ in a bed of Geldart B group solids supported by a porous plate distributor:

$$d_b = 0.853\left[1+0.272\left(U-U_{mf}\right)\right]^{1/3}\left(1+0.0684z\right)^{1.21} \quad (5.24)$$

It was found in the present study that best results were obtained using the Khan et. al. expression for bubble diameter.

5.2.9 Bubble velocity

The absolute rise velocity of an isolated single rising bubble, $u_{br,}$ was first suggested by Davidson and Harrison (1963) to be given by;

$$u_{br} = 0.711\sqrt{g.d_b}\ ; \qquad \text{When } d_b/d_t < 0.125 \tag{5.25}$$

According to Wallis, the wall effects retard the rise of bubbles when d_b/d_t > 0.125, hence he suggested;

$$u_{br} = \left[0.711\left(gd_b\right)^{1/2}\right]1.2\exp\left(-1.49\frac{d_b}{d_t}\right);\ \text{When } 0.125 < d_b/d_t < 0.6 \tag{5.26}$$

He further recommended that for d_b/d_t >0.6, the bed should not be considered as bubbling, but slugging.

Kunni & Levenspiel (1991), Geldart (1973) & Werther (1973) also recommended the following relation:

$$u_b = 1.6\left[\left(U - U_{mf}\right) + 1.13d_b^{0.5}\right]d_t^{1.35} + u_{br} \tag{5.27}$$

Davidson and Harrison (1963) also proposed on theoretical grounds that the average absolute velocity of a crowd of bubbles in a fluidized bed may be expressed as

$$u_b = U - U_{mf} + u_{br} \tag{5.28}$$

5.2.10 Bubble properties

According to Rowe and Partridge (1965), the ratio between the volumes of wake dragged upward behind a rising bubble to the volume of bubble, $f_{w,}$ may be taken to be roughly as 0.25.

For estimating the size of cloud, ratio of cloud volume to bubble volume (f_c), the Davidson and Harrison (1963) correlation was tried;

$$f_c = \frac{3U_{mf}}{(\varepsilon_{mf}.u_{br} - U_{mf})} \tag{5.29}$$

The ratio of volume of cloud-wake phase to the volume of bubble f_{cw} is obtained as follows;

$$f_{cw} = f_w + f_c \tag{5.30}$$

But, it was found that equation (5.15) gave absurd values of f_c, for the present case. We have therefore taken f_c as an adjustable parameter, the value of which lies in between 0.025 and 0.15. This in turn implies that f_{cw} is now an adjustable parameter, with its value varying from 0.275 to 0.4.

5.2.11 Distribution of gas flow among the three phases

Since the volumetric flow rate of fluidising gas, Q, is distributed among the three phases, thus we have;

$$Q = Q_{mf} + Q_{cw} + Q_b \tag{5.31}$$

Where Q_{mf} : Volumetric flow rate via emulsion phase

Q_{cw} : Volumetric flow rate via cloud-wake phase

Q_b : Volumetric flow rate via bubble phase

Dividing equation (5.17) by the cross-sectional area of the bed, we can get the superficial velocity of fluidising gas;

$$U = U_{mf} + U_{cw} + U_b \tag{5.32}$$

Here U_b is the superficial gas velocity of the bubble phase and it is different from the average absolute rise velocity of a crowd of bubbles.

U_{cw} is the velocity of cloud-wake phase.

The cross-sectional area of the bed occupied by bubbles is;

$$A_b = \varepsilon_b . A \tag{5.33}$$

where ε_b is the volume fraction of bubbles in the bed or the fraction of the bed consisting of bubbles.

The cross-sectional area of bed occupied by cloud-wake phase is given below;

$$A_{cw} = f_{cw} . \varepsilon_b . A \tag{5.34}$$

In the model, the void fraction in the cloud-wake phase is assumed to be ε_{mf}. Hence the cross-sectional area of bed available for gas flow in the cloud-wake phase is expressed by;

$$A_{cw_g} = f_{cw} . \varepsilon_b . \varepsilon_{mf} . A \tag{5.35}$$

The bubble and its associated cloud and wake is assumed to rise at the same absolute rise velocity of crowd of bubbles, u_b. So the volumetric flow rate of gas flowing through the cloud-wake phase is expressed as;

$$Q_{cw} = u_b A_{cw_g} = U_{cw} A \tag{5.36}$$

Substituting the value of A_{cw_g} from equation (5.35) into equation (5.36), we get

$$u_b = \frac{U_{cw}}{(f_{cw} . \varepsilon_b . \varepsilon_{mf})} \tag{5.37}$$

The volumetric flow rate of gas through the bubble phase;

$$Q_b = u_b A_b = U_b \ (A) \tag{5.38}$$

Now substituting the value of A_b from equation (5.33) into equation (5.38), we get

$$u_b = \frac{U_b}{\varepsilon_b} \tag{5.39}$$

Equating equations (5.37) & (5.39), we have

$$U_{cw} = f_{cw} . \varepsilon_{mf} . U_b \tag{5.40}$$

After substituting equation (5.40) into equation (5.32), we get

$$U_b = \frac{U - U_{mf}}{(1.0 + f_{cw} . \varepsilon_{mf})} \tag{5.41}$$

From equations (5.40) & (5.41) the cloud-wake phase velocity may be calculated as;

$$U_{cw} = f_{cw} . \varepsilon_{mf} \frac{(U - U_{mf})}{(1.0 + f_{cw} . \varepsilon_{mf})} \tag{5.42}$$

Also,

$$\frac{(A_b + A_{cw})}{A} \langle 1.0 \tag{5.43}$$

$$\varepsilon_b (1.0 + f_{cw}) \langle 1.0 \tag{5.44}$$

It is because the cross-sectional area occupied by bubble, cloud and wakes should always be less than the total cross-sectional area of the bed as pointed out by Bukur et al. (1978). This condition is of special significance in AFBC because the same is operated relatively at higher operating velocity.

5.2.12 Volume fraction of bubbles in the bed, ε_b

Now substituting the value of A_b from equation (5.33) into equation (5.38), we get

$$\varepsilon_b = \frac{U_b}{u_b} \tag{5.45}$$

5.2.13 Expanded bed height, H

The bed expansion above the height at minimum fluidisation is assumed to be entirely due to the presence of bubbles and hence it is related to expanded bed height;

$$H = \frac{H_{mf}}{(1.0 - \varepsilon_b)} \tag{5.46}$$

5.2.14 Number of equivalent stages, N

As height of each stage is taken to be equal to the average equivalent bubble diameter so, the number of equivalent stages can be calculated as below;

$$N = \frac{H}{d_b} \tag{5.47}$$

5.2.15 Interphase gas exchange coefficients

It is of particular importance because it is one of the determining factors in predicting the performance of fluidised bed combustors. The interphase gas exchange coefficient between any two phases can be looked upon as the flow of gas from one phase to the other and vice – versa. The interphase coefficient between bubble and emulsion phases can be defined as;

$$\left(\mathrm{K_{be}}\right)_{\mathrm{b}} = \frac{\left[\begin{array}{c}\text{volume of gas going from bubbles to emulsion} \\ \text{or from emulsion to bubbles}\end{array}\right]}{(\text{volume of bubbles in the bed})(\text{time})} \tag{5.48}$$

The overall coefficient of gas interchange between bubble and emulsion phase, therefore, has been investigated by several authors.

Davidson and Harrison (1963) assumed that there were both convective and diffusional flows contributing to the gas interchange and the correlation is given by;

$$\left(K_{be}\right)_b = 4.5\frac{U_{mf}}{d_b} + 5.85\frac{D_e^{1/2}\, g^{1/4}}{d_b^{5/4}} \tag{5.49}$$

In the above equation the second term represents the mass transfer which is given by analogy with the liquid-film controlled diffusion process from a rising bubble.

Kunii and Levenspiel (1969) then proposed a new theory for estimating the interchange coefficients. They assumed that there were two transfer steps, namely the transfer between the bubble and cloud phase and that between the cloud and emulsion phases.

They further assumed that the coefficient for the former step is given by Davidson and Harrison (1963) equation and the coefficient for the latter step is given by Higbie's penetration model. Their correlation is as follows;

$$\frac{1}{(K_{be})_b}=\frac{1}{(K_{bc})_b}+\frac{1}{(K_{ce})_b} \tag{5.50}$$

$$(K_{bc})_b=4.5\frac{U_{mf}}{D_b}+5.85\frac{D_e^{1/2}g^{1/4}}{D_b^{5/4}} \tag{5.51}$$

$$(K_{ce})_b=6.78(\frac{\varepsilon_{mf}D_e u_b}{D_b^{3}})^{1/2} \tag{5.52}$$

D_e, the oxygen diffusivity is expressed in terms of surrounding temperature using Bird et al. (1960) correlation as;

$$D_e=5.14\times10^{-9}\times(T_b)^{1.5} \tag{5.53}$$

5.2.16 Reaction rate constant

The chemical reaction rate constant K at any instant which is controlled by surface reaction and gas diffusion coefficients and is obtained from the above equation as;

$$\frac{1}{K}=\frac{1}{K_s}+\frac{1}{K_g} \tag{5.54}$$

where K_s the surface reaction rate constant for carbon particles is adopted from the expression given by Parker and Hotel (1936);

$$K_s=4.32\times10^{11}\,T_p^{-0.5}\,\exp(-44000/RT_p) \tag{5.55}$$

The mass transfer coefficient K_g is expressed by dimensionless Sherwood number (Sh) as;

$$K_g=\frac{Sh\times D_e}{d_p} \tag{5.56}$$

Sherwood number can be defined as a dimensionless concentration gradient at the surface, and it provides a measure of the convection mass transfer occurring at the surface.

Khan et. al. (2007) gave a correlation for this using Schmidt number, Reynold's number and voidage at minimum fluidization, given as:

$$Sh = 2\varepsilon_{mf} + 0.69 S_c^{0.33}\,\mathrm{Re}^{0.5} \tag{5.57}$$

where Schmidt number 'Sc' is given as;

$$Sc = \frac{\mu_g}{\rho_g D_e} \tag{5.58}$$

Many a correlation were available for estimating the Sherwood number but in this model, La Nauze et al. (1984) correlation has been adopted and the correlation is given as;

$$\mathrm{Sh} = 2\varepsilon_{mf} + [4.0\varepsilon_{mf} d_p (U_{mf}/\varepsilon_{mf} + U_b)/\pi D_e]^{1/2} \quad \text{for } d_p/d_{pbed} \geq 4.0 \tag{5.59}$$

$$\text{and } \mathrm{Sh} = 2.0\varepsilon_{mf} + [4.0 d_p U_{mf}/\pi D_e]^{1/2} \quad \text{for } d_p/d_{pbed} < 4.0 \tag{5.60}$$

In the calculation $d_p/d_{pbed} < 4.0$ has been assumed.

5.2.17 Particle shrinkage rate

According to shrinking core model, as soon as the fuel enters into the FBC, it decomposes into volatiles and combustible matter. During a short ignition period, pores start to form, while the fuel softens and re-solidifies to become char, where combustion reaction takes place till final burnout of char is achieved.

Wen (1968) and Ishida et al. (1971) on the basis of studies of numerous systems, conclude that the shrinking core model is the best simple representation for the majority of reacting gas solid systems.

$$\left(\frac{dd_p}{dt}\right)_{\text{over all}} = \left(\frac{dd_p}{dt}\right)_{\text{attrition}} + \left(\frac{dd_p}{dt}\right)_{\text{combustion}} \tag{5.61}$$

The shrinkage rate by attrition was determined by Merick and Highly (1974) correlation as follows;

$$(\frac{dd_p}{dt})_{attrition} = \frac{1}{3} A_{kt} (U - U_{mf}) \tag{5.62}$$

where: A_{kt} is a dimension less attrition rate constant.

According to Turnbull et al. (1984);

$$(\frac{dd_p}{dt})_{combustion} = \frac{2M_c}{\rho_p} (\frac{1}{K_s} + \frac{d_p}{Sh\, D_e})^{-1} C_p \tag{5.63}$$

Where, M_c is the molecular weight of carbon

$$\frac{dd_p}{dt} = \frac{1}{3} A_{kt} (U_0 - U_{mf}) + \frac{2M_c}{\rho_p} (\frac{1}{K_s} + \frac{d_p}{ShD_g})^{-1} .C_p \tag{5.64}$$

5.2.18 Inlet oxygen concentration

The inlet oxygen molar concentration is evaluated at the bed temperature, at 1 atm. pressure as;

$$C_0 = \left[(\frac{0.21}{22400})(\frac{273.0}{T_b}) \right] \times 1000 \text{ kg-mole/m}^3 \tag{5.65}$$

5.2.19 Elutriation rate constant

In the literature, we have two somewhat different looking, but essentially similar, approaches to the determination of elutriation rate from the vessels. Both approaches assume that that the flux rate of any particular size of solid 'i' is proportional to its weight fraction x_i in the bed.

The approach of Zenz et. al. involved dividing the size distribution into narrow intervals and finding out which intervals have $U_t < U$. These solids are entrained. It uses a flux rate constant (G_{si}^*) which is determined from a graph, then:

$$\text{Total entrainment} = G_s = \sum_i x_i G_{si}^* \tag{5.66}$$

The other approach uses elutriation constant (κ_i^*) such that:

$$\begin{pmatrix} rate\ of\ removal\ of \\ solids\ i \end{pmatrix} = \kappa_i^* \begin{pmatrix} weight\ of\ that\ size \\ of\ solid\ in\ the\ bed \end{pmatrix} \tag{5.67}$$

Various correlations available for κ_i^* are given as under:

in which $\mathrm{Re}_t = \dfrac{d_{pi}\rho_g U_{ti}}{\mu}$

Yagi and Aochi (1955):

$$\frac{\kappa_i^* g d_{pi}^2}{\mu\left(U - U_{ti}\right)^2} = 0.0015\,\mathrm{Re}_t^{0.5} + 0.01\,\mathrm{Re}_t^{1.2} \tag{5.68}$$

Tanaka et. al. (1960):

$$\frac{\kappa_i^*}{\rho_g\left(U - U_{ti}\right)} = 0.046\frac{\left(U - U_{ti}\right)}{\left(g d_{pi}\right)^{0.5}} \times \mathrm{Re}_t^{0.3}\left(\frac{\rho_s - \rho_g}{\rho_g}\right)^{0.15} \tag{5.69}$$

Colakyan and Levenspiel (1984):

$$\kappa_i^* = 0.011\rho_s\left(1 - \frac{U_{ti}}{U}\right)^2 \tag{5.70}$$

Wen and Hashinger (1985):

$$\frac{\kappa^*}{\rho_g\left(U - U_t\right)} = 1.52\times10^{-5}\left[\frac{\left(U - U_t\right)^2}{g d_p}\right]^{0.5} \mathrm{Re}_t^{0.725}\left[\frac{\left(\rho_s - \rho_g\right)}{\rho_g}\right]^{1.15} \tag{5.71}$$

Merrick and Highley (1988):

$$\frac{\kappa^*}{\rho_g U} = A + 130\times\exp\left[-10.4\left(\frac{U_t}{U}\right)^{0.5}\left(\frac{U_{mf}}{U - U_{mf}}\right)^{0.25}\right] \tag{5.72}$$

All of the above correlations were tried; one given by Yagi and Aochi gave the most appropriate results. So in the present model development, Yagi and Aochi's expression was used to determine the elutriation rate.

5.3 Determination of $p_0(d_p)$:

Kunni & Levenspiel reiterated that before considering the behaviour of beds containing solids of different sizes, we must be able to describe usefully the size distribution of a batch of solid particles. For this, they defined the size distribution functions P and p as follows. Let P be the volume fraction of particles smaller than size dp and let $pd(d_p)$ be the volume fraction of particles of size between d_p and $d_p + d(d_p)$.

The relationship between p and P can be found by considering particles of any particular size, dp1, for which we have

$$p_1 = \left(\frac{dp}{d\left(dp\right)} \right)_1 \qquad \text{or} \qquad P_1 = \int_0^{d_{p1}} pd\left(d_p\right) \tag{5.73}$$

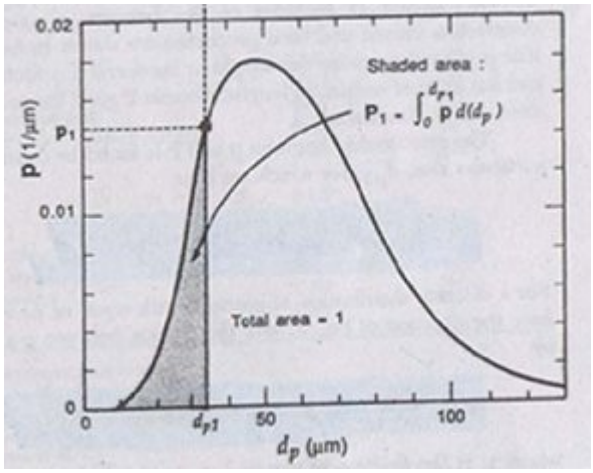

Figure 5.1: Typical size distribution functions

For discrete distribution of particles with equal or unequal size intervals, we have the following relation between p and P at any given dpi:

$$p_i = \left(\frac{\Delta P}{\Delta d_p} \right)_i \qquad \text{or} \qquad P_i = \sum_1^i \left(p \Delta d_p \right)_i = \sum_1^i x_i \tag{5.74}$$

From this, we get to know that p gives volume (or weight or numbers) distribution of particles directly and has units of reciprocal length, whereas P gives the cumulative distribution of sizes and is dimensionless.

Kunni & Levenspiel also gave this relation for average diameter of particle:

$$\bar{d}_p = \frac{1}{\sum_{all...i} \left[\left(p \Delta d_p \right)_i / d_{pi} \right]} = \frac{1}{\sum_{all...i} \left(x / d_p \right)_i} \tag{5.75}$$

So we get;

d_p(mm)	d_p(mm)	d_{pi}(mm)	Weight fraction in interval (x_i)	$(x/d_p)_i$
0.6	1.18	0.89	0.01762	0.019799
1.18	2.36	1.77	0.01762	0.009955
2.36	4.75	3.555	0.02643	0.007435
4.75	10	7.375	0.12775	0.017322
10	20	15	0.21586	0.014391
20	40	30	0.33921	0.011307
40	80	60	0.25551	0.004258

Table 5.2: Calculations for mean diameter of particle

$$\bar{d}_p = \frac{1}{\sum_{all...i} \left(x / d_p \right)_i} = 11.8388 \text{ mm}$$

σ = standard deviation= 26.73843

Using the above calculated mean and standard deviation, various functions were used to find out the probability density function and then the curve fitting tool of MATLAB was used to fit the given size distribution data. The fit of the data is judged according to the residuals given by cftool of the MATLAB. Residuals are defined as the difference between the observed values of the dependent variable and the values that are predicted by the model. When you fit a model that is appropriate for your data, the residuals approximate independent random errors. To calculate fit parameters for a linear model, MATLAB minimizes the sum of the squares of the residuals to produce a good fit. This is called a least-squares fit. You can gain insight into the "goodness" of a fit by visually examining a plot of the residuals: if the residual plot has a pattern, this indicates that the model does not properly fit the data. Notice that the "goodness" of a fit must be determined in the context of your data. For example, if your goal of fitting the data is to extract coefficients that have physical meaning, then it is important that your model reflect the physics of the data. In this case, understanding what your data represents and how it was measured is just as important as evaluating the goodness of fit.

These are the results obtained from curve fitting tool of MATLAB where the abbreviations stand for:

SSE: Sum of squares due to error

R-square: Coefficient of determination

RSME: Root mean squared error (standard error)

1. General model Gauss1 (Normal distribution):

$f(x) = a_1*exp(-((x-b_1)/c_1)^2)$

Coefficients (with 95% confidence bounds)

a_1 = 0.01529 (0.0145, 0.01608), b_1 = 13.57 (11.2, 15.94)

c_1 = 34.53 (29.75, 39.31)

Goodness of fit:

SSE: 7.634e-007 R-square: 0.9929 RMSE: 0.0004369

2. General model Exp1 (exponential):

*f(x) = a*exp(b*x)*

Coefficients (with 95% confidence bounds):

a = 0.0155 (0.01223, 0.01878)

b = -0.01591 (-0.02994, -0.001877)

Goodness of fit:

SSE: 2.575e-005 R-square: 0.7619 RMSE: 0.002269

3. General model Weibull:

*f(x) = a*b*x^(b-1)*exp(-a*x^b)*

Coefficients (with 95% confidence bounds):

a = 0.02743 (-3.378, 3.433)

b = 0.02041 (-2.438, 2.479)

Goodness of fit:

SSE: 5.004e-007 R-square: -4359 RMSE: 0.0003164

Warning: A negative R-square is possible if the model does not contain a constant term and the fit is poor (worse than just fitting the mean). Try changing the model or using a different Start Point.

In the above given results, the goodness of fit of Weibull distribution is accompanied by a warning that clearly indicates that it gives a poor fit. Hence, we reject the Weibull distribution.

Further, comparing the results of Normal & Exponential distribution, we get to know that the degree of errors is least in case of normal distribution. Hence in this study,

the normal distribution has been used while dealing with probability distribution functions associated with feed and carryover of particles.

The figure shows the curve (dp versus $p0(d_p)$), it is consistent with the data collected from the sieve analysis of the cotton stalk fuel sample collected from the plant. Hence the normal distribution and the given curve are accepted.

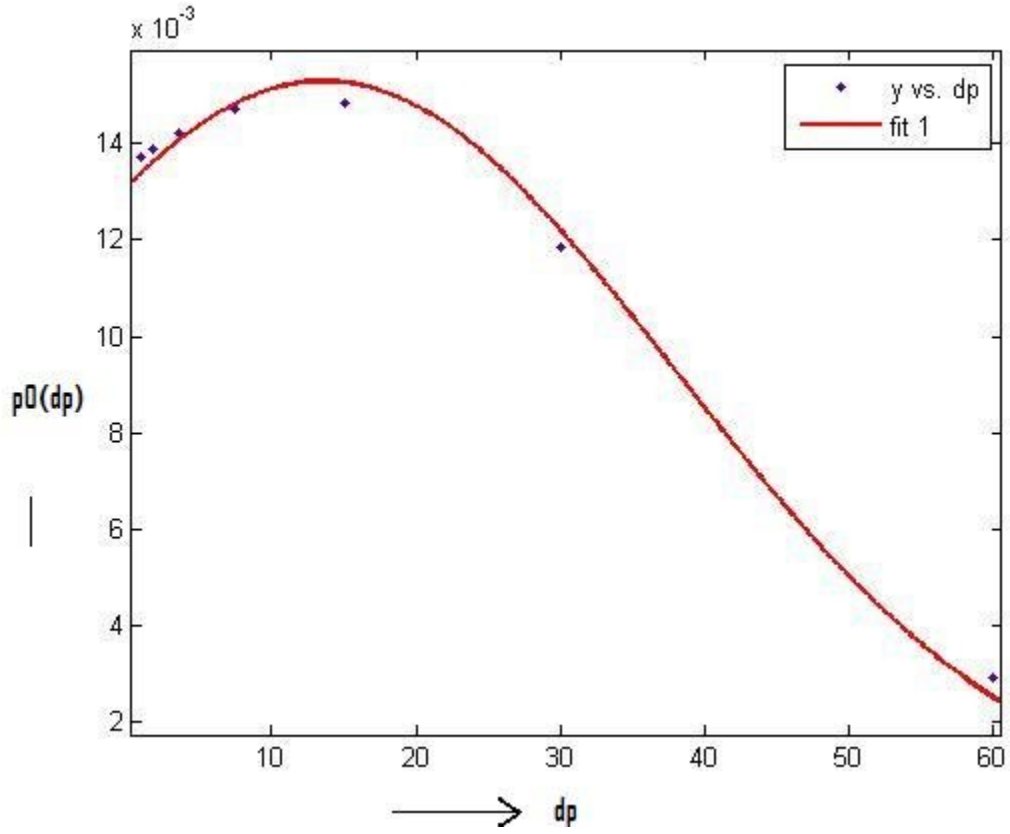

Figure 5.2: Normal probability distribution curve

5.3.1 Size distribution of solids in Fluidized Beds:

The particles in the fluidized beds can be treated as being of:

Unchanging size

Growing and shrinking particles

In both the cases, numerical methods are needed to find the size distribution in the bed, however, the procedure is straightforward and follows same strategy throughout. In our case, the development is limited to steady state operations.

5.3.1.1 Feed of one size:

For a given bed weight and flow rate of solids of unchanging density, as shown in figure, a material balance gives

$$F_0 = F_1 + F_2 \tag{5.76}$$

And the mean residence time of solids in a single fluidized bed becomes

$$t = W/F_0 = W/(F1 + F_2) \tag{5.77}$$

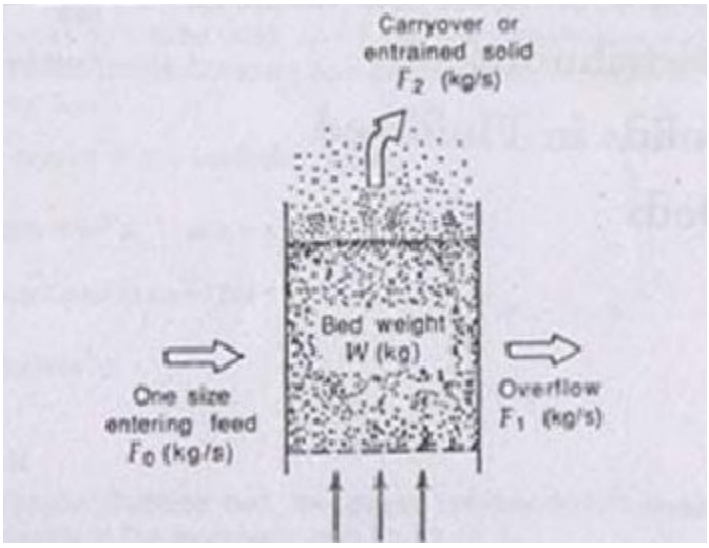

Figure 5.3: Flows in single-stage fluidized bed with single-size feed

5.3.1.2 Feed of Wide Size Distribution:

When particles of wide size distribution $p_0(d_p)$ are fed continuously into a bed as shown in figure, fine particles are likely to be entrained by the gas stream while the remainder of the solids is discharged through an overflow pipe.

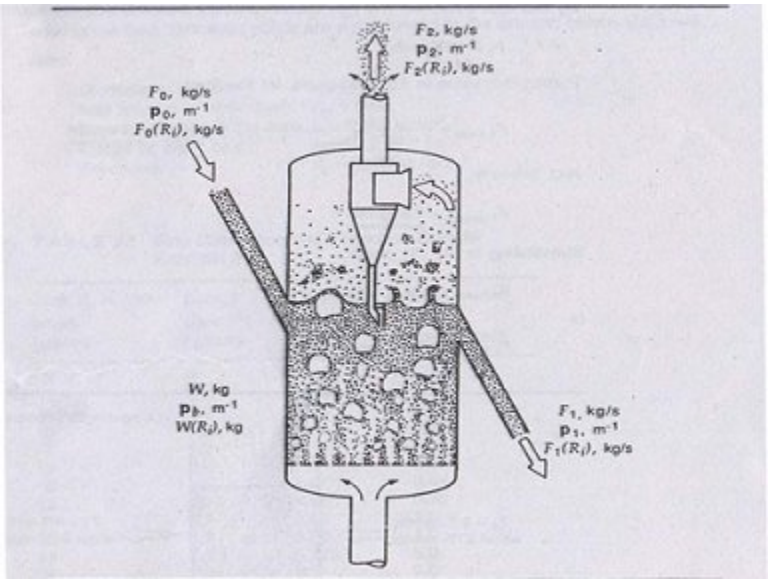

Figure 5.4: Fluidized bed operating with a wide size distribution of solids

Normally, knowing the bed weight W, the feed properties F0, $p_0(d_p)$ and elutriation constant $\kappa(d_p)$ for all sizes of solids, we can determine $p_b(d_p)$ and the solids leaving the vessel $p_1(d_p)$. Up to this point we have already determined size distribution of the feed $p_0(d_p)$ and the elutriation constant $\kappa(d_p)$.

We assume the backmix flow of solids in the bed, in which case the size distribution in the overflow stream is that of the bed, or

$$p_1(d_p) = p_b(d_p) \tag{5.78}$$

The elutriation constant is a function of particle size and for any size 'dp' in the bed is

$$\kappa(d_p) = \frac{F_2 p_2(dp)}{W p_b(dp)} \tag{5.79}$$

The overall mass balance for all of the flowing solid streams gives

$$F_0 = F_1 + F_2 \tag{5.80}$$

And for any size interval between dp and $d_p + d(d_p)$, a mass balance gives

$$F_0 p_0\left(d_p\right) dd_p = F p_1\left(d_p\right) dd_p + F_2 p_2\left(d_p\right) dd_p \tag{5.81}$$

Since the entrainment preferentially removes the small particles from the bed, the fines on the average spend a shorter time in the bed. Thus, the average length of stay of particles varies with size, and for any particular size it is

$$\bar{t}\left(d_p\right) = \frac{\text{weight of a particular size in the bed}}{\text{Flow rate of that size into the bed}}$$

$$= \frac{W p_b\left(d_p\right)}{F_0 p_0\left(d_p\right)} = \frac{W p_b\left(d_p\right)}{F_1 p_1\left(d_p\right) + F_2 p_2\left(d_p\right)} \tag{5.82}$$

Combining equation (5.82) with equations (5.78) and (5.79) gives

$$\bar{t}\left(d_p\right) = \frac{1}{F_1 / W + \kappa\left(d_{p)}\right.} \tag{5.83}$$

This equation shows that the fines have a smaller $\bar{t}\left(d_p\right)$ than the coarse, the reason being larger elutriation rate $\kappa\left(d_p\right)$ values for the fines. In the extreme case, for fine solids where $\kappa\left(d_p\right) >> F_1 / W$,

$$\bar{t}_{fines}\left(d_p\right) = \frac{1}{\kappa\left(d_p\right)} \tag{5.84}$$

At the other extreme, for the coarse fractions that are not entrained, $\kappa\left(d_p\right)$=0, it becomes

$$\bar{t}_{coarse} = \frac{W}{F_1} \tag{5.85}$$

To find the composition of the outflow streams, combine equations (5.78), (5.79) and (5.81) and rearrange to give

$$F_1 p_1\left(d_p\right) = \frac{F_0 p_0\left(d_p\right)}{1 + \left(W / F_1\right) \kappa\left(d_p\right)} \tag{5.86}$$

Noting that the area under probability distribution curve is unity,

$$\int_0^{d_M} p(d_p)dd_p = 1, \quad \text{where } d_M \text{ is largest size in feed} \tag{5.87}$$

On integrating and rearranging equation (5.)

$$\frac{F_1}{F_0} = 1 - \frac{F_2}{F_0} = \int_{d_m}^{d_M} \frac{p_0(d_p)dd_p}{1+(W/F_1)\kappa(d_p)} \tag{5.88}$$

d_m is the smallest size in feed

5.3.2 Particles of changing size:

Considering the operations where the solid particles shrink and lose mass because of reaction, incineration, attrition or sublimation, or else grow larger and increase in mass because of deposition of material from the fluid and where the density of deposited material is that of particles themselves.

Rate Expressions for Growing and Shrinking particles:

The following are the rate expressions used to describe the change in particle size. For linear particle growth by deposition or condensation of material,

$$\Re(d_p) = \frac{d(d_p)}{dt} = k \tag{5.89}$$

For linear particle shrinkage by dissolution, sublimation, reaction or slow attrition,

$$\Re(d_p) = \frac{d(d_p)}{dt} = -k \tag{5.90}$$

In these expressions k is independent of particle size, but does depend on bed conditions. These kinetics are relatively easy to handle and closely represent most growth and shrinkage phenomenon.

5.4 General Performance Equation:

The general material balance equations and their various final integrated forms have been expresses here. The assumptions include steady state operations, an entering stream of solids F_0 (kg/s), an outflow stream F_1 (kg/s), an elutriating outflow stream of solids F_2 (kg/sec), spherical particles of constant density ρ_s, backmix flow in the bed (hence $p_b(d_p) = p_1(d_p)$), and the particle growth or shrinkage given by general rate expression $\Re(d_p)$. Then the mass balance on particles of size between d_p and $d_p + d(d_p)$ gives

$$\begin{pmatrix}\text{solids}\\ \text{entering in}\\ \text{feed}\end{pmatrix} - \begin{pmatrix}\text{solids}\\ \text{leaving in}\\ \text{overflow}\end{pmatrix} - \begin{pmatrix}\text{solids}\\ \text{leaving in}\\ \text{carryover}\end{pmatrix} + \left[\begin{pmatrix}\text{solids growing into}\\ \text{the interval from}\\ \text{a smaller size}\end{pmatrix} - \begin{pmatrix}\text{solids growing out}\\ \text{of the interval to}\\ \text{a larger size}\end{pmatrix}\right] + \begin{pmatrix}\text{solid generation}\\ \text{due to growth}\\ \text{within interval}\end{pmatrix} = 0 \quad (5.91)$$

Or, in symbols,

$$F_0 p_0(d_p) - F_1 p_1(d_p) - W\kappa(d_p) p_1(d_p) - W\frac{d\left[\Re(d_p) p_1(d_p)\right]}{dd_p} + \frac{3W}{d_p} p_1(d_p)\Re(d_p) = 0 \quad (5.92)$$

An overall mass balance represents the rate of generation or disappearance of all solids in the bed and is given by

$$F_1 + F_2 - F_0 = \int \frac{3W p_b(d_p)\Re(d_p) dd_p}{d_p} \quad (5.93)$$

For a feed of wide size distribution, integration of equation (5.) relates the flows and size distributions of the flowing streams. Thus, for growing particles the flows F_0 and F_1 are related by

$$\frac{W}{F_0} = \int_{d=d_m}^{d_t\to\infty} \frac{d_p^{\,3}}{\Re(d_p)} I(d_p, d_m) \int_{d_i=d_m}^{d_i=d} \frac{p_0(d_i)_i\, d(d_{pi})}{d_{pi}^3 I(d_{pi}, d_m)} d(d_p) \quad (5.94)$$

For shrinking particles

$$\frac{W}{F_0} = \int_{d_i \to \infty}^{d_M} \frac{d_p^{\,3}}{\Re(d_p)} I(d_p, d_M) \int_{d_i = d_p}^{d_i = d_M} \frac{p_0(d_i)_i \, d(d_{pi})}{d_{pi}^3 I(d_{pi}, d_m)} d(d_p) \tag{5.95}$$

For growing particles, the size distribution of feed and carryover streams are related by

$$p_1(d_p) = \frac{F_0 d_p^{\,3}}{W \Re(d_p)} I(d_p, d_m) \int_{d_i = d_m}^{d_i = d} \frac{p_0(d_i)_i \, d(d_{pi})}{d_{pi}^3 I(d_{pi}, d_m)} \tag{5.96}$$

And, for shrinking particles, by

$$p_1(d_p) = \frac{F_0 d_p^{\,3}}{W \Re(d_p)} I(d_p, d_M) \int_{d_i = d}^{d_i = d_M} \frac{p_0(d_i)_i \, d(d_{pi})}{d_{pi}^3 I(d_{pi}, d_M)} \tag{5.97}$$

In the above expressions d_m represents the smallest feed size for particle growth, d_M represents the largest feed size for particles and $I(d_p, d_{pi})$ represents the following

$$I(d_p, d_{pi}) = \exp\left[- \int_{d_{pi}}^{d_p} \frac{F_1 / W + E(d_p)}{\Re(d_p)} d(d_p) \right] \tag{5.98}$$

Where

$$E(d_p) = \frac{\kappa^*(d_p)}{L_{mf}(1 - \varepsilon_{mf}) \rho_s} \tag{5.99}$$

The last part of equation (5.95) was named as $F(d_p)$, such that:

$$F(d_p) = \int_{d_i = d}^{d_i = d_M} \frac{p_0(d_i)_i \, d(d_{pi})}{d_{pi}^3 I(d_{pi}, d_M)} \tag{5.100}$$

5.5 Procedure adopted:

Based on the smallest and largest particle size obtained in the sieve analysis, an approximate minimum and maximum size of particle was assumed, an imaginary interval was chosen and a grouped data of 11 elements was achieved. Then for each size of particle, the probability density function $p_0\left(d_p\right)$, elutriation rate $\kappa^*\left(d_p\right)$, elutriation constant $E\left(d_p\right)$, the function $I\left(d_p, d_{pi}\right)$ and the term $F\left(d_p\right)$ was calculated. To arrive at the $F\left(d_p\right)$ value, Simpson's 1/3rd rule was used.

After the $F\left(d_p\right)$ had been calculated for each size, it was used to evaluate the value given by

$$\frac{W}{F_0} = \int_{d_t \to \infty}^{d_M} \frac{{d_p}^3}{\Re\left(d_p\right)} I\left(d_p, d_M\right) F\left(d_p\right) \tag{5.101}$$

We have already calculated the value of shrinkage rate $\Re\left(d_p\right)$, so by assuming the value of F_0 as unity we can easily determine the value of W.

Then the value of W was used in the equation (5.97) to calculate $p_1\left(d_p\right)$. The values of $p_0\left(d_p\right)$ and $p_1\left(d_p\right)$ were plotted against d_p, the graph obtained was in consistence with the principles of fluidization.

5.6 Performance of a boiler:

The performance of a boiler is often measured in terms of its evaporative capacity. The amount of steam generated by the boiler in kg per hour at full load is known as evaporative capacity. This can also be represented in terms of kg/kg of fuel burnt.

Mathematically,

Evaporation rate = (Total steam produced) / (total fuel burnt) (kg/kg)

5.6.1 Boiler Efficiency:

According to the direct method, it is the ratio of heat required to convert water into steam to the heat liberated by the combustion of fuel at the same time. It is also said to be thermal efficiency of the boiler. Mathematically,

$$\eta_b = \left(\frac{heat\ required\ to\ produce\ the\ steam}{heat\ liberated\ \ from\ fuel} \right) = \left(\frac{m_s \left(h - h_{f1} \right)}{m_f \times CV} \right)$$

Where m_s = mass of steam produced in kg.

m_f = mass of fuel burnt in kg

The indirect method is also called the heat loss method. The efficiency can be calculated by subtracting the heat loss fractions from 100 as follows:

Efficiency of boiler (n) = 100 - (i + ii + iii + iv + v + vi + vii)

Whereby the principle losses that occur in a boiler are loss of heat due to:

i. Dry flue gas
ii. Evaporation of water formed due to H_2 in fuel

iii. Evaporation of moisture in fuel

iv. Moisture present in combustion air

v. Unburnt fuel in fly ash

vi. Unburnt fuel in bottom ash

vii. Radiation and other unaccounted losses

Losses due to moisture in fuel and due to combustion of hydrogen are dependent on the fuel, and cannot be controlled by design.

The data required for calculation of boiler efficiency using the indirect method are:

- Ultimate analysis of fuel (H_2, O_2, S, C, moisture content, ash content)
- Percentage of oxygen or CO_2 in the flue gas
- Flue gas temperature in ^oC (T_f)
- Ambient temperature in ^oC (T_a) and humidity of air in kg/kg of dry air
- GCV of fuel in kcal/kg
- Percentage combustible in ash (in case of solid fuels)
- GCV of ash in kcal/kg (in case of solid fuels)

A detailed procedure for calculating boiler efficiency using the indirect method is given below.

Step 1: Calculate the theoretical air requirement

$$= [(11.43 \times C) + \{34.5 \times (H_2 - O_2/8)\} + (4.32 \times S)]/100 \text{ kg/kg of fuel}$$

Step 2: Calculate the % excess air supplied (EA)

$$= \frac{O_2\% \times 100}{(21 - O_2\%)}$$

Step 3: Calculate actual mass of air supplied/ kg of fuel (AAS)

$$= \{1 + EA/100\} \times \text{theoretical air}$$

Step 4: Estimate all heat losses

i. Percentage heat loss due to dry flue gas

$$= \frac{m \times C_p \times (T_f - T_a) \times 100}{\text{GCV of fuel}}$$

Where, m = mass of dry flue gas in kg/kg of fuel

m = (mass of dry products of combustion / kg of fuel) + (mass of N_2 in fuel on 1 kg basis) + (mass of N_2 in actual mass of air we are supplying).

Cp = Specific heat of flue gas (0.23 kcal/kg)

ii. Percentage heat loss due to evaporation of water formed due to H_2 in fuel

$$= \frac{9 \times H_2 \{584 + C_p (T_f - T_a)\} \times 100}{\text{GCV of fuel}}$$

Where, H_2 = percentage of H_2 in 1 kg of fuel

Cp = specific heat of superheated steam (0.45 kcal/kg)

iii. Percentage heat loss due to evaporation of moisture present in fuel

$$= \frac{M \{584 + C\,p (T_f - T_a)\} \times 100}{\text{GCV of fuel}}$$

Where, M – % moisture in 1kg of fuel

C_p – Specific heat of superheated steam (0.45 kcal/kg)

iv. Percentage heat loss due to moisture present in air

$$= \frac{\text{AAS x humidity factor x } C_p (T_f - T_a)\} \text{ x } 100}{\text{GCV of fuel}}$$

Where, C_p – Specific heat of superheated steam (0.45 kcal/kg)

v. Percentage heat loss due to unburnt fuel in fly ash

$$= \frac{\text{Total ash collected/kg of fuel burnt x GCV of fly ash x } 100}{\text{GCV of fuel}}$$

vi. Percentage heat loss due to unburnt fuel in bottom ash

$$= \frac{\text{Total ash collected per Kg of fuel burnt x G.C.V of bottom ash x } 100}{\text{GCV of fuel}}$$

vii. Percentage heat loss due to radiation and other unaccounted loss

The actual radiation and convection losses are difficult to assess because of particular emissivity of various surfaces, its inclination, airflow patterns etc. In a relatively small boiler, with a capacity of 10 MW, the radiation and unaccounted losses could amount to between 1% and 2% of the gross calorific value of the fuel, while in a 500 MW boiler; values between 0.2% to 1% are typical. The loss may be assumed appropriately depending on the surface condition.

Step 5: Calculate boiler efficiency

Efficiency of boiler (n) = 100 - (i + ii + iii + iv + v + vi + vii)

Evaporation Ratio = Heat utilized for steam generation/Heat addition to the steam

Table 5.4: Heat balance sheet of the boiler

Heat supplied	KJ	%	Heat utilized	KJ	%
Heat supplied by The fuel	130200000	100			
			Heat utilized in raising the steam	101405000	77.88
			Heat lost to flue gases	1188	7.30
			Heat lost in moisture	362.32	2.23
			Heat lost due to unburnt carbon	440	2.7
			Heat lost due to incomplete combustion	11.82	0.073
			Heat lost to steam due by combustion of hydrogen	1583.1	9.727
			Losses unaccountable such as radiation, convection etc.		0.1
Total	Q	100%	----	Q	100%

Table 5.3: Heat balance sheet

CHAPTER 6

Results and Discussion

6.1 Input Data:

The input data required for the model development has been taken from the Malwa power Ltd., Muktsar (Punjab). The plant is a 7.5 MW thermal power plant using the FBC process. The following table shows the data collected from the plant:

Parameter	**Symbol**	**Value**	**Units**
Fuel feed rate	W_{fuel}	2.7778	kg/s
Moisture content	XW	0.1388	-
Carbon content	XC	0.4237	-
Hydrogen content	XH	0.0567	-
Sulphur content	XS	0.0	-
Oxygen content	XO	0.3658	-
Nitrogen content	XN	1.5014	-
Fractional excess air	E_{xair}	0.3	-
Bed temperature	T_b	1023	K
Pressure in the combustor	P_{av}	1.01	atm
Cross-sectional area of the bed	A_t	19.43	m^2
Number of orifice openings	N_d	842	-
Bed height at minimum fluidization	H_{mf}	0.7	m
Particle density	ρ_p	116.1	kg/m^3
Particle size	d_p	0.01183	m
Gas constant	R_g	0.08206	atm-m^3/ (kg-mole K)
Bed diameter	D_R	4.9738	m
Ratio of coud-wake volume to bubble volume	f_{cw}	0.5	-
Mean voidage under minimum fluidization	ε_{mf}	0.3	-

Table 6.1: Input Data for the model

After the hydrodynamic parameters have been calculated, we start with the development of mathematical model. First of all, the fuel sample collected from the plant is passed through a sieve analysis in sand testing laboratory, thereby, getting the fraction of weight lying in particular size intervals. The distribution obtained is given as under:

dp(mm)	dp(mm)	dpi	Weight in interval(gms)	%age weight fraction
-80mm	+40mm	60mm	29	25.56
-40mm	+20mm	30mm	38.5	33.92
-20mm	+10mm	15mm	24.5	21.58
-10mm	+4.75mm	7.375mm	14.5	12.77
-4.75mm	+2.36mm	3.555mm	3	2.643
-2.36mm	+1.18mm	1.77mm	2	1.762
-1.18mm	+600µm	0.89mm	2	1.762

Table 6.2: Size distribution of feed particles

The model has been developed to predict the solid population balance in the fluidized bed which enables it to conclude about the solid population density being carried out of the vessel when a given size density is being fed into the vessel. It helps to decide about the sizes that have maximum and minimum probability of being carried out of vessel; hence, it signifies the equilibrium between the solids being fed to bed and being carried out of the bed.

Figure 6.1 shows the change in minimum fluidization velocity due to particle size, the figure includes the results obtained by using different expressions given by a variety of authors. Though all the expressions gave satisfactory results, but those of Chitester et. al. were most reliable and appropriate, so Chitester et. al.'s expression was used in this model. As the figure indicates, the minimum fluidization velocity increases with increase in particle size. As the weight of the particle increase with size, hence the drag force

required to hold and counter the weight also increases. Thus, the fluidization velocity also increases with the particle size.

The superficial velocity depends upon various factors, out of which moisture content of the fuel is one variable. Given that the other parameters involved are kept constant, the superficial velocity decreases with the increase in moisture content as shown in figure 6.2. This is because, the superficial velocity is dependent upon the stochiometrical oxygen supply (kg-mole/sec) required for complete combustion of the fuel being fed to the bed, which in-turn is inversely proportional to the moisture content in the fuel. More is the moisture content, lesser is the oxygen requirement. Hence, the superficial velocity decreases with the increase in moisture content. The bed temperature also affects the superficial velocity. As the volumetric flow rate of fluidizing air is directly proportional to the bed temperature, thus the superficial velocity increases with rise in bed temperature, as shown in figure 6.3. Whereas figure 6.4, shows the effect of excess air on superficial velocity. The stochiometrical oxygen supply required for complete combustion of the fuel is used to calculate the actual air being supplied to the fluidized. The actual supply is directly proportional to the excess air being supplied which is further directly proportional to the superficial velocity. Thus, superficial velocity increases with increase in excess air.

Bubble diameter constitutes one of the important parameter of bubble properties. Figure 6.6 shows the effect of superficial velocity on bubble diameter. The literature provides us the fact that the air in excess of minimum fluidization velocity is responsible for bubbles. From this, we can conclude that the bubble diameter should increase as the superficial velocity rises, which is, in consistence with the curve in the figure 6.6. The bubble grows in size as it moves up in the fluidized bed; this phenomenon has been indicated by the figure 6.7. The bubble diameter at various heights in the bed has been shown in the figure.

As discussed earlier that the air in excess of minimum fluidization velocity moves up the bed in form of bubbles. So it sums up that an increase in minimum fluidization velocity, while keeping the superficial velocity unchanged, would result in bubbles of lesser diameter. In accordance, the figure 6.8 shows that the bubble diameter decreases with increase in minimum fluidization velocity. As we know that the minimum

fluidization velocity is directly proportional to the particle diameter, thus we can predict that, keeping all other variables unchanged, the bubble diameter would decrease with increase in particle size.

The particles that are fed into the bed, many a time, shrink due to heat. Flaking ash or gaseous products cause shrinkage in size and with time the particles may even disappear. Firstly the gases diffuse to the surface of the particle, and then it either reacts at the surface of the particle or penetrates a short distance into the fine pores of the solid before reacting. Hence the shrinkage rate depends upon the surface reaction rate constant and mass transfer coefficient. Further, the shrinkage rate is directly proportional to the oxygen concentration in particulate phase, thus shrinkage rate increases with rise in oxygen concentration in particulate phase as shown in figure 6.9. The particle shrinkage rate is also affected by particle diameter size. The figure 6.10 shows the change in shrinkage rate with particle size. As the correlation for the shrinkage rate has particle diameter in inverse proportion, thus the shrinkage rate decreases with the increase in particle size. It's in consistence with the shrinkage model that predicts the diffusion of gases into the particle before reacting with the particle; thus the gases would take longer time to diffuse into a large particle and the shrinkage rate would be low for a larger particle.

The expression for the initial oxygen concentration shows that it is inversely proportional to the bed temperature. The figure 6.11 shows the change in initial oxygen concentration with change in bed temperature.

The Transport Disengagement Height (TDH) is the height above which the entrainment rate becomes constant and it is recommended that the exit of flue gases must be kept above TDH for minimum particulate entrainment from the vessel. The literature gives an expression for estimating the TDH in accordance with the bubble diameter. Figure 6.12 shows the effect of bubble diameter on TDH and it shows that the fluidized beds with large bubbles have higher TDH.

In figure 6.13, variation of Sherwood number with feed particle has been shown. It can be seen in the expression for Sherwood number that it is directly proportional to the particle size so, as particle size increases, Sherwood number also tends to increase.

Figures 6.14 and 6.15 show the variation of reaction rate constant (K) with char surface temperature and the variation of gas phase diffusion coefficient with bed temperature. It can be observed that as bed temperature increases, gas phase diffusion coefficient also tends to increase. Further, reaction rate constant also increases with an increase in char temperature. The reasons for an increase gas phase diffusion coefficient is that with an increase in temperature, the movement of molecules gets enhanced, because of which more molecules are able to diffuse through.

Figure 6.16 shows the probability density of the particles being fed into the bed. It shows the number/weight/volume of the particles between particular intervals of size that are being fed. It shows that the probability is high for medium range of particles and it is relatively low for very large and small particles.

Scope of future work:

- Actual particle shrinkage rate needs to be found out.
- Particle attrition in freeboard needs to be studied.
- Effect of distribution plate on fluidization parameters needs to be studied.

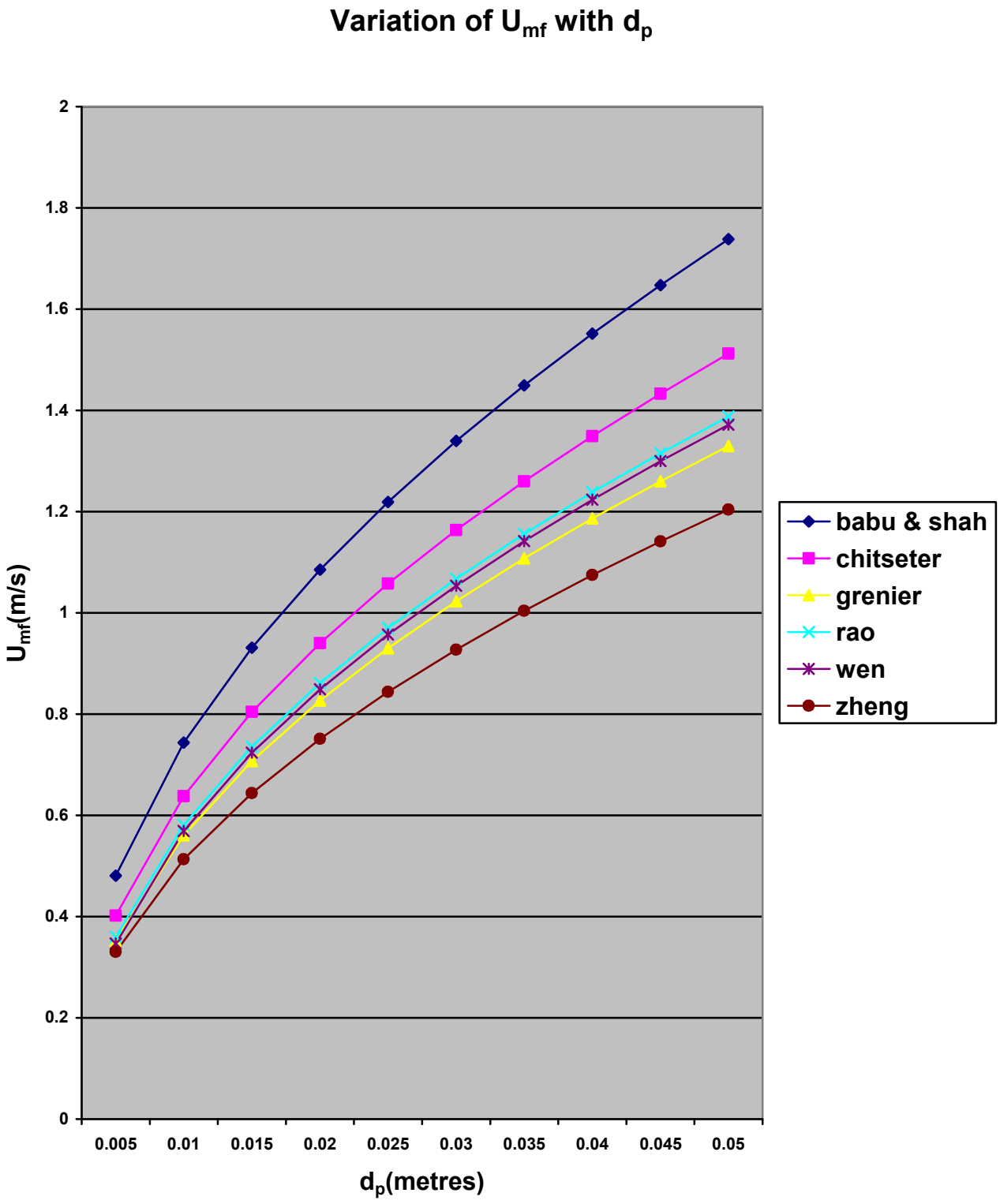

Figure 6.1: Effect of particle diameter on minimum fluidization velocity

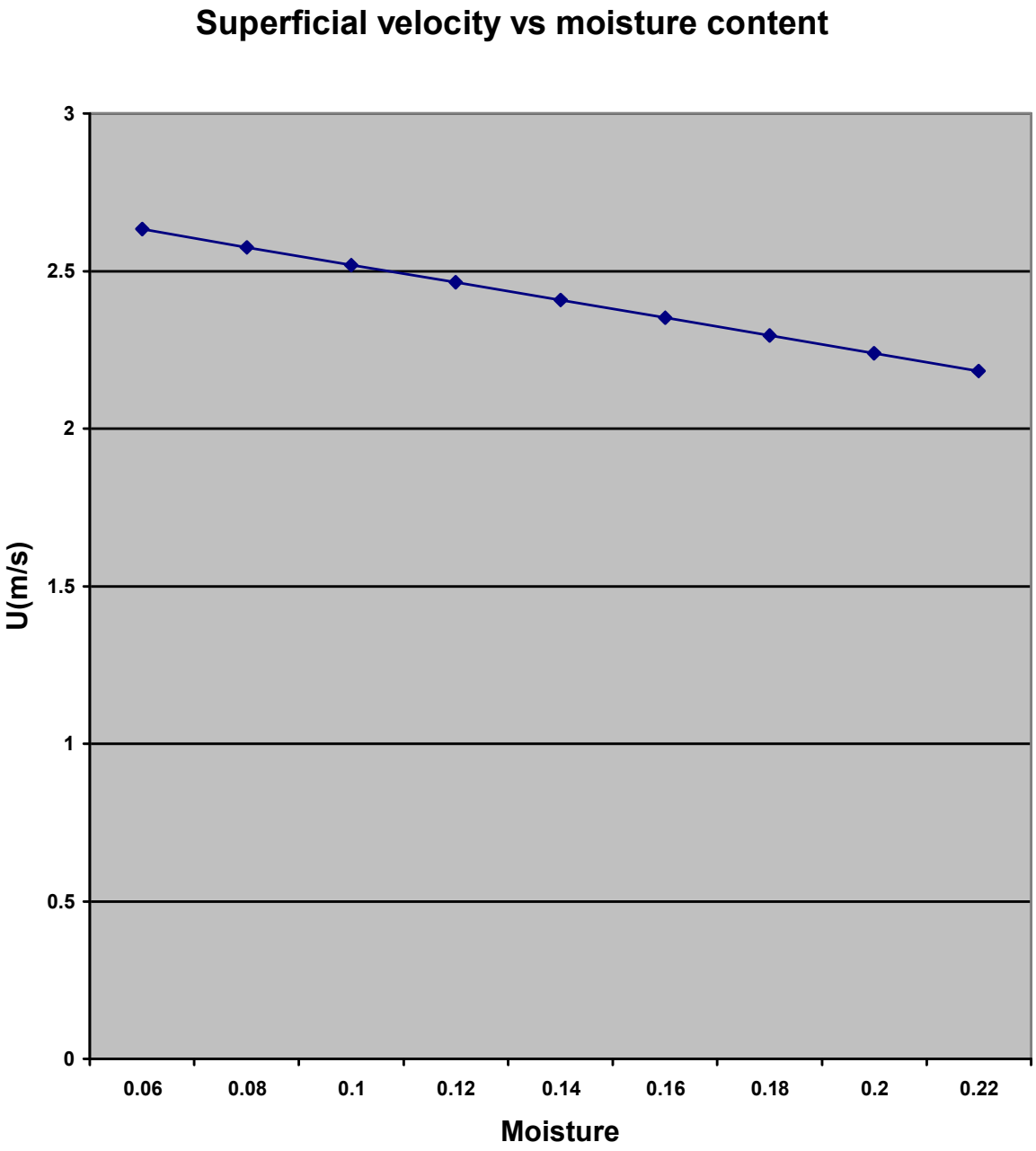

Figure 6.2: Effect of moisture content on superficial velocity

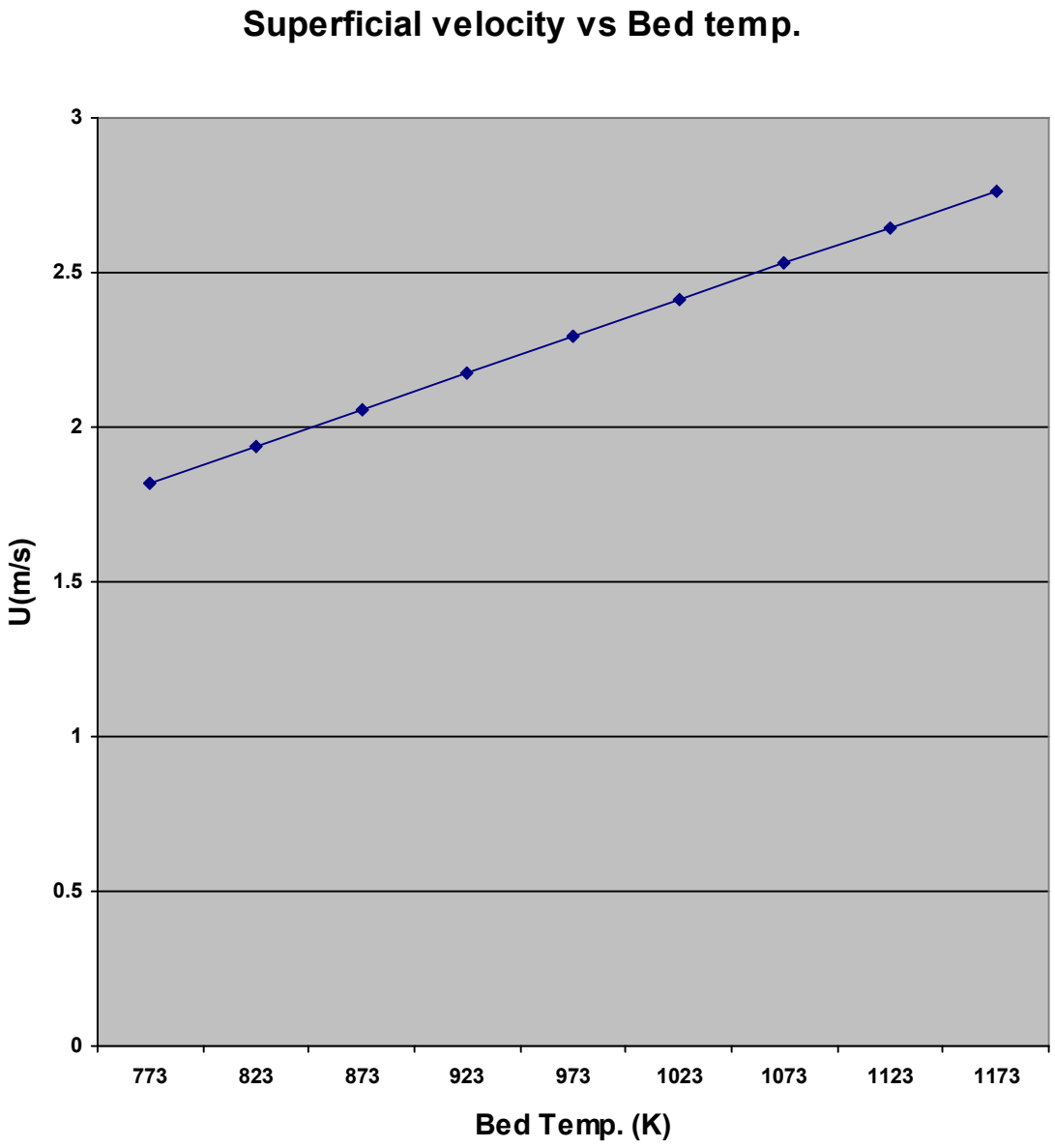

Figure 6.3: Effect of bed temperature on superficial velocity

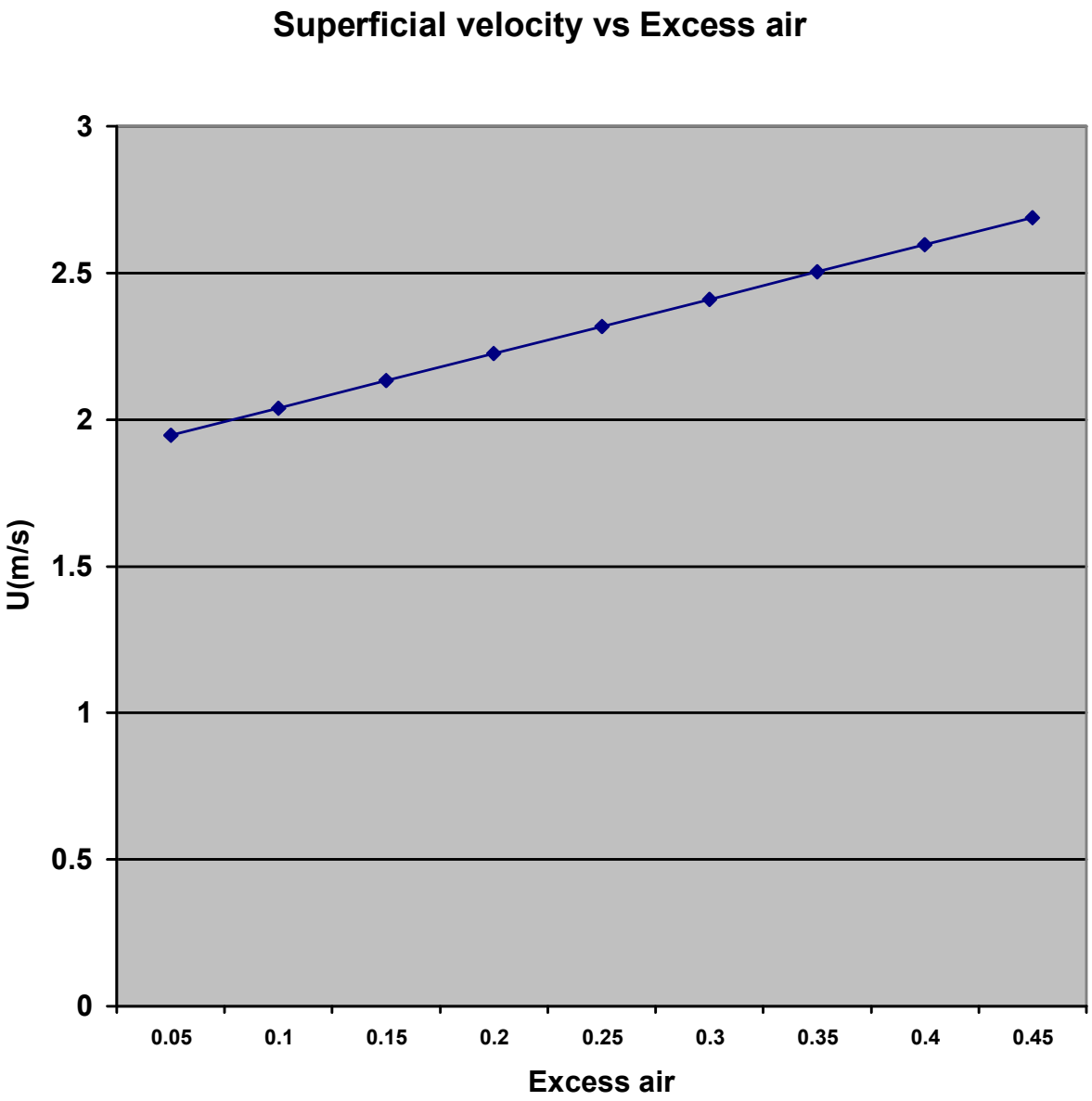

Figure 6.4: Effect of excess air on superficial velocity

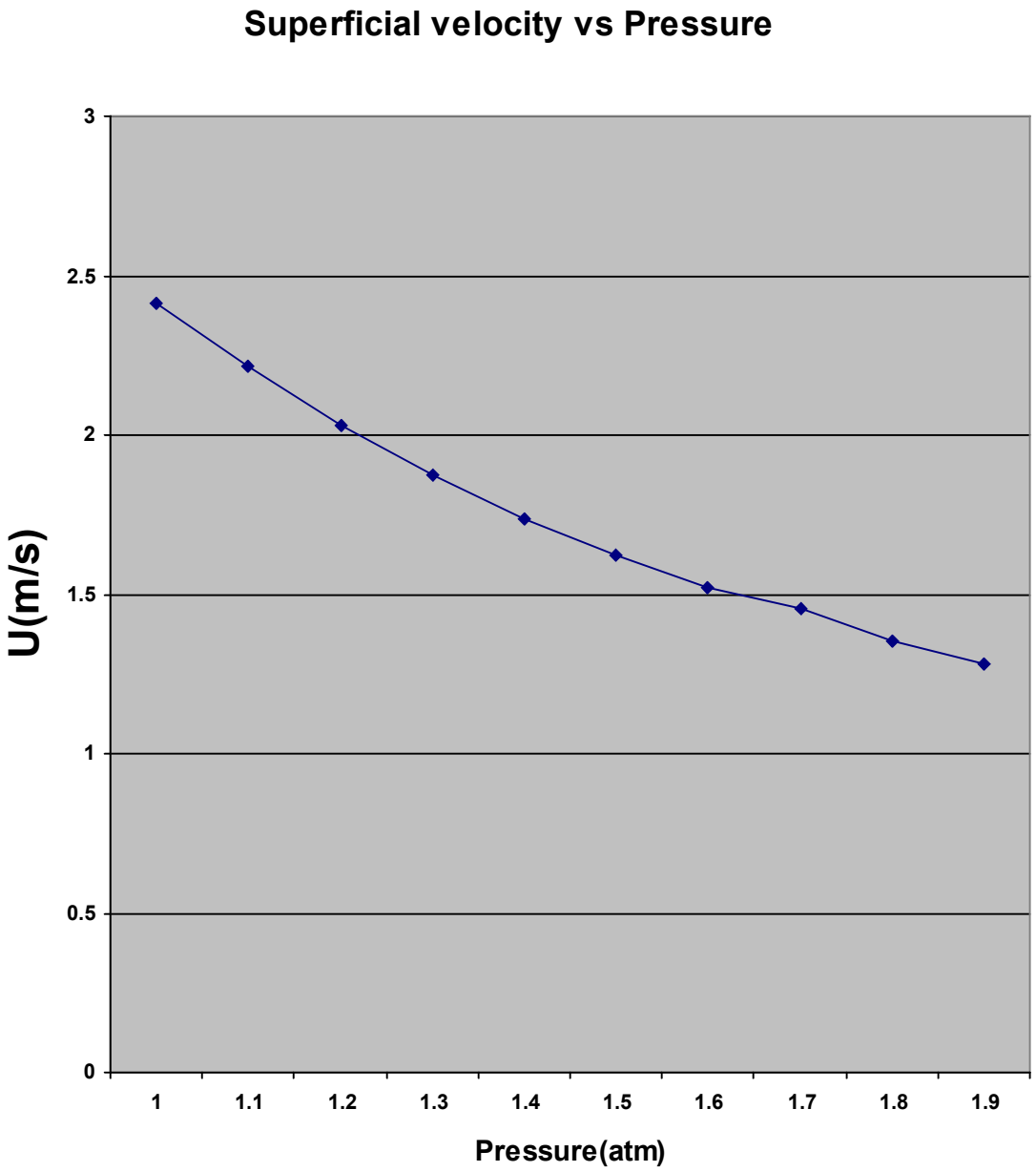

Figure 6.5: Effect of pressure on superficial velocity

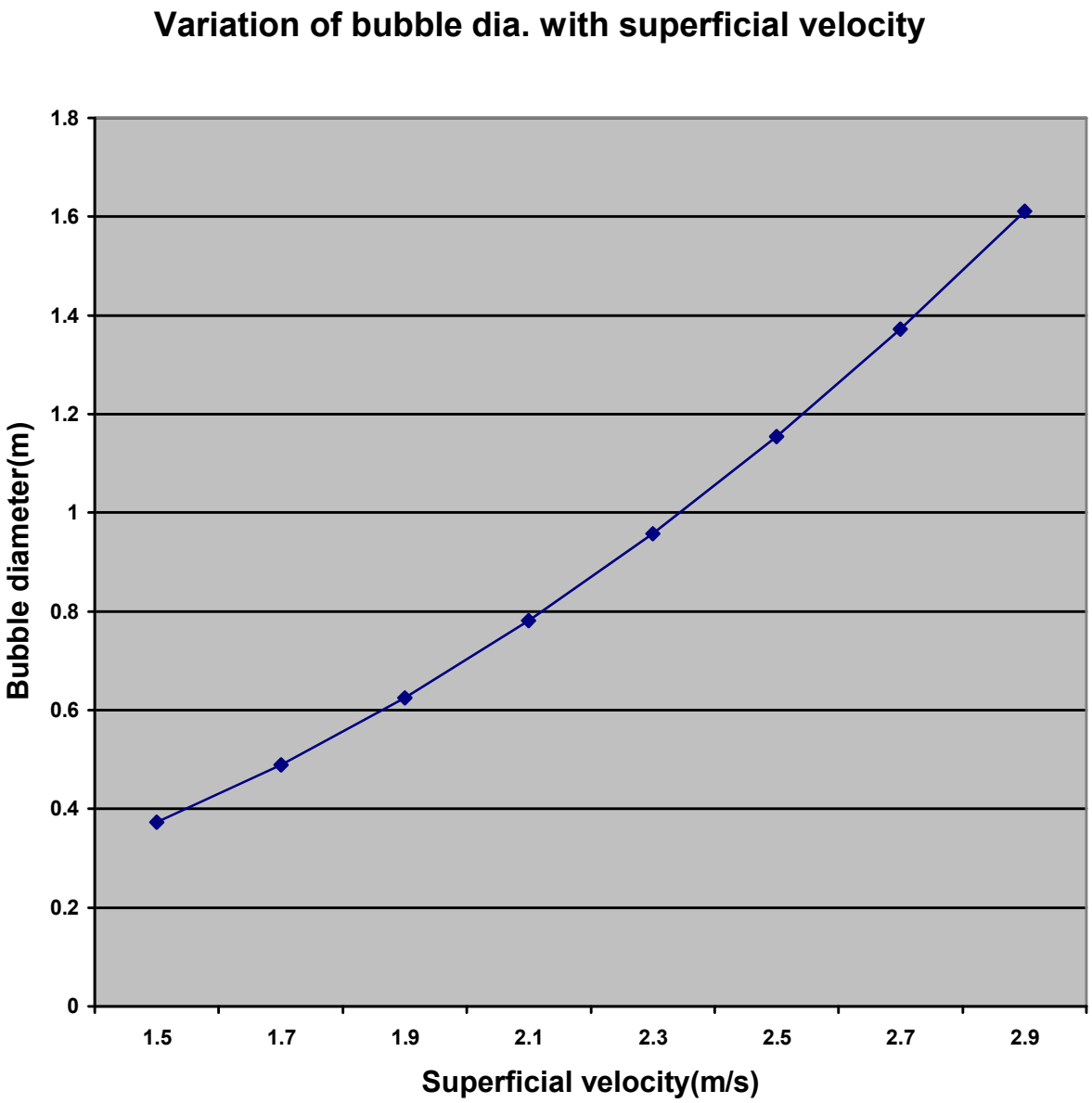

Figure 6.6: Effect of superficial velocity on bubble diameter

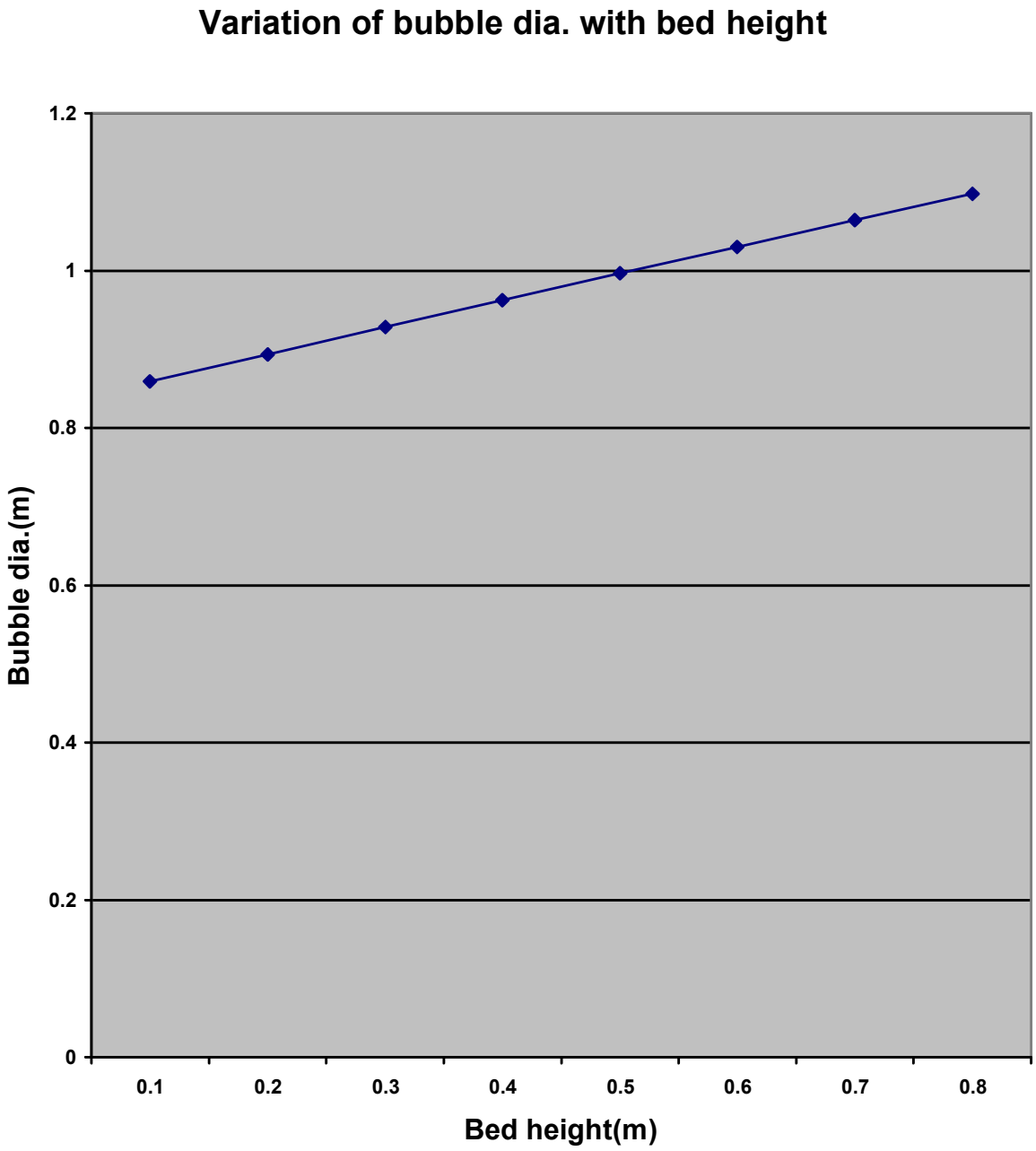

Figure 6.7: Bubble diameter at various bed heights

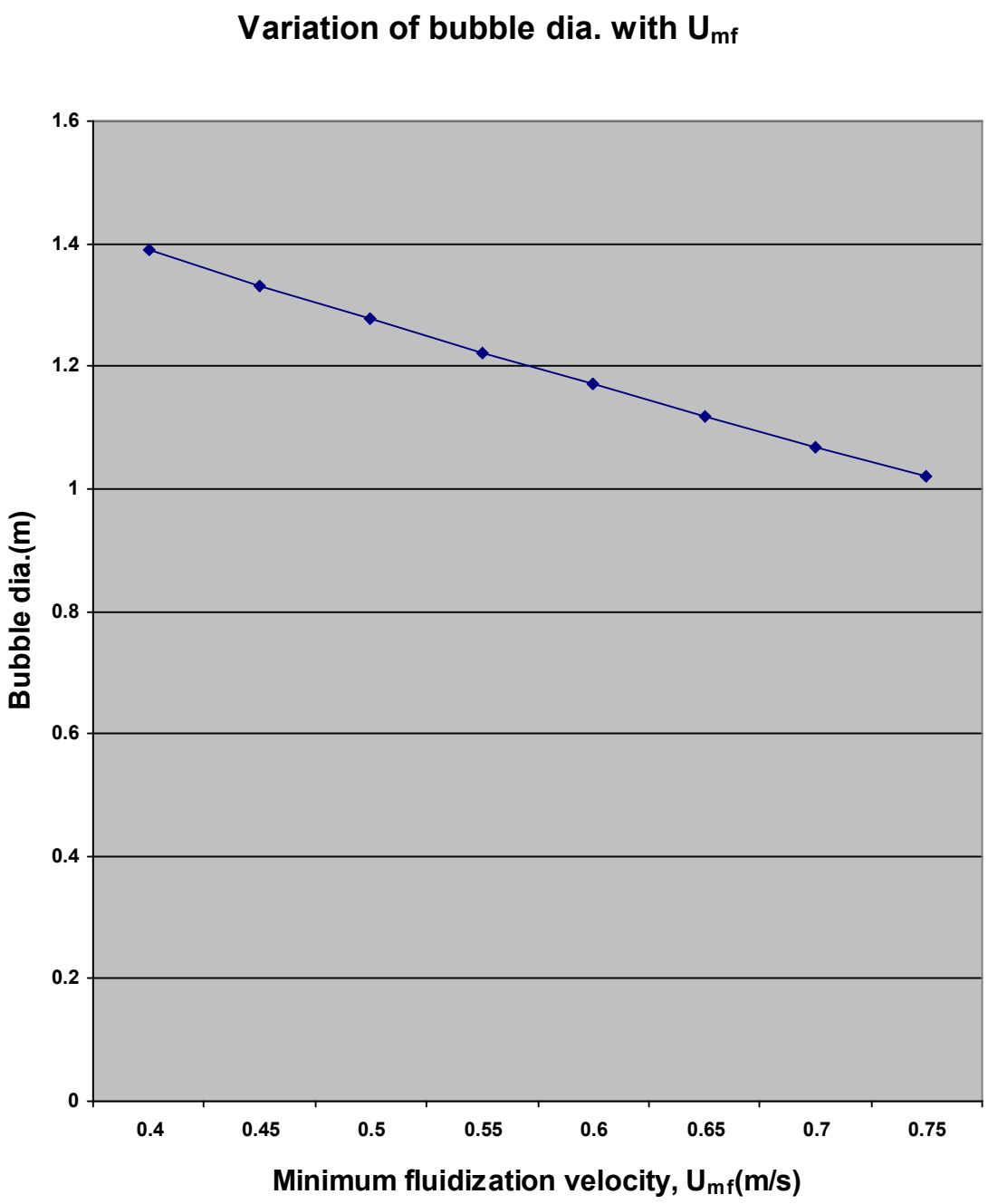

Figure 6.8: Effect of minimum fluidization velocity on bubble diameter

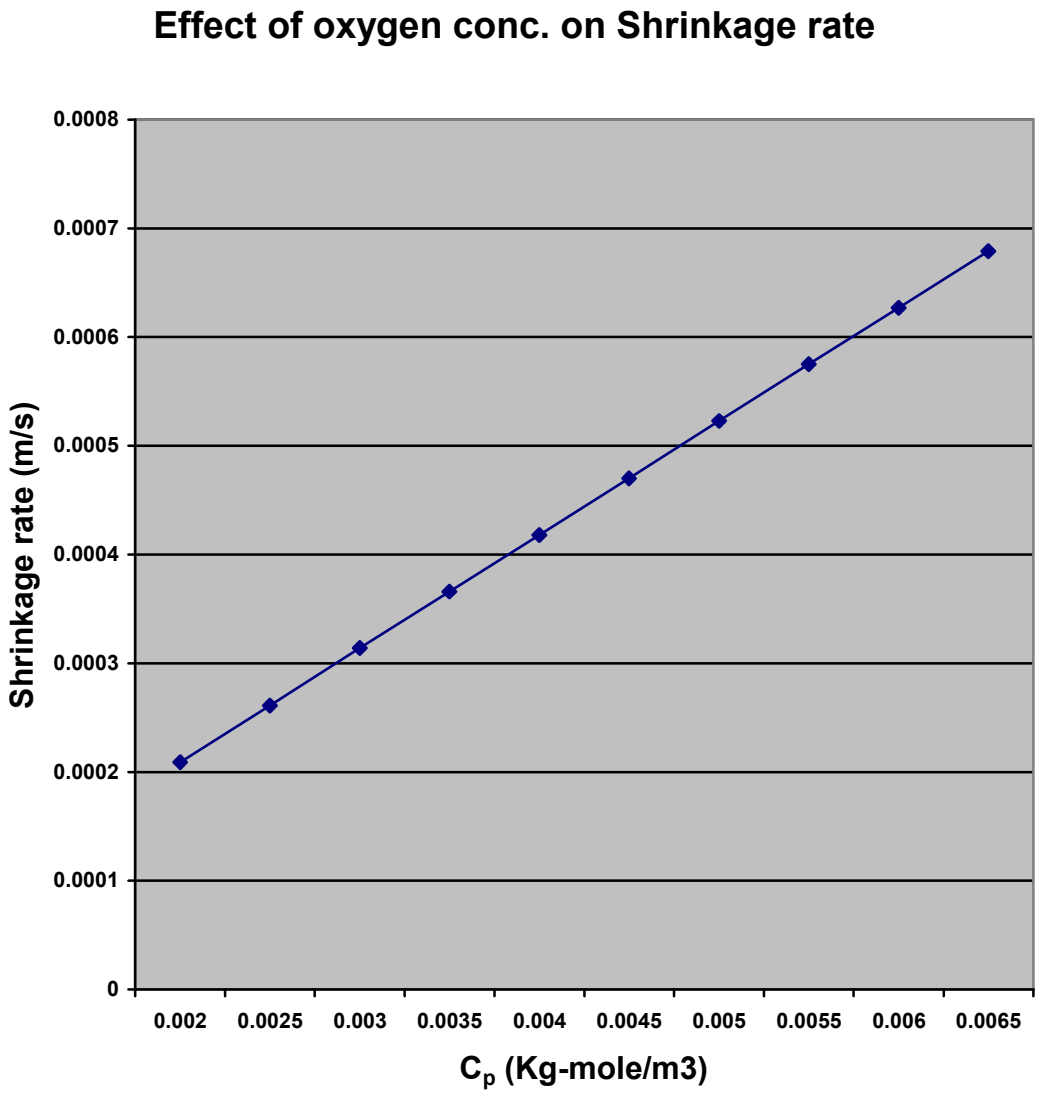

Figure 6.9: Effect of oxygen in particulate phase on shrinkage rate

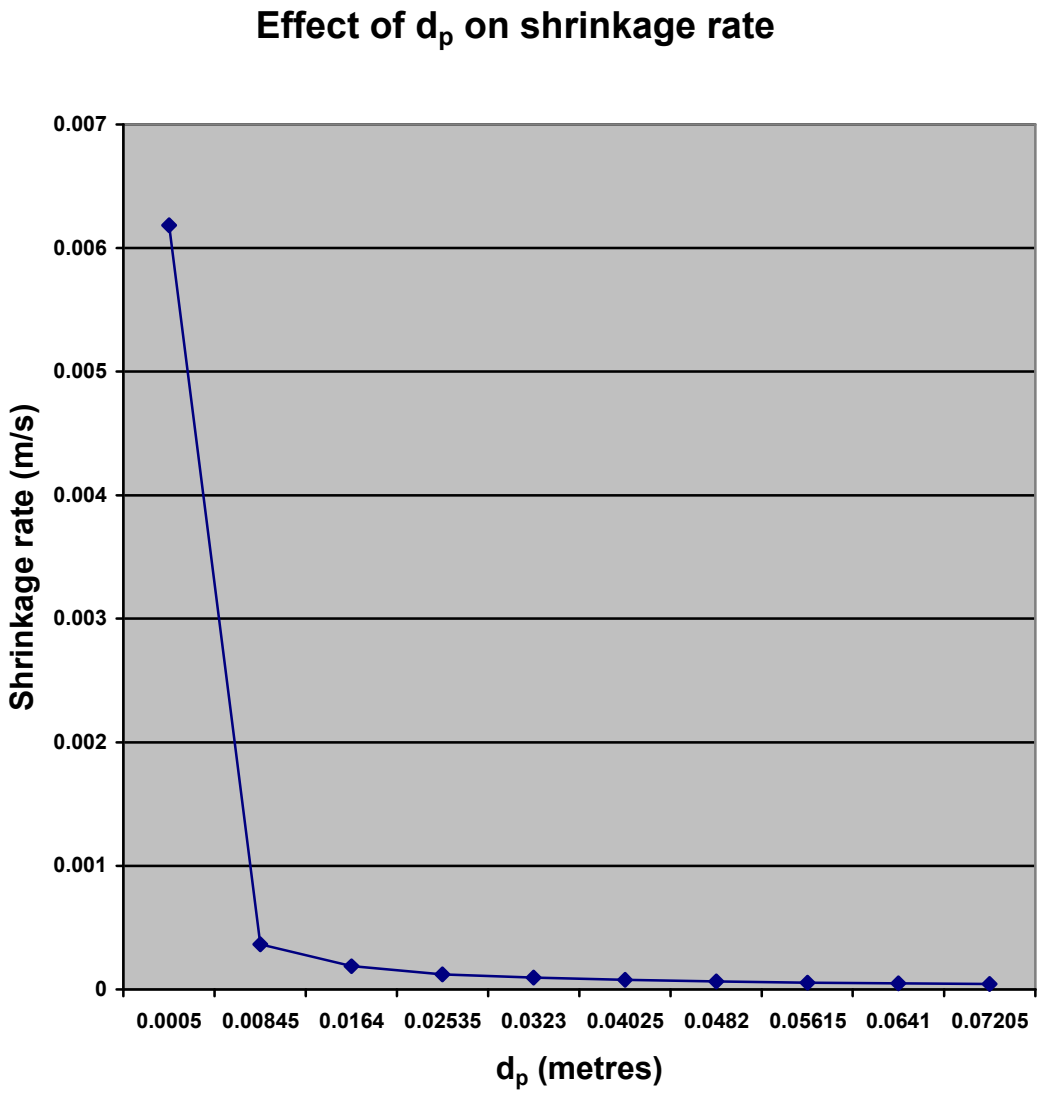

Figure 6.10: Change in shrinkage rate with particle diameter

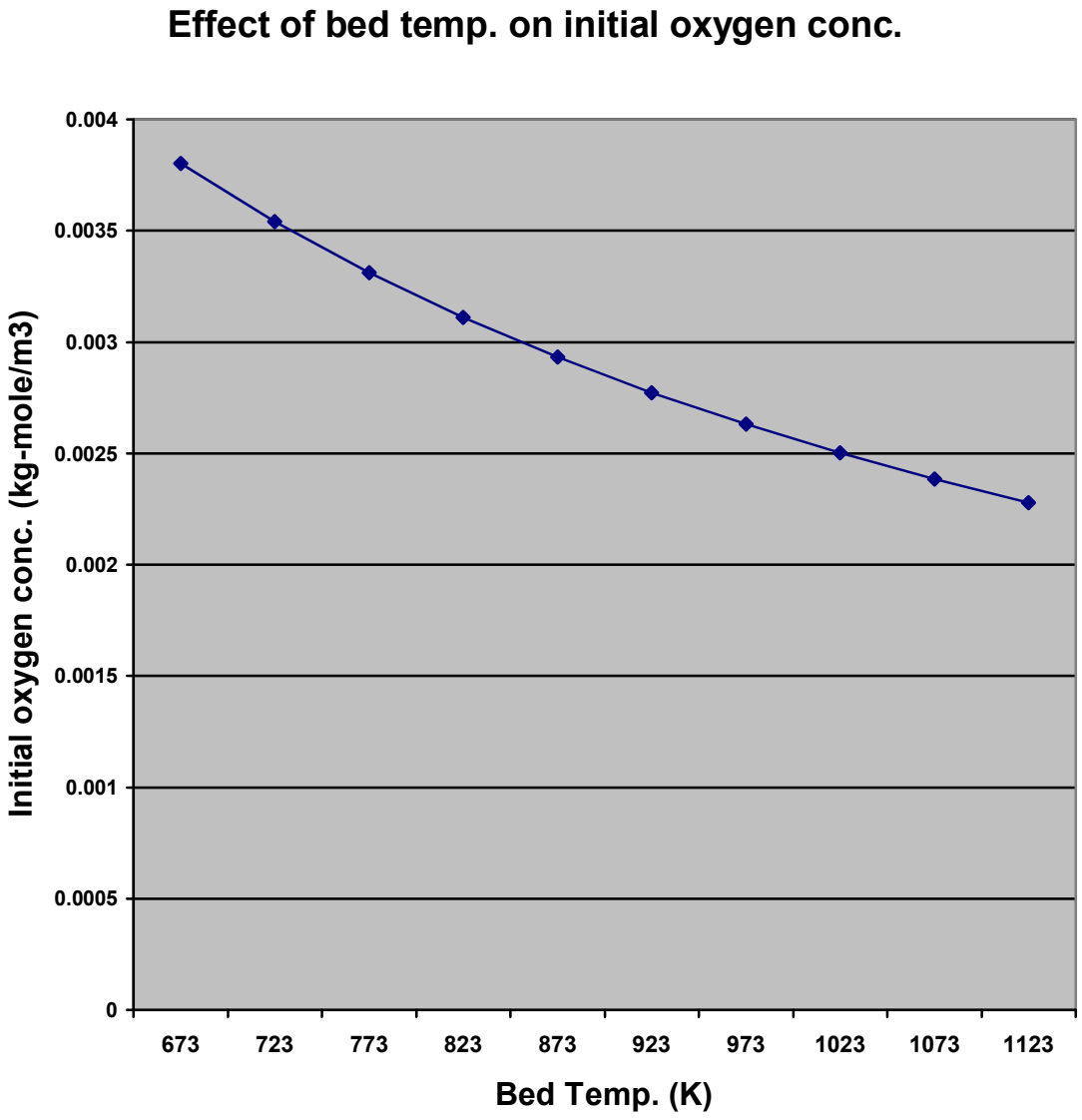

Figure 6.11: Effect of bed temperature on initial oxygen concentration

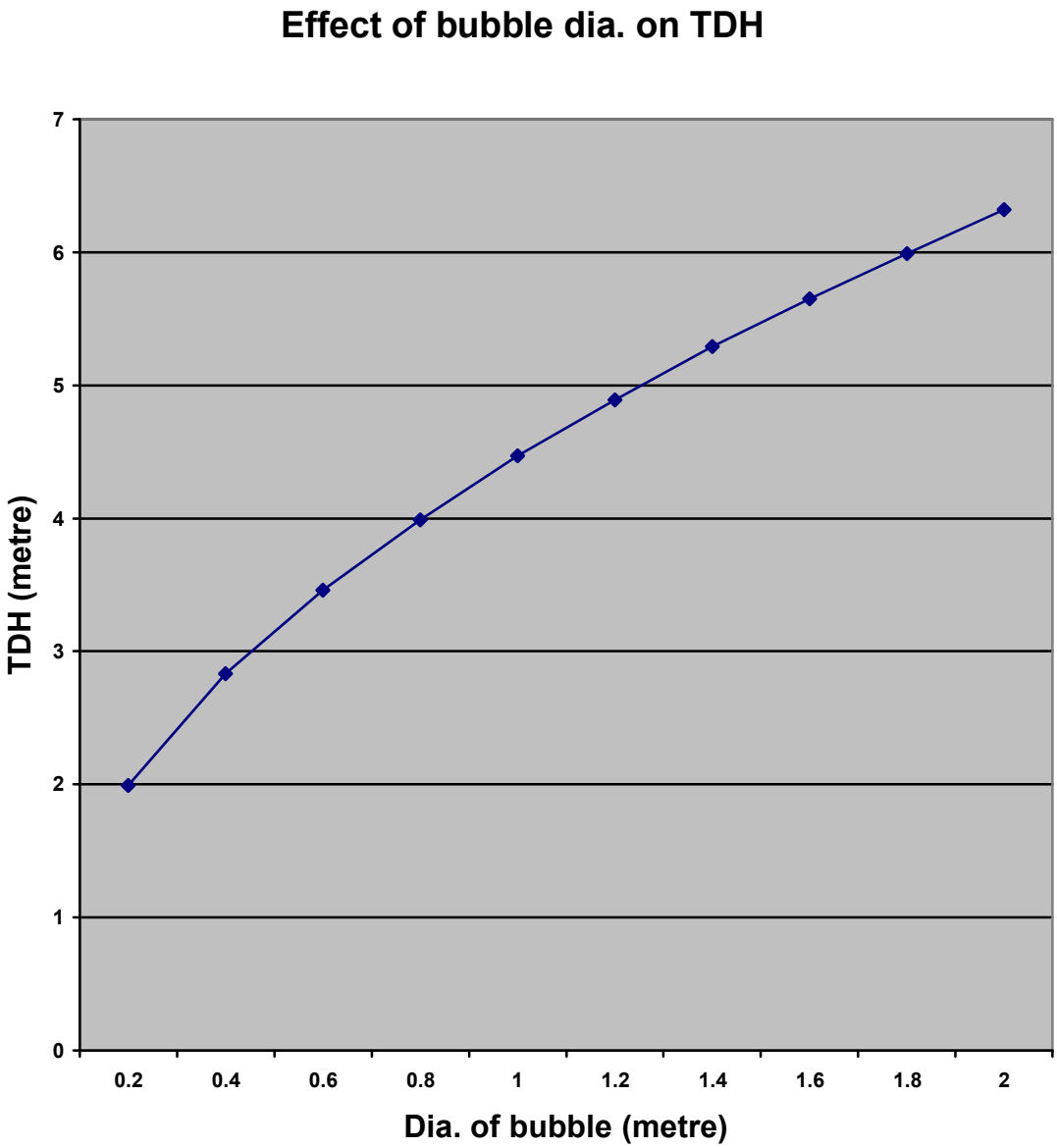

Figure 6.12: Effect of bubble diameter on TDH

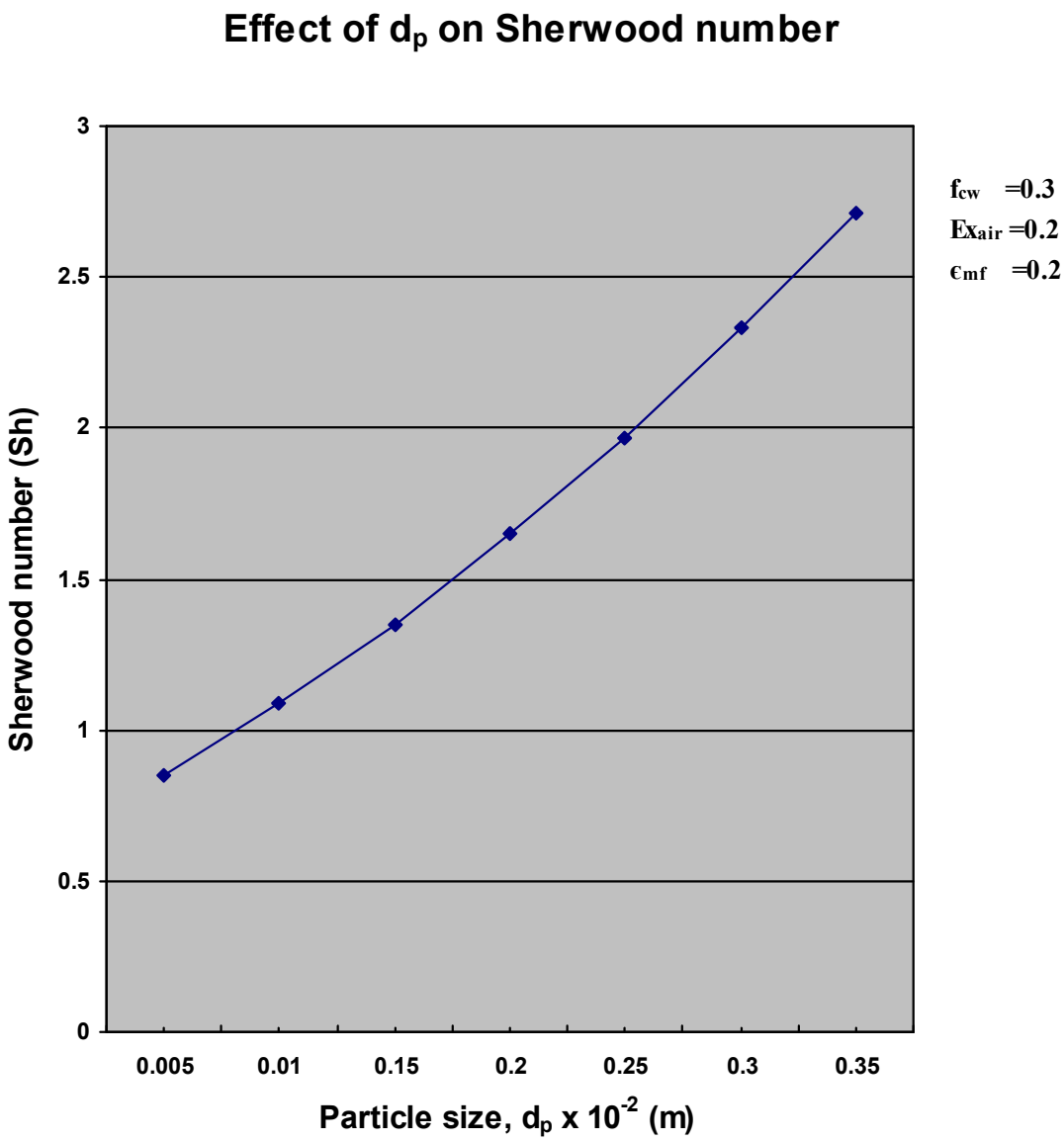

Figure 6.13: Effect of particle size on Sherwood number

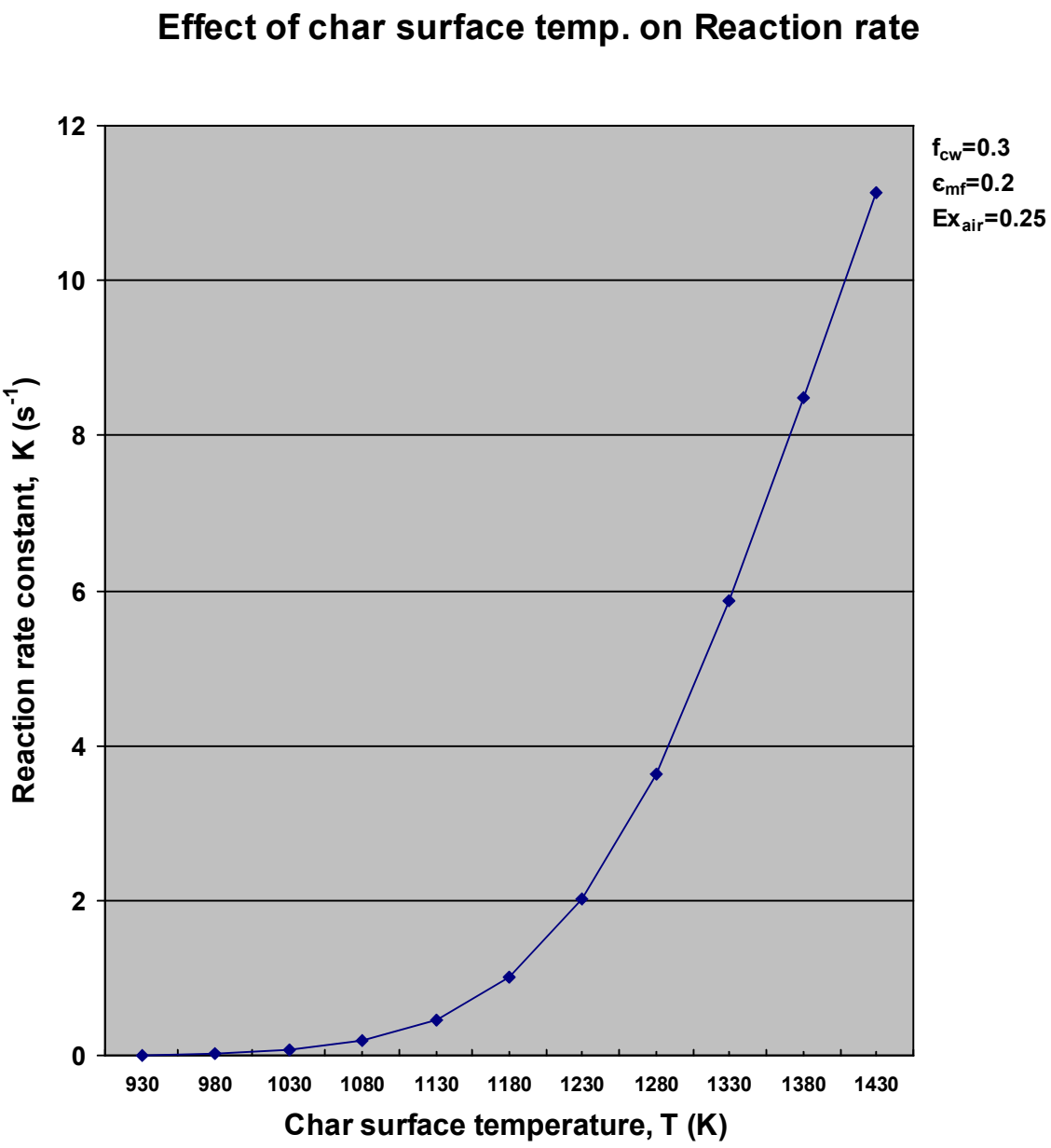

Figure 6.14: Change in reaction rate constant with change in char surface temperature

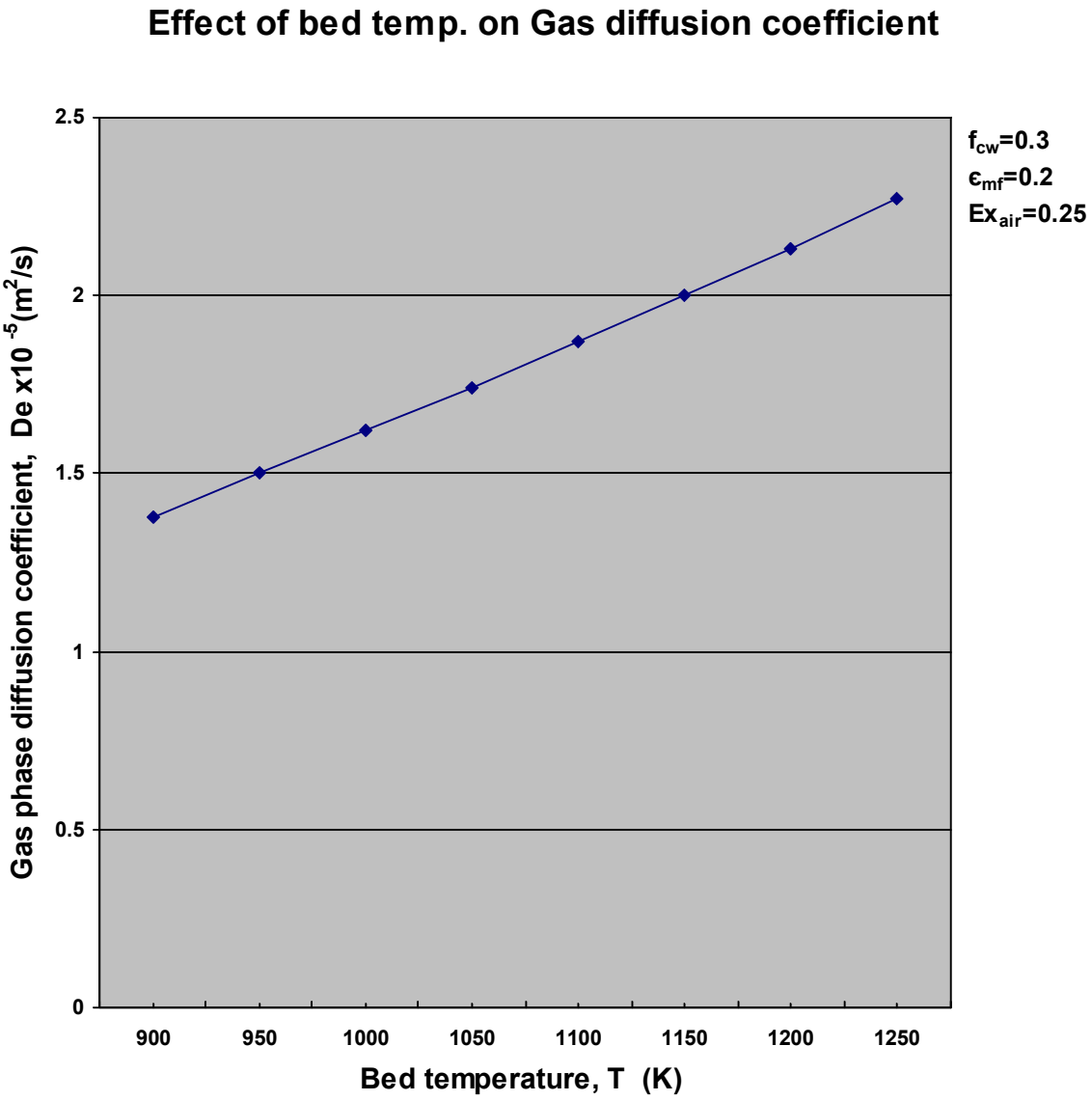

Figure 6.15: Effect of bed temperature on Gas diffusion constant

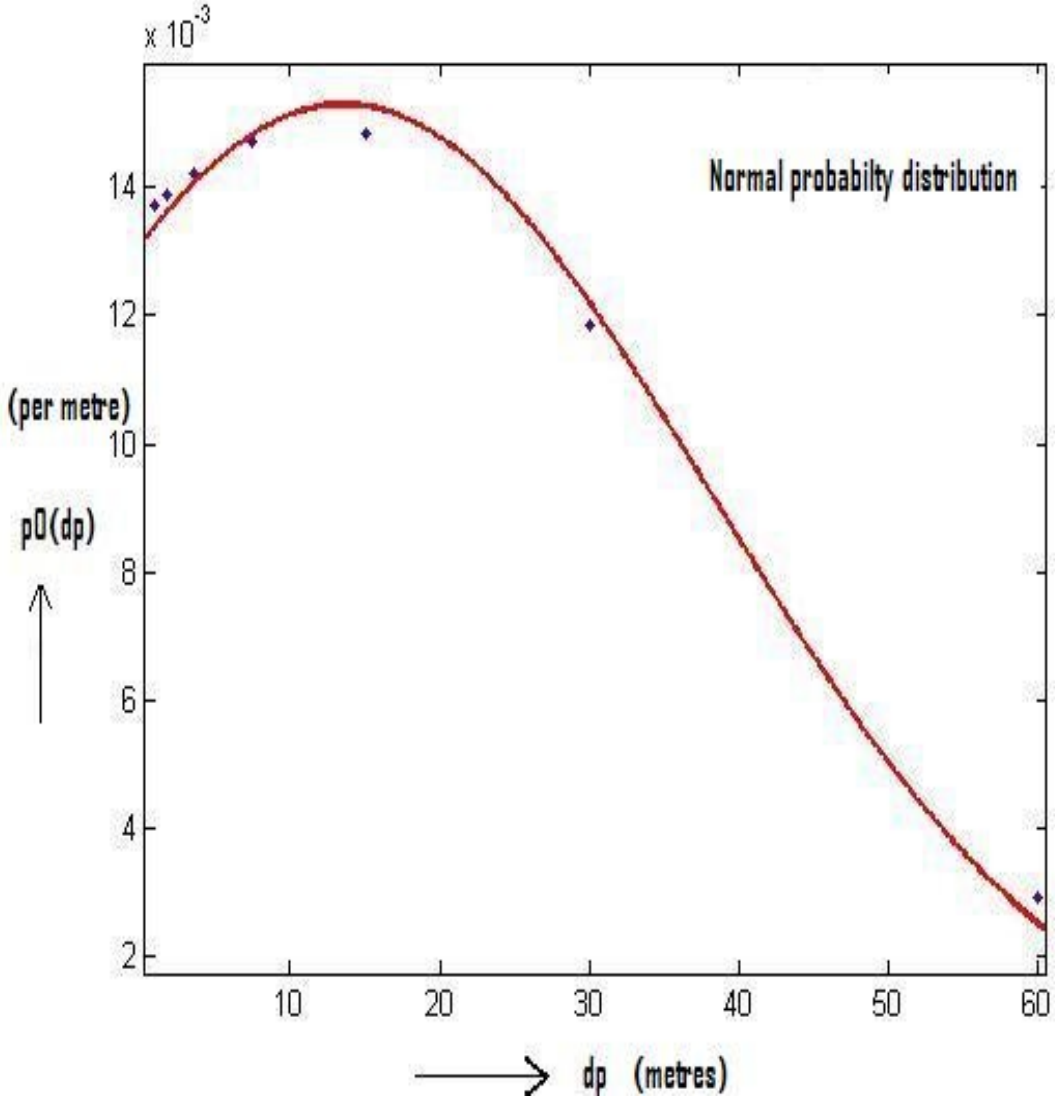

Figure 6.16: Probability density function

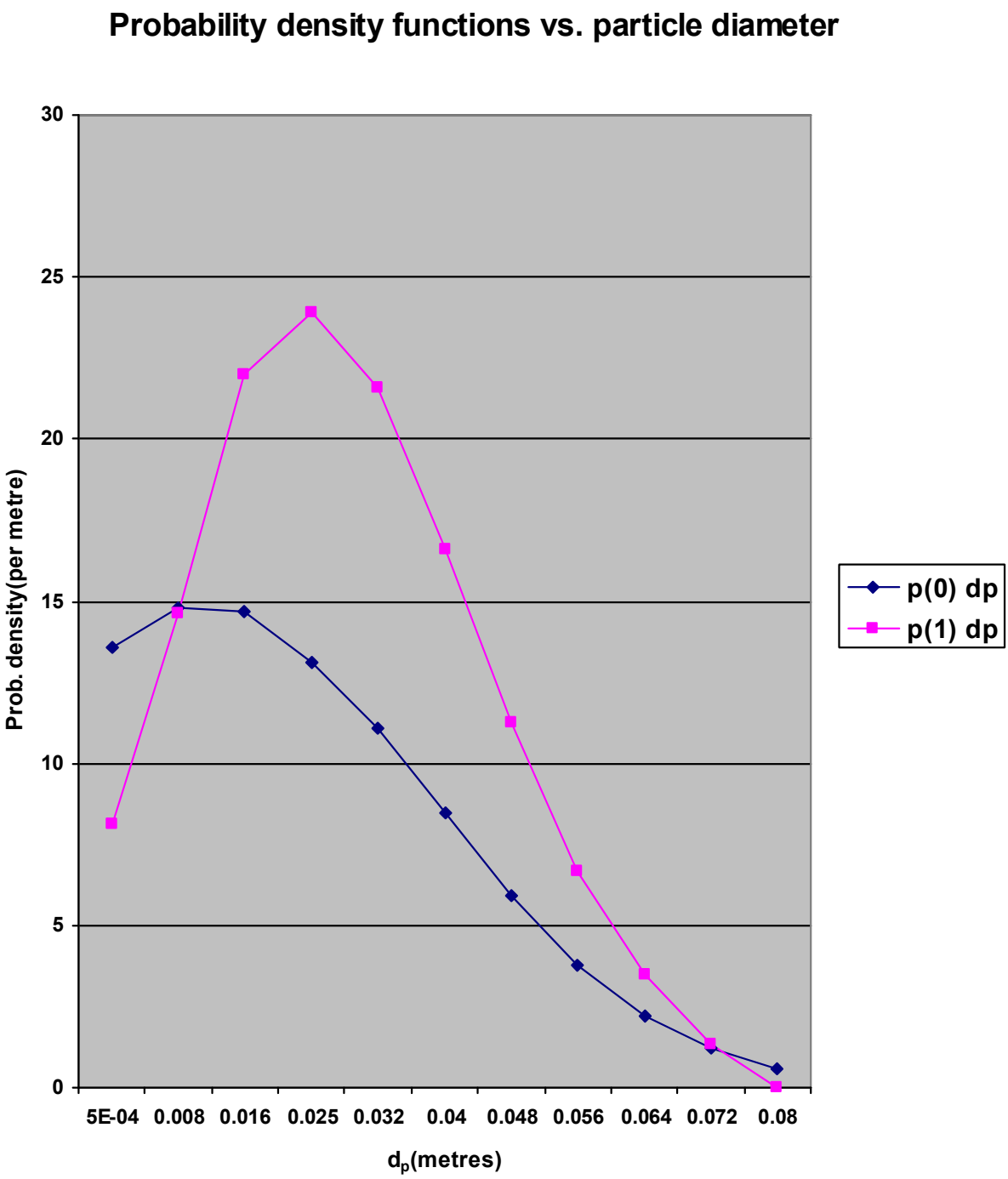

Figure 6.17: $p_0(d_p)$ & $p_1(d_p)$ versus particle diameter

References

[1] Ahmadzadeh, A., Arastoopour, H. and Teymour, F., Numerical simulation of gas and particle flow in a rotating fluidized bed, *Ind. Eng. Chem. Res.*, Vol.**42**, 2627-2633, (2003).

[2] Bizon, K., Fluidized bed combustion of fossil and alternate fuels, *30th Meet on combustion*, Italian Section of the Combustion Institute, (2006).

[3] Chang, S., Kang, Y. and Kim, S., Mass transfer in two and three-phase fluidized beds, *Department of Chemical Engineering,* Korea Advanced Institute of Science and Technology, Seoul, (1987).

[4] Choi, J., Son, J., and Kim, S., Solid entrainment in Fluidized bed combustors, *Journal of Fluids Engineering,* Vol.**22**, no.6, ASME, (1989).

[5] Degirmenci, E., Seluk, N., and Gogebakan, Y., Modeling of a bubbling fluidized bed combustor with volatiles release, *Journal of Energy Resources Technology,* 72-125, (2003).

[6] Delebarre, A., Does the minimum fluidization exist? , *Journal of Fluids Engineering,* ASME, Vol. **124**, 595-600, (2002).

[7] Faravelli, T., Frassoldati, A., and Ranzi, E., Modeling homogeneous combustion in bubbling beds burning liquid fuels, *Journal of energy resources technology,* ASME, Vol. **129**, 33-41, (2007).

[8] Fu, Y. and Liu, D., Novel experimental phenomenon of fine-particle fluidized beds, *Experimental Thermal and Fluid Science*, Vol. **32**, 341-344, (2007).

[9] Garbett, E., Nigassa, M. and Hedley, M., The effect of coal particle size on the performance of a fluidized bed coal combustor, *Sheffield coal research unit,* Department of Chemical Engineering and Fuel Technology, U.K, (1983).

[10] Grosso, W. and Chiovetta, M., Modeling fluidized bed reactor for the catalytic polymerization of ethylene: Particle size distribution effects, *Latin American Applied Research,* Vol.**35**, 67-76, (2005).

[11] Janvijitsakul, K., Kuprianov, V. and Permchart, W., Co-firing of rice husk and bagasse in a conical fluidized-bed combustor, *The Joint International Conference on "Sustainable Energy and Environment (SSE)"*, Hua Hin, Thailand, **3-016(O)**, 232-237, (2004).

[12] Jiang, H., Zhu, X., Guo, Q. and Zhu, Q., Gasification of rice husk in a fluidized-bed gasifier without inert additives, *Ind. Eng. Chem. Res.,* Vol.**42**, 5745-5750, (2003).

[13] Khan, A., Jong, W., Gort, D. and Spliethoff, H., A fluidized bed biomass combustion model with discretized population balance. 1. Sensitivity analysis, *Energy and Fuels,* Vol.**21**, 2346-2356, (2007).

[14] Kim, S. and Kang, Y., Heat and mass transfer in three phase fluidized bed reactors: An overview, *Elsevier Science Ltd., Chemical Engineering Science,* Vol. **52**, Nos. 21, 22, 3639-3660, (1997).

[15] Kunii, D., and Levenspiel, O., Fluidization Engineering, Butterworth-Heinemann, a division of Reed Publishing, USA, (1991).

[16] Larachi, F., Iliuta, I., Rival, O. and Grandjean, B., Prediction of minimum fluidization velocity in three-phase fluidized-bed reactors, *Ind. Eng. Chem. Res.,* Vol.**39**, 563-572, (2000).

[17] Liu, H., Li, Y. and Guo, Q., Fluidization quality improvement for cohesive particles by fine powder coating, *Ind. Eng. Chem. Res.,* Vol.**45**, 1805-1810, (2006).

[18] Loffler, G., Andahazy, D., Wartha, C., Winter, F., and Hofbauer, H., NOx and N_2O formation mechanisms- Detailed chemical kinetic modeling study on a single fuel particle in a Laboratory-Scale fluidized bed, ASME, Vol.**123**, 228-235, (2001).

[19] Mancuhan, E., Modeling of combustion of low grade lignites in fluidized beds with heat extraction, *Proceedings of the 15th International Conference on Fluidized Bed Combustion*, Paper No. FBC99-0015, (1999).

[20] Mansaray, K.G., Al-Taweel, A.M., and Hamdullapur, F., Mathematical modeling of fluidized bed rice husk gasifier: Part-III-Model Verification, *Energy Sources,* Vol.**22**, 281-296, (2000).

[21] Mastral, A., Garcia, T., Callen, M., Lopez, J., Murillo, R. and Navarro, M., Effects of limestone on polycyclic aromatic hydrocarbon emissions during coal atmospheric fluidized fed combustion, *Energy and Fuels,* Vol.**15**, 1469-1474, (2001).

[22] Miccio, F., Scala, F, and Chirone, R., Fluidized bed combustion of a biomass fuel: Comparision between pilot scale experiments and model simulations, *Journal of Heat Transfer*, ASME, Vol. **127**, 117-122, (2005).

[23] Mihalyko, C., Lakatos, B., Matejdesz, A. and Blickle, T., Population balance model for particle-to-particle heat transfer in gas-solid systems, *International Journal of Heat and Mass Transfer*, Vol.**47**, 1325-1334, (2004).

[24] Mitchell, R., Campbell, P. and Ma, L., Characterization of coal and biomass conversion behaviors in advanced energy systems, *GCEP Technical Report,* (2004).

[25] Muthukrishnan, M., Sundararajan, S., Viswanathan, G., Rajaram, S., Kamalanathan, N., and Ramakrishnan, P., Salient features and operating experience with world's first rice straw fired fluidized bed boiler in a 10 MW power plant, Bharat Heavy Electricals Limited.

[26] Ngampradit, N., Piumsomboon, P., and Sajjakulnukit, B., Simulation of a circulating fluidized bed combustor with shrinking core and emission models, *ScienceAsia,* Vol.**30**, 365-374, (2004).

[27] Niu, F. and Subramaniam, B., Particle fluidization with supercritical carbon dioxide: Experiments and theory, *Ind. Eng. Chem. Res.,* Vol.**46**, 3153-3156, (2007).

[28] Ohman, M. and Nordin, A., Bed agglomeration characteristics during fluidized bed combustion of biomass fuels, *Energy and fuels,* Vol.**14**, 169-178, (2000).

[29] Ramirez, J., Martinez, J. and Petro, S., Basic design of a fluidized bed gasifier for rice husk on a pilot scale, *Latin American Applied Research,* Vol.**37**, 299-306, (2007).

[30] Ravelli, S., Perdichizzi, A. and Barigozzi, G., Description, applications and numerical modeling of bubbling fluidized bed combustion in waste-to-energy plants, *Progress Energy Combustion Science,* 1-34, doi:10.1016/j.pecs.2007.07.002, (2007).

[31] Rawlings, J., Witkowski, W. and Eaton, J., Control issues arising in population balance models, Department of Chemical Engineering, *The University of Texas at Austin*, Texas, 677-682, (1989).

[32] Saastamoinen, J., Tourunen, A., Hamalainen, J., Hyppanen, T., Loschkin, M. and Kettunen, A., Analytical solutions for steady and unsteady state particle size distributions in FBC and CFBC boilers for non-breaking char particles, *Combustion and Flame*, Vol.**132**, 395-405, (2003).

[33] Skinner, D.G., The Fluidized combustion of coal, Mills & Boon, London, 59-85, (1971).

[34] Skrifvars, B.G., Zevenhoven, M., Backman, R., and Hupa, M., Predicting the ash behavior of different fuels in fluidized bed combustion, Process Chemistry Group, Abo Akademi University, Finland.

[35] Subramani, H., Balaiyya. M.B. and Miranda, L., Minimum fluidization velocity at elevated temperatures for Geldart's group-B powders, *Experimental Thermal and Fluid Science,* Vol.**32**, 166-173, (2007).

[36] Toomey, R.D. and Johnstone, H.F., Gaseous fluidization of solid particles, *Chem. Eng. Prog*., **48**, pp. 220–226, (1952).

[37] Wang, F., Chen, S., Lei, P. and Wu, C., Effects of pressure drop and superficial velocity on the bubbling fluidized bed incinerator, *Journal of Environmental Sciences and Health Part A,* Vol.**42**, 2147-2158, (2007).

[38] Yagi, S., and Kunii, D., Studies on combustion of carbon particles in flames and fluidized bed, *5th Int. Symposium on combustion,* Reinhold, NY, (1955).

[39] Yates, Y., Fundamentals of Fluidized Bed Chemical Processes, *Butterworths,* page 40, (1983).

Appendix

Output of the C++ program prepared for the development of the model:

Enter the value of rhos = 116.1 kg/cubic metre

Enter the value of dp= 0.0118388 metre

The Archimedes no. is = 6797993

The minimum fluidization velocity is = 0.704192 m/s

The Reynold's no. at minimum fluidization is= 551.510803

The voidage at minimum fluidization is = 0.413374

Fth is = 0.433472

Fme is = 0.563513

The superficial velocity U is =2.410555 m/s

Terminal velocity =5.862228 m/s

The dia. of the bubble just above the distributor = 0.824004 m

The maximum bubble dia. is= 6.651791 m

The effective bubble diameter is = 0.861182 m

Rise velocity of bubble w.r.t emulsion phase = 1.918576 m/s

The bubble velocity is = 3.624938 m/s

The T.D.H is = 4.148156 m

The ratio of cloud to bubble volume is = 23.76413

This gives absurd value so we assume fc=0.5 & fw=0.3

Enter the value of fc & fw
0.5
0.3

The ratio of cloud-wake to bubble volume is= 0.8

Superficial velocity of bubble is= 1.282305 m/s

Superficial velocity of cloud-wake is=0.424058 m/s

Fraction of bubbles in the bed= 0.353745

The cross-sectional area of bubble is= 6.873272 sq.metre

Cross-section area of bed occupied by cloud-wake is= 5.498618 sq.metre

Area of bed available for gas flow in cloud-wake phase is= 2.272987 sq.metre

The volumetric flow rate through cloud-wake phase is= 8.239439 cubic metre per second

The volumetric flow rate through bubble phase is= 24.915186 cubic metre per second

The volumetric flow rate through emulsion phase is= 13.682455 cubic metre per second

The total volumetric flow rate is= 46.837082 cubic metre

The gas interchange coefficient Kbc is = 3.785119

The coefficient Kce is = 0.063746

The coefficient Kbe is= 0.062691
enter the value of bed particle size = 0.001 m

The Sherwood number is = 16.96899

Schmidt number is = 0.211713

The mass transfer coefficient is = 0.10234

The overall reaction rate constant is = 0.102339

The oxygen concentration in particulate phase is = 0.002502 Kg-mole/cubic metre

Shrinkage rate is = 0.000261 m/s

Enter the value of dp = 0.0005 metre

$p_0(d_p)$	Elutriation	$E(d_p)$	$I(d_p)$	$F(d_p)$
13.637178	0.000004	0.000000	0.999974	109100204032.000000
14.800833	0.000000	0.000000	1.000000	24531046.000000
14.704670	0.000000	0.000000	1.000000	3333679.750000
13.373092	0.000000	0.000000	1.000000	926264.437500
11.133094	0.000000	0.000000	1.000000	330375.875000
8.484130	0.000000	0.000000	1.000000	130109.695312
5.918427	0.000000	0.000000	1.000000	52852.453125
3.779312	0.000000	0.000000	1.000000	21348.306641
2.209157	0.000000	0.000000	1.000000	8387.888672
1.182083	0.000000	0.000000	1.000000	3160.429443
0.578998	0.000000	0.000000	1.000000	1130.855103

F0is = 289406752.000000

F1 0is = 0.036176

****

****

Enter the value of dp = 0.00845

$p_0(d_p)$	Elutriation	$E(d_p)$	$I(d_p)$	$F(d_p)$
14.800833	0.000000	0.000000	1.000000	24531046.000000
14.772908	0.000000	0.000000	1.000000	3887538.500000
13.726124	0.000000	0.000000	1.000000	1164209.500000
11.872217	0.000000	0.000000	1.000000	443470.531250
9.559117	0.000000	0.000000	1.000000	187650.593750
7.164829	0.000000	0.000000	1.000000	82832.773437
4.999146	0.000000	0.000000	1.000000	36856.445313
3.247042	0.000000	0.000000	1.000000	16189.778320
1.963280	0.000000	0.000000	1.000000	6926.029785
1.105041	0.000000	0.000000	1.000000	2858.769287
0.578997	0.000000	0.000000	1.000000	1130.854004

F1is = 107456.234375

F1 1is = 0.064834

****

****

Enter the value of dp = 0.01640

$p_0(d_{p)}$	Elutriation	$E(d_{p)}$	$I(d_{p)}$	$F(d_{p)}$
14.704669	0.000000	0.000000	1.000000	3333678.500000
13.726124	0.000000	0.000000	1.000000	1164209.500000
12.107915	0.000000	0.000000	1.000000	490337.656250
10.092984	0.000000	0.000000	1.000000	225979.343750
7.950574	0.000000	0.000000	1.000000	108548.390625
5.918426	0.000000	0.000000	1.000000	52852.429687
4.163348	0.000000	0.000000	1.000000	25634.181641
2.767629	0.000000	0.000000	1.000000	12241.315430
1.738609	0.000000	0.000000	1.000000	5708.787109
1.032107	0.000000	0.000000	1.000000	2584.539795
0.578997	0.000000	0.000000	1.000000	1130.853149

F2is = 22104.679688

F1 2is = 0.097503

****

****

Enter the value of dp = 0.02535

$p_0(d_p)$	Elutriation	$E(d_p)$	$I(d_p)$	$F(d_p)$
13.131917	0.000000	0.000000	1.000000	806109.812500
11.598543	0.000000	0.000000	1.000000	396384.687500
9.825087	0.000000	0.000000	1.000000	205747.453125
7.982281	0.000000	0.000000	1.000000	109727.007812
6.219784	0.000000	0.000000	1.000000	59111.667969
4.648163	0.000000	0.000000	1.000000	31802.964844
3.331540	0.000000	0.000000	1.000000	16951.957031
2.290164	0.000000	0.000000	1.000000	8900.054687
1.509890	0.000000	0.000000	1.000000	4582.230957
0.954733	0.000000	0.000000	1.000000	2305.691895
0.578997	0.000000	0.000000	1.000000	1130.854004

F3is = 6515.207031

F1 3is = 0.106136

****

****

Enter the value of dp = 0.03230

$p_0(d_p)$	Elutriation	$E(d_p)$	$I(d_p)$	$F(d_p)$
11.133094	0.000000	0.000000	1.000000	330375.875000
9.559119	0.000000	0.000000	1.000000	187650.687500
7.950575	0.000000	0.000000	1.000000	108548.429688
6.405573	0.000000	0.000000	1.000000	63258.769531
4.999149	0.000000	0.000000	1.000000	36856.476562
3.779313	0.000000	0.000000	1.000000	21348.316406
2.767632	0.000000	0.000000	1.000000	12241.332031
1.963281	0.000000	0.000000	1.000000	6926.036133
1.349072	0.000000	0.000000	1.000000	3856.623535
0.897980	0.000000	0.000000	1.000000	2109.081543
0.578997	0.000000	0.000000	1.000000	1130.854004

F4is = 2829.697510

F1 4is = 0.095356

****
****

Enter the value of dp = 0.04025

$p_0(d_p)$	Elutriation	$E(d_p)$	$I(d_p)$	$F(d_p)$
8.484130	0.000000	0.000000	1.000000	130109.695312
7.164830	0.000000	0.000000	1.000000	82832.804687
5.918427	0.000000	0.000000	1.000000	52852.453125
4.781990	0.000000	0.000000	1.000000	33668.304688
3.779312	0.000000	0.000000	1.000000	21348.306641
2.921587	0.000000	0.000000	1.000000	13441.677734
2.209157	0.000000	0.000000	1.000000	8387.888672
1.633941	0.000000	0.000000	1.000000	5179.327637
1.182083	0.000000	0.000000	1.000000	3160.427002
0.836491	0.000000	0.000000	1.000000	1903.670166
0.578997	0.000000	0.000000	1.000000	1130.853149

F5is = 1127.365479

F1 5is = 0.073513

****
****

Enter the value of dp = 0.04820

$p_0(d_p)$	Elutriation	$E(d_p)$	$I(d_p)$	$F(d_p)$
5.918427	0.000000	0.000000	1.000000	52852.453125
4.999147	0.000000	0.000000	1.000000	36856.457031
4.163348	0.000000	0.000000	1.000000	25634.189453
3.418588	0.000000	0.000000	1.000000	17758.912109
2.767630	0.000000	0.000000	1.000000	12241.318359
2.209156	0.000000	0.000000	1.000000	8387.879883
1.738610	0.000000	0.000000	1.000000	5708.791504
1.349072	0.000000	0.000000	1.000000	3856.623535
1.032108	0.000000	0.000000	1.000000	2584.544189
0.778525	0.000000	0.000000	1.000000	1717.314209
0.578998	0.000000	0.000000	1.000000	1130.855957

F6is = 445.867523

F1 6is = 0.049928

****

****

Enter the value of dp = 0.05615

$p_0(d_p)$	Elutriation	$E(d_p)$	$I(d_p)$	$F(d_p)$
3.779312	0.000000	0.000000	1.000000	21348.306641
3.247043	0.000000	0.000000	1.000000	16189.787109
2.767630	0.000000	0.000000	1.000000	12241.318359
2.340306	0.000000	0.000000	1.000000	9224.833984
1.963280	0.000000	0.000000	1.000000	6926.029785
1.633941	0.000000	0.000000	1.000000	5179.327637
1.349072	0.000000	0.000000	1.000000	3856.623535
1.105042	0.000000	0.000000	1.000000	2858.771484
0.897980	0.000000	0.000000	1.000000	2109.083252
0.723935	0.000000	0.000000	1.000000	1548.327148
0.578998	0.000000	0.000000	1.000000	1130.855957

F7is = 169.135818

F1 7is = 0.029942

****

****

Enter the value of dp = 0.06410

$p_0(d_p)$	Elutriation	$E(d_p)$	$I(d_p)$	$F(d_p)$
2.209157	0.000000	0.000000	1.000000	8387.888672
1.963281	0.000000	0.000000	1.000000	6926.036133
1.738611	0.000000	0.000000	1.000000	5708.796387
1.534217	0.000000	0.000000	1.000000	4696.742188
1.349073	0.000000	0.000000	1.000000	3856.626221
1.182084	0.000000	0.000000	1.000000	3160.432373
1.032109	0.000000	0.000000	1.000000	2584.546631
0.897981	0.000000	0.000000	1.000000	2109.084717
0.778526	0.000000	0.000000	1.000000	1717.316040
0.672578	0.000000	0.000000	1.000000	1395.175537
0.578999	0.000000	0.000000	1.000000	1130.857178

F8is = 58.513706

F1 8is = 0.015411

****

****

Enter the value of dp = 0.07205

$p_0(d_p)$	Elutriation	$E(d_p)$	$I(d_p)$	$F(d_p)$
1.182083	0.000000	0.000000	1.000000	3160.429443
1.105042	0.000000	0.000000	1.000000	2858.771484
1.032108	0.000000	0.000000	1.000000	2584.544189
0.963137	0.000000	0.000000	1.000000	2335.374268
0.897980	0.000000	0.000000	1.000000	2109.083252
0.836492	0.000000	0.000000	1.000000	1903.673462
0.778525	0.000000	0.000000	1.000000	1717.314209
0.723935	0.000000	0.000000	1.000000	1548.327148
0.672578	0.000000	0.000000	1.000000	1395.174316
0.624312	0.000000	0.000000	1.000000	1256.447021
0.578998	0.000000	0.000000	1.000000	1130.855957

F9is = 15.771186

F1 9is = 0.005899

****

****

Enter the value of dp = 0.08

$p_0(d_p)$	Elutriation	$E(d_p)$	$I(d_p)$	$F(d_p)$
0.578998	0.000000	0.000000	1.000000	1130.855103
0.578998	0.000000	0.000000	1.000000	1130.855103
0.578998	0.000000	0.000000	1.000000	1130.855103
0.578998	0.000000	0.000000	1.000000	1130.855103
0.578998	0.000000	0.000000	1.000000	1130.855103
0.578998	0.000000	0.000000	1.000000	1130.855103
0.578998	0.000000	0.000000	1.000000	1130.855103
0.578998	0.000000	0.000000	1.000000	1130.855103
0.578998	0.000000	0.000000	1.000000	1130.855103
0.578998	0.000000	0.000000	1.000000	1130.855103
0.578998	0.000000	0.000000	1.000000	1130.855103

F10is = 0.000002

F1 10is = 0.000000
****

Wc is = 16.963829 Kg

Values for $p_1(d_p)$:

enter the value of dp= 0.0005

$p_1(d_p)$ for 0.000500is = 8.155533

enter the value of dp= 0.00845

$p_1(d_p)$ for 0.008450is = 14.616227

enter the value of dp= 0.01640

$p_1(d_p)$ for 0.016400is = 21.981098

enter the value of dp= 0.02535

$p_1(d_p)$ for 0.025350is = 23.927412

enter the value of dp= 0.03230

$p_1(d_p)$ for 0.032300is = 21.497162

enter the value of dp= 0.04025

$p_1(d_p)$ for 0.040250is = 16.572803

enter the value of dp= 0.04820

$p_1(d_p)$ for 0.048200is = 11.255908

enter the value of dp= 0.05615

$p_1(d_p)$ for 0.056150is = 6.750228

enter the value of dp= 0.06410

$p_1(d_p)$ for 0.064100is = 3.474283

enter the value of dp= 0.07205

$p_1(d_p)$ for 0.072050is = 1.329841

enter the value of dp= 0.08

$p_1(d_p)$ for 0.080000is = 0.000000